ADDIS ABABA UNIVERSITY

ADDIS ABABA INSTITUTE OF TECHNOLOGY

SCHOOL OF CIVIL AND ENVIRONMENTAL ENGINEERING

Developing a Finite Element Computer Code for the Analysis of Rectangular Raft Foundations for a New Two Parameter Subgrade Model

By

Gebreegziabher Gebretnsea

July 2019

Addis Ababa, Ethiopia

Addis Ababa University
Addis Ababa Institute of Technology
School of Civil and Environmental Engineering
Geotechnical Engineering Stream

Developing a Finite Element Computer Code for the Analysis of Rectangular Raft Foundations for a New Two Parameter Subgrade Model

By

Gebreegziabher Gebretnsea

Advisor

Asrat worku (Dr.Ing.)

A Thesis submitted at Addis Ababa Institute of Technology in partial fulfillment of the requirements for the Degree of Master of Science in Geotechnical Engineering.

The undersigned have examined the thesis entitled '**Developing a Finite Element Computer Code for the Analysis of Rectangular Raft Foundations for a New Two Parameter Subgrade Model**' presented by **Gebreegziabher Gebretnsea**, a candidate for the degree of Master of Science and hereby certify that it is worthy of acceptance.

Board of Examiners

Dr.-Ing. Asrat Worku	_____	_____
Advisor	**Signature**	**Date**
_____	_____	_____
External Examiner	**Signature**	**Date**
_____	_____	_____
Internal Examiner	**Signature**	**Date**
_____	_____	_____
Chair Person	**Signature**	**Date**

DECLARATION

I, the undersigned, declare that this thesis is my original work, has not presented for a degree in this or any other universities, and all the sources of materials used for this thesis work have been fully acknowledged.

Name: Gebreegziabher Gebretnsea

Signature:

Advisor: Asrat worku (Dr.Ing.)

Signature:

ABSTRACT

In order to design safe and economical foundation structure, it has to be analyzed appropriately. An analysis method is said to be appropriate if the real behavior of the materials is implemented in the computational model. In order to implement the real behavior of the materials, advanced material models have to be applied. Formulating a computational model that uses advanced material models accurately is difficult. However, it is possible to formulate computational models that implement the advanced material models approximately. This is possible by using sophisticated 3D numerical methods. Nevertheless, running sophisticated 3D numerical models in routine personnel computers need significant time. Therefore, alternative computational models that are simplified and yet effective have to be formulated or selected.

There are practical cases in which soil behavior is characterized by elastic material models. In addition to this, there are poor practices of including a soil effect on a foundation structure. This study is intended to develop a linear 3D equivalent finite element model for a plate on an elastic foundation based on the current findings of subgrade models. This model is formulated such that design oriented results can be obtained easily by running the program on routine personal computers.

The developed finite element model is formulated based on a Kerr-equivalent subgrade model and Mindlin's theory for plates of intermediate thickness. In order to run the developed program on common personal computers easily, computer implementation techniques of finite element formulation are applied. All the operations of the developed program are coded by using the programming language of MATLAB. The results of the developed finite element model are compared with the results of PLAXIS 3D FOUNDATION. As per the observation of the comparison results, an attempt has been made to adjust the subgrade model. PLAXIS 3D FOUNDATION has been used for this purpose.

The final comparison after the application of adjustment factors shows that the solution of the developed finite element model is fairly in good agreement with the solutions of full-fledged finite element software such as PLAXIS 3D FOUNDATION. The developed elastic finite element computer program is used for the analysis of rectangular raft foundations.

ACKNOWLEDGEMENT

First of all, I would like to thank to Ethiopian Road Authority for the full sponsorship of my education expenses in the Master's Program.

Secondly, I would like to thank my thesis advisor Dr.-Ing. Asrat Worku of Geotechnical Engineering stream at Addis Ababa Institute of Technology, Addis Ababa University. The door to Dr.-Ing. Asrat office was always open whenever I need any assistance about my research. He gave me constructive guidance with great patience starting from the proposal stage. Therefore, I have a deepest gratitude for all his contributions.

Finally, I have appreciation for all my friends who give me constructive suggestions in case of difficulties.

TABLE OF CONTENTS

LIST OF TABLES

LIST OF FIGURES

1. Introduction

1.1. Background

Engineering structures are subjected to static and dynamic loads. The effects of these loads are transferred to the foundation structure and then finally to the underlying soil stratum. Thus, the stiffness of the underlying soil stratum is critical for the stability of the whole structure. In order to prevent post-construction structure failures, prior-construction simulation of the whole structure including the underlying soil stratum under the application of the design loads is required. If the simulation of the whole structure incorporates appropriate material models, then a structure designed as per the analysis result of the simulation is safe and economical. Even if we have material models, formulating computational model that implements the material models exactly is a challenging task. Hence, formulating a computational model by simplifying the material model and/or computational technique is the usual practice.

In order to analyze foundation structures, both the supporting soil medium and plate models have to be selected. If the selected soil and plate models are advanced, then these models can only be implemented in realistic approximate way by using 3D numerical methods. In general, it is possible to model realistic simulation of total stress, pore-water pressure, seepage, consolidation, and the interface between soil and structure at any stage of construction. This can be done effectively by using sophisticated 3D finite element computer codes [19, 20]. However, applying sophisticated 3D finite element computer codes for all practices is disadvantageous, because the cost of analysis is high. This is mainly due to the demand of high speed computer, expensive software, and expertise requirement. Therefore, by considering all the difficulties of formulating and implementation of sophisticated 3D finite element computer codes, there is a need to formulate simplified versions of the sophisticated 3D finite element computer codes that can be applied for moderately critical engineering projects.

When a greater safety factor is employed for foundation soils, there is a great chance of characterizing the soil behaving almost elastically under working loads. Not only this, in most local practices, the most common methods of including the soil effect on the foundation structure

are, a) considering the soil contact pressure as uniform or linearly varying, b) modeling contact pressure by Winkler model. Therefore, it is possible at least to modify these practices by applying current findings on analytical subgrade modeling.

Worku (2010) has derived a generalized continuum model for elastic soil foundations without any simplifications. This model has contributed in solving the confusions/challenges that were raised in mechanical as well as in the earliest continuum subgrade models. The significant findings of the generalized continuum model include: the model is equivalent to the three-parameter mechanical model of Kerr; and the open constants of the mechanical models can be determined by direct comparison with special cases of this model (generalized continuum model) [32].

A further study of Worku (2014) has recommended applying Kerr-equivalent Pasternak model for practical use. This has an advantage over the existing two-parameter simplified subgrade models, because it has been derived by adjusting the two-parameter Pasternak model to the adjusted three-parameter generalized Kerr-type continuum model to give identical results [33].

Hence, this research is aiming to develop static linear finite element computer program, which is based on the Kerr-equivalent Pasternak model and Mindlin plate theory. Detail literature review on the soil models, plate models, computational techniques and related literatures are given in the next chapter.

1.2. Objectives of the Study

The objective of this study is to develop 3D equivalent static linear finite element computer code for the analysis of flexible rectangular plate on an elastic foundation based on the Kerr-equivalent two-parameter Pasternak model. The developed finite element computer code will enable the generation of deflection, shear force, and bending moment so that it is possible to design flexible rectangular plate-like foundations for punching and flexure easily.

1.3. Scope of the Work

This study is limited to the analysis of shallow foundation structures with rectangular geometry and with no openings and beams. It can be used effectively for the analysis of rectangular mat foundations. The foundation structure is assumed to directly rest on the soil, and no pile foundation is attached to this structure. The application of the developed finite element model is limited to the elastic responses of the plate and the soil.

1.4. Methodology

In order to decide on the formulation of the computational model, literature on soil models, plate models and methods of analysis are reviewed. After selecting the appropriate analytical soil and plate models, the computational model is formulated by using the finite element method. The finite element method demands many operations, which are mandatory to use a programming language. In this study, MATLAB is used to code all the operations of the finite element as per the selected soil and plate models.

When a new computational model is formulated, it has to be verified, and/or if possible, validated. In this study, PLAXIS 3D FOUNDATION is used to verify and adjust the developed 3D equivalent finite element model.

1.5. Organization of the Thesis

This thesis is organized in 7 chapters. The content of each chapter is as described below:

Chapter one: describes the general view of analysis of foundation structures and then clarifies why this research needs to be done. In addition to this, the study's objectives, scopes, and methodologies are explained.

Chapter two: the intention of this chapter is to review appropriate literature that focus on soil models, plate models, analysis methods and related studies. This chapter gives benchmark information on the organization of the computational model.

Chapter three: solving the differential equation for a plate on a two parameter subgrade for any loading type is difficult. Therefore, the purpose of this chapter is to formulate an approximate computational model. As a result, this chapter discusses the finite element formulation of plate-soil element stiffness matrix, boundary condition, equivalent nodal loading and internal shear force and bending moment.

Chapter four: in this chapter the computer implementation of the finite element formulation is presented. The finite element programming techniques of generating finite element model information, element connectivity, assembling element stiffness matrix and load vector, solution method and post-processing results are discussed. In order to create a clear view of the developed finite element model, only the flow charts of the subroutines are presented.

Chapter five: this chapter deals with the verification, adjustment and convergence of the developed finite element model.

Chapter six: in this chapter different numerical examples are solved by both the developed finite element model and PLAXIS 3D FOUNDATION, then the solution of the two models are compared.

Chapter seven: in this chapter the conclusions and the recommendations for further studies are discussed.

2. Review of Soil Models, Plate Models, Analysis Methods & Related Studies

2.1. General Introduction

Safe and economically designed engineering structures cannot be achieved without applying accurate or appropriate methods of analysis. Therefore, attention should be given to the development of new methods of analysis or using the best available methods. An analysis method is said to be acceptable if it can be supported by experimental results or at least verified and the entire expertise requirement are applied.

In order to analyze foundation structures effectively, two types of models are required. They are models for the foundation structure and for its interaction with the supporting soil. The most common foundation structure models are: 1) Kirchhoff plate theory, 2) Reissner-Mindlin plate theory, 3) 3D model [25]. The most widely used soil models are: elastic subgrade models and advanced soil models.

After modeling the foundation structure and the supporting soil, the next step is to identify the solution method. This step plays a key role in finding a solution that reflects the real loading configuration. Except for simple problems, it is difficult to find a closed form solution as the loading, material properties and geometry are generally complicated. For this reason, approximate solution methods, i.e., numerical solution methods become the most common analysis method in most engineering fields, as is also the case in the analysis of plates on a deformable subgrade.

The intention in this chapter is to review plate models, soil models, analysis methods, and similar studies. Reviewing plate models, soil models and analysis methods give helpful information in formulating new computation models.

2.2. Flat Foundation Structure (Plate) Models

2.2.1. Introduction to Plates

Plates are straight, plane, two-dimensional structural components the thickness, h, being much smaller than the other dimensions. Plates predominantly carry perpendicular transverse loads, in which the external loads are internally carried by bending moments and transverse shear forces, which resemble the carrying action of beams or cables to certain extent. Statically, plate boundary conditions can be free, simply supported, fixed, or elastic supports and elastic restraints. In some cases, even point supports are employed [25]. Plates are widely used in the construction industry or engineering fields, typically in architectural structures, bridges, hydraulic structures, pavements, aircraft hangars, containers, airplanes, missiles, ships, instruments, and machine parts.

The governing differential equation of plates is dependent in the magnitude of the plate deflection. If plate deflection is small, the middle surface stress is negligible. However, for a large plate deflection the middle surface stress is included in the differential equation of plates, which becomes much more complicated [27].

If rigorous analysis is required, plates should be considered as three-dimensional continuum. However, obtain solution for all types of problems faces mathematical difficulties. Even if a solution could be found, the resulting costs would be, in most cases, prohibitively high. Consequently, in order to rationalize the plate analysis, we distinguish among four different plate categories with inherently different structural behavior and hence, different governing differential equations [25]. Although the boundaries are somewhat fuzzy, subdivision of the plates is done based on thickness (h) to length (L) ratio as follows:

1. Membrane ($h/L<1/50$): carries load by axial and central shear forces, which is approximated by a network of stressed cables.
2. Stiff plate ($h/L=1/50$ to $1/10$): carries load mainly by bending moments, generally in a manner similar to beams. Such plates are commonly analyzed by Kirchhoff's plate theory.

3. Moderately thick plate (h/L=1/10 to 1/5): similar to stiff plate, with the notable exception that the effects of transverse shear forces on the normal stress components are also taken into account. Such plates are commonly analyzed by Reissner-Mindlin plate theory.
4. Thick plate (h/L>1/5): have an internal stress condition that resembles that of a three-dimensional continuum.

2.2.2. Classical Small-Deflection Theory of Thin Plates

A mathematical exact stress analysis of thin plates with small deflections subjected to transverse loads require solution of the differential equations of three-dimensional elasticity [8, 27]. In most cases, such approach would encounter insurmountable mathematical difficulties. Yet, for the vast majority of technical applications Kirchhoff's classical theory of thin plates yields sufficiently accurate results without the need for carrying out a full three-dimensional stress analysis [25].

Kirchhoff's classical plate theory is formulated in terms of transverse deflections, w(x, y), for which the governing differential equation is of fourth order, requiring only two boundary conditions to be satisfied at each edge. In order to establish the behavior of Kirchhoff plate theory and reduce the three-dimensional theory of elasticity, the following approximations are used [25, 27]:

1. The normal stress, which is in the direction of the thickness, is assumed to be zero.
2. The transverse deflection, w(x, y), is small as compared to the plate thickness.
3. Sections that are taken normal to the middle surface before deformation remain plane and normal to the deflected middle surface. Consequently, shear deformations are neglected. This assumption represents an extension of Bernoulli's hypothesis for beams to plates.
4. The plate thickness is either uniform or varies slowly, so three-dimensional stress effects are ignored.
5. The middle surface of the plate remains unstrained during bending.
6. The material is homogeneous, isotropic, and linear elastic; that is, it follows Hooke's law.
7. The plate is symmetric in fabrication about the middle surface.

According to the above assumptions, there exists only the in-plane stresses and strains and the out of plane stresses and strains vanish. However, the internal out of plane shear forces are

necessary for equilibrium in the z-direction; which implies the out of plane shear stresses are not zero, but small for thin plate.

The governing differential equation in the Cartesian coordinate system for thin plates subjected to transverse distributed load can be derived easily and is given by [25]:

$$\frac{\partial^4 w(x,y)}{\partial x^4} + 2\frac{\partial^4 w(x,y)}{\partial x^2 \partial y^2} + \frac{\partial^4 w(x,y)}{\partial y^4} = \frac{p_z(x,y)}{D} \tag{2.1}$$

where: w(x, y) is the transverse deflection of the mid plane of the plate.

D=flexural rigidity of the plate, P_z (x, y) =transverse distributed load.

To arrive at Equation (2.1), the equilibrium equations are not enough; additional elasticity equations should be utilized. If elasticity equations are not used, the plate problem becomes statically indeterminate. Such a problem occurs in all two and three-dimensional problems of elasticity.

A plate problem is considered solved, if a suitable expression for the deflected plate surface w(x, y) is found that satisfies the differential equation of equilibrium (2.1) and the boundary conditions.

2.2.3. Theories for Moderately Thick Plates

Although the classical Kirchhoff's plate theory yields sufficiently accurate results for thin plates, its accuracy decreases with growing thickness of the plate. Exact three-dimensional elasticity analysis of some plate problems indicates that its error is in the order of plate thickness square. Such an inherent limitation of classical Kirchhoff's plate theory for moderately thick plates necessitated the development of more refined theories in order to obtain reliable results for the behavior of these structures [25].

The major difference between moderately thick plate theories and classical Kirchhoff's plate theory is that the out-of-plane shear deformation is included in the former. This implies, for moderately thick plates, due to E. Reissner and R. D. Mindlin, the assumption that particles of the plate originally on a straight line that is normal to the undeformed middle surface remain on a straight line during deformation is modified to, this line is not necessarily normal to the

deformed middle surface. With this assumption, the section rotations and transverse deflection are independent of each other [3].

Unlike the classical Kirchhoff plate theory, in the moderately thick plate theory only the normal transverse strain and stress vanish, whereas the remaining strains and stresses exist. All these strains and stresses are estimated from the constitutive relationships. The resulting shear strains and corresponding shear stresses are constant throughout the thickness of the plate. Since the real shear stress distribution in moderately thick plates is parabolic, this assumption is incorrect. Furthermore, it fails to satisfy the zero-stress condition on the top and bottom surfaces of the plate. Consequently, it was necessary to introduce a correction factor, k^2, which was evaluated by comparison with the exact elastic solution [3].

Applying the minimum of the potential energy theorem, Mindlin derived the following differential equations of equilibrium for moderately thick plates [25]:

$$k^2Gh(\nabla^2 w(x,y)+¤)+p_z(x,y)=0 \tag{2.2}$$

$$\frac{D}{2}\left[(1-¬)\nabla^2 \cdot_x+(1+¬)\frac{\partial ¤}{\partial x}\right]-k^2Gh\left(\cdot_x+\frac{\partial w(x,y)}{\partial x}\right)=0 \tag{2.3}$$

$$\frac{D}{2}\left[(1-¬)\nabla^2 \cdot_y+(1+¬)\frac{\partial ¤}{\partial y}\right]-k^2Gh\left(\cdot_y+\frac{\partial w(x,y)}{\partial y}\right)=0 \tag{2.4}$$

Where:

ψ_x and ψ_y represent rotations at the mid plane about y-axis and x-axis respectively.

k^2,E, G and v are shear correction factor, Young's modulus of elasticity, shear modulus and Poisson's ratio, respectively. The function ¤ is:

$$¤=\frac{\partial \cdot_x}{\partial x}+\frac{\partial \cdot_y}{\partial y};\nabla^2=\frac{\partial^2}{\partial x^2}+\frac{\partial^2}{\partial y^2} \tag{2.5}$$

The moderately thick plate theory has better benefit in the finite element formulation than the classical Kirchhoff's plate theory, because the finite element derived for moderately thick plate

becomes conformal if C^0 continuity requirement is satisfied in both section rotations and deflection. However, for classical Kirchhoff's plate theory, C^1 and C^0 continuity are required. Where C^0 and C^1 define the continuity of a function with the highest degree of derivative 0 and 1, respectively. To satisfy C^1 continuity requirement, we have to ensure continuity of transverse deflection, w(x,y), as well as its normal derivatives $\partial w/\partial n$ along the element boundaries. However, this is not always an easy task; thus, this requirement is often violated by many successful nonconforming elements [3, 25].

2.2.4. Three-Dimensional Elasticity model for Thick Plates

When the thickness of the plate becomes significant as compared to its smallest span dimension, that is, the thickness-to-span ratio is considerably greater than 1/5; the governing equations of three-dimensional elasticity theory must be applied in order to determine the true three-dimensional distribution of stresses and strains in the plate. Such a three-dimensional approach is rigorous, and finding a solution for such problems is generally extremely difficult [25].

In general, the solution of a three-dimensional elasticity problem consists of finding the 6 stresses, 6 strains and 3 displacements, 15 unknowns in total. The elastic body is subjected to surface forces p_x, p_y, p_z and body forces X, Y, Z. For this purpose, the following field equations and specific boundary conditions are required [23, 25]:

1. Three equilibrium equations,
2. Six kinematic relationships(displacement-strain relations),
3. Six stress-strain equations, and
4. Static, kinematic, and mixed boundary conditions.

The original 15 equations used in a stress-based analysis can be reduced to three differential equations in terms of the displacement components u, v, and w. The three equilibrium differential equations in terms of these displacements, which are referred to as Navier's or Lame's equations of equilibrium are [25]:

$$(\lambda+G)\,\partial\varepsilon/\partial x+G\nabla^2 u+X=0, \qquad (2.6)$$

$$(\lambda+G)\partial\varepsilon/\partial y+G\nabla^2 v+Y=0, \quad (2.7)$$

$$(\lambda+G)\partial\varepsilon/\partial z+G\nabla^2 w+Z=0. \quad (2.8)$$

Where:

$$\lambda=\nu E/((1+\nu)(1-\nu)), \quad (2.9)$$

$$\nabla^2=\partial^2/\partial x^2+\partial^2/\partial y^2+\partial^2/\partial z^2, \quad (2.10)$$

$$\varepsilon=\varepsilon_x+\varepsilon_y+\varepsilon_x. \quad (2.11)$$

The three-dimensional elasticity solutions (closed form solution) of the above Equations (2.6, 2.7, and 2.8) have the ability to express precisely the high-order variation of displacement and stress through the thickness of the plate. Nevertheless, finding closed form solutions is generally extremely difficult. The few analytical solutions available are usually restricted to problems with simple plate geometry, loading conditions and boundary conditions [25].

2.3. Elastic and Non-elastic Support /Soil Models

2.3.1. General Introduction

The analysis of structure rested on soil is not complete without accounting the soil-structure interaction. Soils are often the weakest materials involved in common geotechnical problems. This implies, soils determine the deformation and the possibility of failure of the structure, and it is therefore important to characterize these materials reliably over the entire range of stresses and strains to which they will become exposed. Other construction materials such as concrete and steel may remain stiff in comparison with soils, and it may be sufficient to characterize these materials as elastic or as elastic-perfectly plastic. Thus, selecting the appropriate soil model is a critical stage.

The types of soil models/soil effect accounting methods from the weakest to the strongest form sequentially are rigid method, subgrade (mechanical and continuum) models, and advanced constitutive models. The first method can be used in the analytical solution method for simple problems and the second models are applicable for a soil response in the elastic range. However,

with the development of fast computing machines and software, including advanced constitutive models in the numerical analysis methods gives results with better accuracy.

2.3.2. Subgrade Models

2.3.2.1. Winkler Subgrade Model

The Winkler subgrade model is a mechanical model based on the assumptions of elastic soil response and is commonly used in practice which is also included in some 2D finite element software for routine analysis such as SAFE to analyze plates. This model assumes a uniform spring bed, in which each spring is linear and acts independent of the others. The spring bed is characterized by a single parameter, k_s, called modulus of subgrade reaction. This representation has the desire to increase the contact pressure below columns and is a significant improvement over the rigid method [5]. Even though this method tries to consider the soil-structure interaction (SSI), it is a coarse method as the interaction between the springs is ignored and there is no specific method to determine the k_s value. The transverse deflection is not continuous at the boundary of the foundation. According to Winkler's assumption, the transverse deflection, w(x,y), of the soil medium at any point on the surface is proportional to applied stress at that point, q(x,y), and independent of the neighboring stress.

$$q(x, y) = k_s * w(x, y) \tag{2.12}$$

Where: k_s is the subgrade reaction modulus (force per length cubed).

2.3.2.2. Two-Parameter Mechanical Subgrade Models

Two-parameter mechanical subgrade models are developed with the intention of creating continuity between Winkler springs. To achieve this, a second parameter is incorporated to inter-connect Winkler springs. This creates continuous surface deflection beyond the loaded region. The most common two-parameter mechanical models are: Filonenko-Borodich model (1940, 1945), Hetényi model (1946) and Pasternak model (1954). All these models include a second parameter in order to account the missed interactions between the Winkler springs. In all these models, there are two independent elastic parameters [24]. Although the aim of these models is the same, that is, inter-connecting the Winkler springs/subgrade reaction, they consider the inter-connecting elastic parameter differently.

2.3.2.2.1. Filonenko-Borodich Mechanical Model

In the Filonenko-Borodich mechanical model the inter-connecting element is a membrane under constant tension (T). The differential equation of the Filonenko-Borodich model for 3D case is as follows [24]:

$$q(x,y) = k_s w(x,y) - T\nabla^2 w(x,y) \tag{2.13}$$

Where:

$$\nabla^2 = \frac{\partial^2}{\partial x^2} + \frac{\partial^2}{\partial y^2} \tag{2.14}$$

2.3.2.2.2. Hetenyi Mechanical Model

The difference with Filonenko-Borodich model is, Hetenyi model uses a flexural element as a connecting component to ensure the continuity of the Winkler springs that gives dish-shaped transverse deflection. The differential equation of this model, which defines the relationship between the contact pressure, the elastic parameters (ks and D) and the deflection, w(x,y), for the 3D case is as follows [24]:

$$q(x,y) = k_s w(x,y) - D\nabla^4 w(x,y) \tag{2.15}$$

Where: D is the flexural rigidity of the connecting element, and

$$\nabla^4 = \frac{\partial^4}{\partial x^4} + \frac{\partial^4}{\partial y^4} \tag{2.16}$$

2.3.2.2.3. Pasternak Mechanical Model

This model proposed by Pasternak (1954) assumes the existence of shear interaction between the Winkler springs. This is accomplished by connecting the Winkler spring elements to a layer of incompressible vertical elements, which deform in transverse shear only. By assuming that the shear layer is isotropic in the x, y plane, the shear modulus becomes $G_x=G_y=G_p$. Then for elastic case, the transverse shear stresses of the shear layer are [24]:

$$\left.\begin{aligned} \tau_{xz} &= G_p \gamma_{xz} \\ \tau_{yz} &= G_p \gamma_{yz} \end{aligned}\right\} \tag{2.17}$$

Where: τ_{xz}, τ_{yz} are the transverse shear stresses in the xz and yz planes respectively; γ_{xz}, γ_{yz} are the transverse shear strains in the xz and yz planes respectively.

The partial differential equation of Pasternak Model is identical to Filonenko-Borodich model, except the second model parameter is replaced by Gp :

$$q(x,y) = k_s w(x,y) - G_p \nabla^2 w(x,y) \tag{2.18}$$

2.3.2.3. Three Parameter Mechanical Models

Two-parameter mechanical subgrade models still lack in adequately accounting the behavior of soil media. For this reason, three-parameter mechanical models have been developed to improve the two-parameter mechanical subgrade models. The third parameter is added with the intention of making the subgrade models more realistic [10]. Kerr and Rhines (1967) suggested that more accuracy could be obtained by incorporating additional springs and shear elements. However, Worku (2010) developed a generalized continuum model without ignoring any deformation, strain, and stress, which is equivalent to the three parameter mechanical model developed by Kerr [32]. This proves that using a model with more than three mechanical parameters do not increase accuracy, it rather complicates the subsequent analysis for no additional benefits. Quantifying the additional parameters is also an added disadvantage.

2.3.2.3.1. Three Parameter Kerr Mechanical Model

This model consists of three elastic parameters in which an upper spring, $k_{u,}$ and lower spring, $k_{L,}$ are inter-connected by a shear layer, G_k. This model is introduced as an attempt to improve the two-parameter Pasternak mechanical model. The differential equation of this model is as follows [10]:

$$p(x,y) - \frac{G_k}{K_u + K_l}\nabla^2 p(x,y) = \frac{K_u K_l}{K_u + K_l} w(x,y) - \frac{G_k K_u}{K_u + K_l}\nabla^2 w(x,y) \tag{2.19}$$

Where: p(x,y) is applied stress.

Kerr's model was motivated by the derivation of a differential equation of similar order and form by Reissner [22], who represented the subgrade by a significantly simplified continuum as presented in Section 2.3.2.4.2.

2.3.2.4. Continuum Subgrade Models

The surface deflection obtained from Winkler model is limited to the loaded region, but practically the surface deflection will occur not only immediately under the loaded region but also extends to the zone beyond the loaded region. In attempts to account for the continuity of surface deflection, soil media have often been idealized as three-dimensional elastic continuum. In general, applying three-dimensional theory of elasticity in the soil-foundation interaction demands a complex mathematical problem. Hence, to overcome this mathematical complexity some simplifications were employed by different researchers. Recently, Worku has derived a generalized continuum model by considering the full three-dimensional theory of elasticity [32].

2.3.2.4.1. Vlasov-Leont'ev Continuum Model

This model is based on representing the subgrade by an isotropic elastic stratum of thickness and is derived by neglecting the horizontal displacement components in the subgrade material. Furthermore, it assumes that the vertical displacement has maximum value at the soil surface and vanishes to zero after some depth in accordance with a certain function of depth. The basic differential equation is derived using the variational approach, and is given by [30]:

$$q(x,y) = kw(x,y) - 2t\nabla^2 w(x,y) \tag{2.20}$$

Where: q(x,y) and w(x,y) are the applied stress and surface vertical deflection respectively,

$$k = \frac{E_o}{\left(1-v_o^{\,2}\right)}\int_0^H \left(\frac{\partial h(z)}{\partial z}\right)^2 dz \tag{2.21}$$

$$t = \frac{E_o}{4\left(1+v_o\right)}\int_0^H \left(h(z)\right)^2 dz \tag{2.22}$$

$$E_o = \frac{E_s}{1-v}, v_o = v\left(1-v\right) \tag{2.23}$$

Es, *v* and H are the modulus of elasticity, Poisson's ratio and thickness of soil stratum respectively, and h (z) is a function that shows the variation of the displacement, w(x, y), in the z-direction.

It is evident from Equations (2.21) and (2.23) that different soil types can be modeled by assigning suitable expressions for the function h (z). Note also that Equation (2.20) is similar in form with the two-parameter mechanical models presented above.

2.3.2.4.2. Reissner Continuum Model

Reissner (1958) proposed a continuum model, which is equivalent to a three parameter mechanical model. This model is formulated by making the simplifying assumption of zero in-plane stresses: ($\sigma_{xx} = \sigma_{yy} = \tau_{xy} = 0$)

The consequence of zero in-plane stresses result in a constant vertical shear stress, $\tau_{xz,}\tau_{yz}$ throughout the thickness of the soil medium.

Such an assumption is not realistic for thick soil media. The differential equation of Reissner model is as follows [22]:

$$p(x,y) - \left(\frac{GH^2}{12E_s}\right)\nabla^2 p(x,y) = \frac{E_s}{H} w(x,y) - \frac{GH}{3}\nabla^2 w(x,y) \qquad (2.24)$$

Where: H is the thickness of soil medium; E_s and G are Young's and shear modulus of the soil medium respectively.

Note that this differential equation is similar in form and order with Equation (2.19) representing Kerr's three-parameter mechanical model.

2.3.2.4.3. Generalized Continuum Model

Worku (2010) developed generalized continuum model without making any major simplfying assumption except the assumption on the depth-wise variation of transverse shear stresses (see Equation (2.27)).This model has contributed in solving the confusions/challenges that were raised in the mechanical as well as in the earlier continuum subgrade models. The significant

findings of the generalized continuum model include; the three parameter mechanical models are equivalent to this model and the open parameters of the mechanical models can be determined from the prevailing mathematical equivalence. The depth-wise variation of the normal stresses and transverse shear stresses are described as follows [32]:

$$\sigma_x(x,y,z) = g_x(z)\sigma_z(x,y,z); \qquad \sigma_y(x,y,z) = g_y(z)\sigma_z(x,y,z) \tag{2.25}$$

$$\tau_{xz}(x,y,z) = I_{zx}(z)\tau_{zx}(x,y); \qquad \tau_{yz}(x,y,z) = I_{yz}(z)\tau_{yz}(x,y) \tag{2.26}$$

Where: $g_x(z)$,$g_y(z)$,I_{zx} and I_{yz} are function of z, which shows the depth-wise variation of the normal stresses and shear stresses, respectively. The following assumption is made in the model development:

$$I_{zx}(z)=I_{yz}(z)=I(z) \tag{2.27}$$

This implies that the variation of the vertical shear stresses with depth on the faces perpendicular to x-and y-axis is similar. Note, however that the two stresses are not identical. The generalized continuum model's differential equation for the homogenous soil layer is as follows [32]:

$$p(x,y) - \frac{G}{E_s K_I}\left(L_{gI} - \frac{K_{gI}L_g}{K_g}\right)\nabla^2 p(x,y) = \frac{E_s}{K_g}w(x,y) - \frac{GL_{gI}}{K_g K_I}\nabla^2 w(x,y) \tag{2.28}$$

Where:

$$K_g = \int_0^H g dz; \quad K_{gI} = \int_0^H g\tilde{I}_Z dz; \quad K_I = \int_0^H I_z dz \tag{2.29}$$

$$L_g = \int_0^H \left[\int g dz - \left(\int g dz\right)_{z=H}\right] dz; \quad L_{gI} = \int_0^H \left[\int g\tilde{I}_z dz - \left(\int g\tilde{I}_z dz\right)_{z=H}\right] dz \tag{2.30}$$

$$g(z) = 1 - \nu[g_x(z) + g_y(z)]; \quad \tilde{I}_z(z) = \left(\int I_z dz\right)_{z=0} - \int I_z dz \tag{2.31}$$

Lower order mechanical and continuum models can be obtained by making just the appropriate simplification on deformations, strains and stresses; and different types of model variants can be obtained by using the same model with the variation of the functions, $g_x(z)$, $g_y(z)$ and I_z [32].

2.3.3. Advanced Soil Constitutive Models (General)

All the above presented soil models are formulated based on elastic soil behavior. For more accurate analysis involving inelastic response, appropriate constitutive soil models should be applied. However, incorporating such models is a difficult task without the application of numerical methods. In addition to this, formulation of the numerical models and the associated computer programming and verification of the final model demands huge expertise.

Initial soil constitutive models were relatively simple. However, better models that capture the behavior of soils under complex loading conditions are formulated later on. Recently, more rigorous models are becoming applicable with the aid of numerical models. Characterization of soil behavior is quite involved, because the stress-strain relationships are non-linear in nature. In addition to this, soils are fundamentally frictional, and volume change occurs during drained shearing [11].

Most practical soil constitutive models, which are applicable in numerical models, are developed based on observed behavior in laboratory experiments. Advanced soil constitutive model are required for analysis of strain and deformation at and after failure and for realistic evaluation of pore pressures induced by change in external loads [7].

Simpler soil models are sufficient when, a) the global safety factor is high enough so that deformation is not dominated by plastic behavior, b) the conditions analyzed are either fully drained or completely undrained, so that it is not necessary to calculate change in pore water pressure. As the soil model becomes more sophisticated, more model parameters are selected based on soil investigation data [7], which generally is a daunting task.

2.4. Methods of Analysis

For an exact theoretical solution, the requirements of equilibrium, compatibility, material behavior and boundary conditions both in terms of force and displacement must be all satisfied. Methods of analysis can be categorized into closed form and numerical analysis.

A closed form solution is the ultimate method of analysis. In this approach, all solution requirements are satisfied and the theories of mathematics are used to obtain complete analytical

expressions defining the full behavior of the problem. However, as soil is a highly complex multi-phase material that behaves nonlinearly when loaded, complete analytical solutions to realistic geotechnical problems are not usually possible. Thus, Solutions can only be obtained for very simple classes of problems by using this method [19].

Many physical phenomena in engineering and science can be described in terms of partial differential equations or functionals. In general, solving these equations by classical analytical methods for arbitrary shapes is almost impossible. A numerical approach such as finite element is a widely used method by which these partial differential equations or functionals can be solved approximately. Even though, numerical methods are approximate by nature, the real behavior of the problem can be included better than the simplified closed form solution methods; and ultimately, with the aid of numerical method based computer simulations better solutions are obtained than the simplified closed form solution methods.

If appropriate soil investigation data is provided into the computer aided numerical solution approach, the following results can be obtained without postulating mode of behavior [19]:

- Simulating the construction stage of the subgrade
- Evaluating 3D stresses and deformations for the structural elements and soil
- Simulation of consolidation, effective stress and total stress with respect to time and loading.

2.5. Review of Related Studies

To get the superstructure's real behavior, the subgrade must be modeled sufficiently well. Most often in practice, structural engineers analyze the structural elements in detail, but they represent the subgrade by poor methods/ models. On the other hand, geotechnical engineers analyze the soil behavior by using advanced soil models, but with a simple model of the structure. Therefore, developing computational software by employing the advanced models of the two disciplines gives in an accurate solution. However, this approach has two disadvantages, which are the demand of unrealistic large computational time and the need a great knowledge in both of the subjects. Thus, there is a need of geotechnical engineers to develop simple subgrade models for practical use that are simple to use, but still give reasonable accurate results.

A recently published article by Poulos clearly argues that even though practicing structures engineers are dissuaded from representing the soil by subgrade reaction modulus (k), they continue to request such a simple value. For this reason, the logical procedures for the estimation of an equivalent k are presented in this article [21].

The simplest and oldest elastic subgrade model is Winkler's model. It is well-known and used foundation soil model by structural engineers. Even though this model is easy for implementation, it was recognized as a poor representation of the subgrade. To modify the discrepancies, different elastic mechanical and continuum models were recommended later. The fundamental flaws in the implementation of these models were the lack of straightforward formulas for the parameters of the models and the numbers of elastic parameters required in the subgrade model for the best accuracy of the results were not known. However, the development of generalized continuum model by Worku aids in the estimation of the model parameters in any of the elastic subgrade models. Furthermore, this model confirms that three-parameter model is the ultimate elastic subgrade model [32].

Worku & Degu have implemented the generalized continuum subgrade model for the analysis of beam on elastic foundation. The closed-form of a deflection solution shows that the generalized continuum subgrade model is sensitive to the thickness of the soil stratum. This discrepancy has been identified by comparing with the solution of finite element software, PLAXIS 2D. To correct the sensitiveness of the model, they introduced a constant calibration factor. After the application of a calibration factor of 3, a closed-form solution of a beam on Kerr type subgrade model is in a closer agreement with the solution of PLAXIS 2D [34].

Amlesu's study of strip plate on Kerr-equivalent Pasternak type subgrade has indicated that the subgrade models is sensitive to the thickness of the soil stratum. Unlike the study of Worku & Degu for beam on elastic foundation, in this study it is shown that the calibration factor is not a constant single number. It rather varies with the soil type, loading and the strip plate size [1]. The numerical comparisons for a strip plate given in this study did not consider cases for small thickness of soil stratum. Therefore, it is important to assess the effect of soil stratum thickness on the calibration factor. In general, the significant observation from this study is the calibration factor is not constant as soil-plate relative rigidity and loading are varied.

Meron's study circular plate on Kerr-equivalent Pasternak type subgrade has shown that the subgrade model is sensitive to the soil stratum thickness, which leads to the recommendation variable calibration factor. This study is limited to circular plate problems that can be taken as axisymmetric problems (2D problems). This implies, this study is not applicable for 3D circular problems that can not be represented by axisymmetric problems [14]. The significant finding from this study is the calibration factor varies with respect to the loading type, soil type and plate size. Once more, the given numerical examples in this study have not covered for soil with small thickness.

All the above studies have given a closed-form solution for simple case of a structure on elastic foundation. If plates are subjected to complex loading, reasonable solution are obtained by considering the problem as 3D. Following closed-form solution method for such problems is difficult. In such cases, numerical solution techniques are the most effective alternatives.

Analysis of plate on elastic foundation by using numerical method is not new approach. It is found in wide range of literatures, typically in [4, 25, 28, 29]. Some reviewed literatures show that they differ from each other in the implementation of the type of the numerical method, plate model, boundary condition, verification method and the type of elastic subgrade model.

In this research, a 3D equivalent finite element model will be developed for plates on elastic foundation. The selected plate model is Mindlin's plate theory, because it can be applicable for thin as well as for moderately thick plates. The elastic subgrade is represented by Kerr-equivalent Pasternak model of Worku and the loading type can be concentrated force, bending moment, uniformly distributed load and mixed loading. Since this research uses a subgrade model based on the current findings of the generalized continuum model of Worku, the developed finite model is expected to be sensitive to the soil stratum thickness. As it is already discussed the findings of other researches in the above paragraphs, the calibration factor is variable with respect to soil type, loading type and plate size. The sensitive of the calibration factor is expected to increase for the case of a plate as compared to a beam.

3. Development of the Finite Element Model

3.1. Introduction and Basic Assumptions

The selected numerical approach to represent the behavior of the interacting plate-soil system in this research is the well-known method of finite elements. The advantage of the finite element method for the analysis of plates lies in its easy application to irregular geometry, general loading, and arbitrary boundary condition. However, only rectangular element is used in this research.

In the development of the finite element formulation, the plate is represented by Mindlin's plate theory, which is a generalized plate theory, as it can be applied also for thin plate; whereas the soil is represented by Pasternak's two-parameter model. The elastic parameters of Pasternak's model are taken as advised by Worku [33].

Each plate-soil element is represented by rectangular elements with four nodes. Each node has three degrees of freedoms, which are two section rotations and one transverse displacement located at the middle plane of the plate. Thus, displacement-rotations of the soil will be estimated at the surface of the soil media only, which are taken to be equal with the plate's middle plane displacement-rotations.

In the finite element method, the entire plate-soil system is discretized in to finite elements. The plate and the soil are represented by Mindlin plate theory and Pasternak two-parameter subgrade model, respectively. The element stiffness matrices relate the nodal deformations and loadings to each other. By using the equilibrium of forces and moments, these element equations are combined together to form global stiffness matrix. The global stiffness matrix connects the global deformations and loadings. After the formation of global simultaneous equation, global deformations become the only unknowns.

The boundary conditions are applied at the plate edge as function of plate boundary deformations. The deformations away from the plate region are taken from Vlasov and Leont'ev

assumption (the detail of this assumption is presented in Section 3.5). The boundary conditions are applied at the respective element node before starting stiffness matrix assembling.

3.2. Development of Plate Element Stiffness Matrix

The plate element formulation is a special case of the general shell element formulation and is based on the theory of plates with transverse shear deformations included. In this theory, due to Reissner and Mindlin, it uses the assumption that particles of the plate originally on a straight line that is normal to the undeformed middle surface remain on a straight line during deformation, but this line is not necessarily normal to the deformed middle surface. With this assumption and positive sign convention given in Figure 3.1, the displacement components of a point by assuming the small displacement bending theory are [2, 3]:

$$u = -z\ _x(x,y);\ v = -z\ _y(x,y);\quad \text{w=w(x,y)} \tag{3.1}$$

Where: $_x(x,y)$ and $_y(x,y)$ are the section rotations in the xz and yz-plane, respectively; z is measured from the middle plane and w(x,y) is deflection of the middle plane.

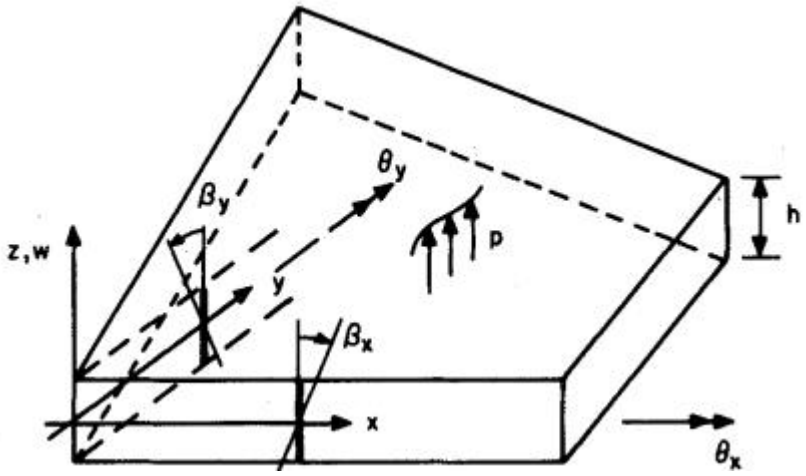

Figure 3. 1: Positive notations/sign conventions for Mindlin plate theory [2].

By considering Figure 3.1, the bending strains, $\varepsilon_{xx}, \varepsilon_{yy}, \gamma_{xy}$ and transverse shear strains , γ_{xz}, γ_{yz} , are given below [25]:

$$\begin{Bmatrix} \gamma_{xz} \\ \gamma_{yz} \end{Bmatrix} = \begin{Bmatrix} \frac{\partial w}{\partial x} + \theta_x \\ \frac{\partial w}{\partial y} + \theta_y \end{Bmatrix} \tag{3.2}$$

$$\begin{Bmatrix} \varepsilon_{xx} \\ \varepsilon_{yy} \\ \gamma_{xy} \end{Bmatrix} = -z \begin{Bmatrix} \frac{\partial \theta_x}{\partial x} \\ \frac{\partial \theta_y}{\partial y} \\ \frac{\partial \theta_x}{\partial y} + \frac{\partial \theta_y}{\partial x} \end{Bmatrix} \tag{3.3}$$

The corresponding in-plane stresses, $\sigma_{xx}, \sigma_{yy}, \tau_{xy}$ and transverse shear stresses, τ_{xz}, τ_{yz} are as given below:

$$\begin{Bmatrix} \sigma_{xx} \\ \sigma_{yy} \\ \tau_{xy} \end{Bmatrix} = -z \frac{E}{1-\nu^2} \begin{bmatrix} 1 & \nu & 0 \\ \nu & 1 & 0 \\ 0 & 0 & \frac{1-\nu}{2} \end{bmatrix} \begin{Bmatrix} \frac{\partial \theta_x}{\partial x} \\ \frac{\partial \theta_y}{\partial y} \\ \frac{\partial \theta_x}{\partial y} + \frac{\partial \theta_x}{\partial x} \end{Bmatrix} \tag{3.4}$$

$$\begin{Bmatrix} \tau_{xz} \\ \tau_{yz} \end{Bmatrix} = \frac{E}{2(1+\nu)} \begin{Bmatrix} \frac{\partial w}{\partial x} + \theta_x \\ \frac{\partial w}{\partial y} + \theta_y \end{Bmatrix} \tag{3.5}$$

Where: E and v are the plate Young's modulus and Poisson's ratio, respectively.

A very important phase of a finite element solution is the calculation of the finite element matrices. Finite element matrices can be calculated using generalized coordinates and isoparametric finite element formulation. However, applying isoparameteric finite element

formulation is found to be more effective. Because, using generalized coordinate involves inverse matrix operation; which becomes tedious, as matrix size is significantly large. However, such operation is not involved in isoparameteric finite element formulation [3].

The basic procedure in the isoparametric finite element formulation is to express the element coordinates and element displacements in the form of interpolations using the natural coordinate system of the element. Relating the Cartesian coordinate and natural coordinate is aimed to relate the strains and stresses in the Cartesian coordinate and natural coordinate. The derivative relationships for these coordinates in 3D are as follow [6]:

$$\begin{bmatrix} \frac{\partial}{\partial r} \\ \frac{\partial}{\partial s} \\ \frac{\partial}{\partial t} \end{bmatrix} = \begin{bmatrix} \frac{\partial x}{\partial r} & \frac{\partial y}{\partial r} & \frac{\partial z}{\partial r} \\ \frac{\partial x}{\partial s} & \frac{\partial y}{\partial s} & \frac{\partial z}{\partial s} \\ \frac{\partial x}{\partial t} & \frac{\partial y}{\partial t} & \frac{\partial z}{\partial t} \end{bmatrix} \begin{bmatrix} \frac{\partial}{\partial x} \\ \frac{\partial}{\partial y} \\ \frac{\partial}{\partial z} \end{bmatrix} \tag{3.6}$$

In matrix notation, $\frac{\partial}{\partial r} = J \frac{\partial}{\partial x}$ (3.7)

Where: J is the Jacobian operator that relates the natural coordinate derivatives to the Cartesian coordinate derivative; and r, s and t are the natural coordinates.

The Jacobian operator for the rectangular element shown in Figure 3.2 can be estimated from the element local and natural coordinate relationships as follow:

$$\left.\begin{aligned} x &= ar \\ y &= bs \end{aligned}\right\} \tag{3.8}$$

$$J = \begin{bmatrix} \frac{\partial x}{\partial r} & \frac{\partial y}{\partial r} \\ \frac{\partial x}{\partial s} & \frac{\partial y}{\partial s} \end{bmatrix} = \begin{bmatrix} a & 0 \\ 0 & b \end{bmatrix} \tag{3.9}$$

Where: a and b are half of the length of the element in x and y, respectively (see Figure 3.2).

To estimate strains and element stiffness matrix in the global coordinate it is necessary to use the following relationship from the respective 2D of Equation (3.6):

$$\frac{\partial}{\partial x} = J^{-1}\frac{\partial}{\partial r} \tag{3.10}$$

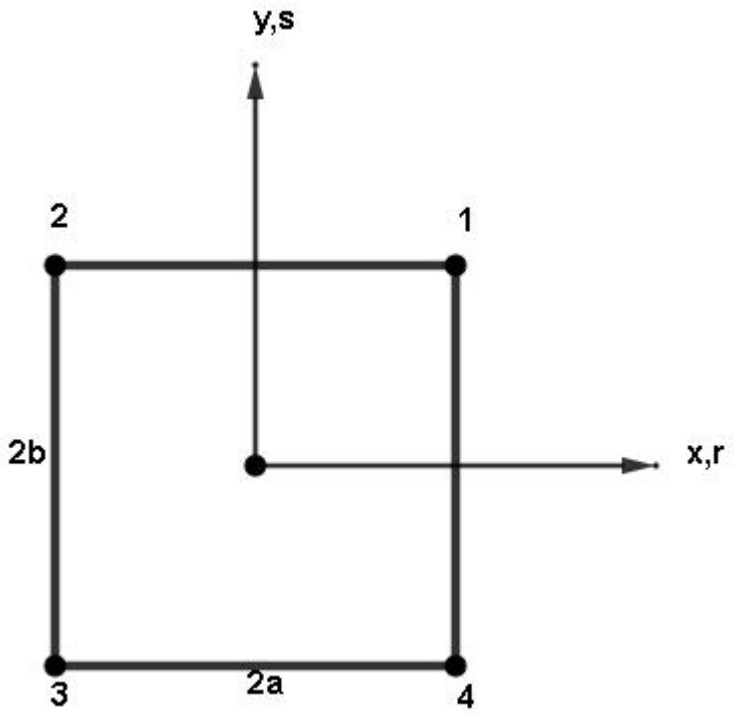

Figure 3.2: Notations for local node numbering, local coordinate, natural coordinate, and dimensions of rectangular plate finite element.

The interpolation functions used in the isoparameteric finite element formulation have a fundamental attractive property, which is, interpolation function in natural coordinate has a value of unity at its node and zero on other nodes. Accordingly, the interpolation functions of a rectangular element (refer Figure 3.2) for each node is as given below:

$$\left.\begin{aligned} h_1 &= \frac{1}{4}(1+r)(1+s) \\ h_2 &= \frac{1}{4}(1-r)(1+s) \\ h_3 &= \frac{1}{4}(1-r)(1-s) \\ h_4 &= \frac{1}{4}(1+r)(1-s) \end{aligned}\right\} \tag{3.11}$$

Using the interpolation functions given in Equation (3.11), the section rotations, and displacement within the element are defined as:

$$w = \sum_{i=1}^{q} h_i w_i; \quad _x = \sum_{i=1}^{q} h_i \bar{}_{yi}; \quad _y = \sum_{i=1}^{q} h_i \bar{}_{xi} \tag{3.12}$$

Where: w_i , $\bar{}_{yi}$ and $\bar{}_{xi}$ are the nodal point values of the displacement and section rotations respectively and q is the number of nodes of the element in Figure 3.2.

Applying pure displacement-based plate element formulation that is using the interpolation functions in Equation (3.11) results in shear locking. Indeed, the least order of interpolation that should be used is a cubic interpolation, which results in a 16-node of quadrilateral element and a 10-node of triangular element [3].

To arrive at efficient and reliable plate bending elements, the pure displacement-based formulation must be extended; and a successful approach is, to use a mixed interpolation. In this approach, the transverse displacement and section rotations are evaluated using the interpolation given in Equation (3.11). However, transverse shear strains are evaluated using independent interpolation function. These elements are referred to as the MITCn elements, where n refers to the number of element nodes and n = 4, 9, 16 for the quadrilateral and n = 7, 12 for the triangular elements (here MITC stands for mixed interpolation of tensorial components) [2, 3].

Considering the MITC4, which is used in this research, the transverse shear strains for rectangular element which are mainly dependent on Equations (3.2) and (3.12) are given below [2, 3]:

$$¥_{xz} = \sqrt{\frac{[(C_x + rB_x)^2 + (C_y + rB_y)^2]}{8\det J}} \left\{ \begin{array}{l} (1+s)\left[\frac{w_1 + w_2}{2} + \frac{x_1 - x_2}{4}(\bar{}_{y1} + \bar{}_{y2}) + (\frac{y_1 - y_2}{4})(\bar{}_{x1} + \bar{}_{x2}) \right] \\ +(1-s)\left[\frac{w_4 - w_3}{2} + \frac{x_4 - x_3}{4}(\bar{}_{y4} + \bar{}_{y3}) + (\frac{y_4 - y_3}{4})(\bar{}_{x4} + \bar{}_{x3}) \right] \end{array} \right\} \quad (3.13)$$

$$¥_{yz} = \sqrt{\frac{[(A_x + sB_x)^2 + (A_y + sB_y)^2]}{8\det J}} \left\{ \begin{array}{l} (1+r)\left[\frac{w_1 - w_4}{2} + \frac{x_1 - x_4}{4}(\bar{}_{y1} + \bar{}_{y4}) + (\frac{y_1 - y_4}{4})(\bar{}_{x1} + \bar{}_{x4}) \right] \\ +(1-r)\left[\frac{w_2 - w_3}{2} + \frac{x_2 - x_3}{4}(\bar{}_{y2} + \bar{}_{y3}) + (\frac{y_2 - y_3}{4})(\bar{}_{x2} + \bar{}_{x3}) \right] \end{array} \right\} \quad (3.14)$$

Where: x_1, x_2, x_3, x_4 and y_1, y_2, y_3, y_4 are the nodal x and y coordinates for MITC4 element per Figure 3.2.

$$\left. \begin{array}{l} \det J = \det \begin{bmatrix} \frac{\partial x}{\partial r} & \frac{\partial y}{\partial r} \\ \frac{\partial x}{\partial s} & \frac{\partial y}{\partial s} \end{bmatrix}; \\ \\ A_x = x_1 - x_2 - x_3 + x_4; \\ B_x = x_1 - x_2 + x_3 - x_4; \\ C_x = x_1 + x_2 - x_3 - x_4; \\ A_y = y_1 - y_2 - y_3 + y_4; \\ B_y = y_1 - y_2 + y_3 - y_4; \\ C_y = y_1 + y_2 - y_3 - y_4 \end{array} \right\} \quad (3.15)$$

Applying Equations (3.13) and (3.14) to the element on Figure 3.2 the transverse shear strains are as given below:

$$¥_{xz} = \begin{bmatrix} \frac{1+s}{4a} & \frac{-1-s}{4a} & \frac{-1+s}{4a} & \frac{1-s}{4a} \end{bmatrix} \begin{Bmatrix} w_1 \\ w_2 \\ w_3 \\ w_4 \end{Bmatrix} + \begin{bmatrix} \frac{1+s}{4} & \frac{1+s}{4} & \frac{1-s}{4} & \frac{1-s}{4} \end{bmatrix} \begin{Bmatrix} \bar{}_{y1} \\ \bar{}_{y2} \\ \bar{}_{y3} \\ \bar{}_{y4} \end{Bmatrix} \quad (3.16)$$

$$¥_{yz} = \begin{bmatrix} \frac{1+r}{4b} & \frac{1-r}{4b} & \frac{-1+r}{4b} & \frac{-1-r}{4b} \end{bmatrix} \begin{Bmatrix} w_1 \\ w_2 \\ w_3 \\ w_4 \end{Bmatrix} + \begin{bmatrix} \frac{1+r}{4} & \frac{1-r}{4} & \frac{1-r}{4} & \frac{1+r}{4} \end{bmatrix} \begin{Bmatrix} \_ \\ x1 \\ \_ \\ x2 \\ \_ \\ x3 \\ \_ \\ x4 \end{Bmatrix} \tag{3.17}$$

Considering loaded plate-soil system, the potential energy of a single element excluding boundary condition is [29]:

$$\prod = \prod_p + \prod_s + \prod_l \tag{3.18}$$

Where: $\prod_p, \prod_s, \prod_l$ are the energy due to plate, soil, and loading, respectively.

Considering only the plate, the strain energy due its deformation is as follows:

$$\prod_P = \frac{1}{2}\int_A \int_{-h/2}^{h/2} \{£_{xx} \quad £_{yy} \quad ¥_{xy}\} \begin{Bmatrix} ±_{xx} \\ ±_{yy} \\ 2_{xy} \end{Bmatrix} dzdA + k_f \frac{1}{2}\int_A \int_{-h/2}^{h/2} \{¥_{xz} \quad ¥_{yz}\} \begin{Bmatrix} 2_{xz} \\ 2_{yz} \end{Bmatrix} dzdA \tag{3.19}$$

Where: k_f is a factor to account for the actual non-uniformity of transverse shear stresses; usually its value is 5/6 and h is thickness of the plate.

Inserting the respective value of Equations (3.3), (3.4), (3.5), (3.16), and (3.17) into Equation (3.19) and then integrating only with respect to z gives the following equation:

$$\prod_p = \frac{1}{2}\int_A k^T C_b k dA + \frac{1}{2}\int_A ¥^T C_s ¥ dA \tag{3.20}$$

Where: $¥ = \begin{Bmatrix} ¥_{xz} \\ ¥_{yz} \end{Bmatrix}$ (3.21)

and $¥_{xz}$ and $¥_{yz}$ are given in Equations (3.16) and (3.17), respectively.

$$k = \begin{Bmatrix} \frac{\partial \quad _x}{\partial x} \\ \frac{\partial \quad _y}{\partial y} \\ \frac{\partial \quad _x}{\partial y} + \frac{\partial \quad _y}{\partial x} \end{Bmatrix} \tag{3.22}$$

$$C_b = \frac{Eh^3}{12(1-v^2)} \begin{bmatrix} 1 & v & 0 \\ v & 1 & 0 \\ 0 & 0 & \frac{1-v}{2} \end{bmatrix}; C_s = \frac{Ehk_f}{2(1+v)} \begin{bmatrix} 1 & 0 \\ 0 & 1 \end{bmatrix} \tag{3.23}$$

After replacing element section rotations as given in Equation (3.12) into Equation (3.22) and then applying Equation (3.10), the following result is obtained:

$$k = \quad _k \tilde{u} \tag{3.24}$$

Where:

$$\tilde{u}^T = \begin{Bmatrix} - & - & - & - & - & - & - & - \\ _{y1} & _{x1} & _{y2} & _{x2} & _{y3} & _{x3} & _{y4} & _{x4} \end{Bmatrix} \tag{3.25}$$

$$_k = [C_1 \quad C_2] \tag{3.26}$$

and,

$$C_1 = \begin{bmatrix} \frac{(1+s)}{4a} & 0 & \frac{-(1+s)}{4a} & 0 \\ 0 & \frac{(1+r)}{4b} & 0 & \frac{(1-r)}{4b} \\ \frac{(1+r)}{4b} & \frac{(1+s)}{4a} & \frac{(1-r)}{4b} & \frac{-(1+s)}{4a} \end{bmatrix} \tag{3.27}$$

$$C_2 = \begin{bmatrix} \frac{-(1-s)}{4a} & 0 & \frac{(1-s)}{4a} & 0 \\ 0 & \frac{-(1-r)}{4b} & 0 & \frac{-(1+r)}{4b} \\ \frac{-(1-r)}{4b} & \frac{-(1-s)}{4a} & \frac{-(1+r)}{4b} & \frac{(1-s)}{4a} \end{bmatrix} \tag{3.28}$$

To evaluate element stiffness matrix, the first variation theorem is applied; and this is equal to minimization of the total potential energy of the system [12]:

$$\frac{\partial \prod}{\partial u_i} = 0 \tag{3.29}$$

Where: u_i is a vector containing the degree of freedom of a single finite element; in this research, it contains 12 elements as per Figure 3.2 and Mindlin plate theory.

Focusing only on the plate finite element stiffness matrix, its finite element stiffness equation due to bending, which is obtained after applying Equation (3.29) is:

$$k_b = \int_{-1}^{1}\int_{-1}^{1} {}_k{}^T C_b \; {}_k \det J dr ds \tag{3.30}$$

Where: k_b is plate finite element stiffness equation due to bending; which gives 12x12 matrix after applying numerical integration.

Equation (3.30) is further simplified as follow:

$$k_b = \frac{Eh^3 ab}{12(1-v^2)} \int_{-1}^{1}\int_{-1}^{1} {}_k{}^T C_b{}^m \; {}_k dr ds \tag{3.31}$$

Where:

$$C_b^{\,m} = \begin{bmatrix} 1 & \nu & 0 \\ \nu & 1 & 0 \\ 0 & 0 & \dfrac{1-\nu}{2} \end{bmatrix} \tag{3.32}$$

After applying numerical integration on Equation (3.31), it gives 12x12 symmetric matrix. A very important numerical integration procedure in which both the positions of the sampling points and the weights have been optimized to increase accuracy is the Gauss quadrature method. Gauss quadrature method requires n unequally spaced sampling points to integrate exactly a polynomial of order at most (2n - 1). For 2D integration, the numerical integration is given below [3]:

$$\int_{-1}^{+1}\int_{-1}^{+1} F(r,s)\,dr\,ds = \sum_{i,j} \sim_i \sim_j F(r_i, s_j) \tag{3.33}$$

Where: r_i and s_j are the sampling points in r and s directions, respectively. $\sim_i$ and $\sim_j$ are the weight integrations in r and s directions, respectively.

In this research fully integrated finite element matrix (i.e. analytically integrated matrix) is obtained by applying the sampling points given in Figure 3.3; and the weight integrations are unity.

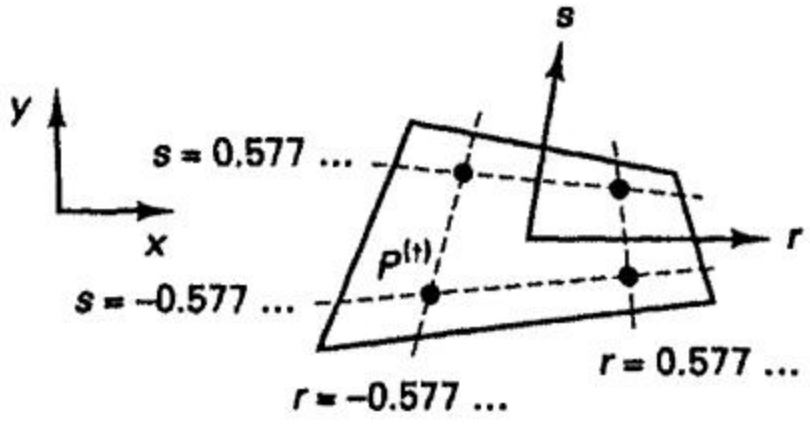

Figure 3. 3: Gauss quadrature sampling points for full integration of four-node element [3].

After performing numerical integration on Equation (3.31), which needs using Equation (3.33) and sampling points given on Figure 3.3 and its respective weight integrations; the plate bending element stiffness matrix is:

$$k_b = \frac{Eh^3 ab}{12(1-v^2)}\begin{bmatrix} k_{b1} & k_{b2} \\ & k_{b3} \end{bmatrix} \tag{3.34}$$

Where: the values of k_{b1}, k_{b2} and k_{b3} are 6x6 matrix as given below:

$$k_{b1} = \begin{bmatrix} 0 & 0 & 0 & 0 & 0 & 0 \\ \frac{5.332}{16b^2} + \frac{5.332(1-v)}{32a^2} & \frac{1+v}{8ab} & 0 & \frac{2.668}{16b^2} + \frac{5.332(v-1)}{32a^2} & \frac{-3v+1}{8ab} & \\ & \frac{5.332}{16a^2} + \frac{5.332(1-v)}{32b^2} & 0 & \frac{3v-1}{8ab} & \frac{2.668(1-v)}{32b^2} - \frac{5.332}{16a^2} & \\ & & 0 & 0 & 0 & \\ & & & \frac{5.332}{16b^2} + \frac{5.332(1-v)}{32a^2} & \frac{-(1+v)}{8ab} & \\ & \textit{symmetric} & & & \frac{5.332}{16a^2} + \frac{5.332(1-v)}{32b^2} & \end{bmatrix}$$

$$k_{b2}=\begin{bmatrix}
0 & 0 & 0 & 0 & 0 & 0\\
0 & \frac{-2.668}{16b^2}+\frac{2.668(\nu-1)}{32a^2} & \frac{-(1+\nu)}{8ab} & 0 & \frac{-5.332}{16b^2}+\frac{2.668(1-\nu)}{32a^2} & \frac{3\nu-1}{8ab}\\
0 & \frac{-(\nu+1)}{8ab} & \frac{2.668(\nu-1)}{32b^2}-\frac{2.668}{16a^2} & 0 & \frac{-3\nu+1}{8ab} & \frac{2.668}{16a^2}+\frac{5.332(\nu-1)}{32b^2}\\
0 & 0 & 0 & 0 & 0 & 0\\
0 & \frac{-5.332}{16b^2}+\frac{2.668(1-\nu)}{32a^2} & \frac{-3\nu+1}{8ab} & 0 & \frac{-2.668}{16b^2}+\frac{2.668(\nu-1)}{32a^2} & \frac{1+\nu}{8ab}\\
0 & \frac{3\nu-1}{8ab} & \frac{2.668}{16a^2}+\frac{5.332(\nu-1)}{32b^2} & 0 & \frac{\nu+1}{8ab} & \frac{-2.668}{16a^2}+\frac{2.668(\nu-1)}{32b^2}
\end{bmatrix}$$

$$k_{b3}=\begin{bmatrix}
0 & 0 & 0 & 0 & 0 & 0\\
 & \frac{5.332}{16b^2}+\frac{5.332(1-\nu)}{32a^2} & \frac{1+\nu}{8ab} & 0 & \frac{2.668}{16b^2}+\frac{5.332(\nu-1)}{32a^2} & \frac{-3\nu+1}{8ab}\\
 & & \frac{5.332(1-\nu)}{32b^2}+\frac{5.332}{16a^2} & 0 & \frac{3\nu-1}{8ab} & \frac{-5.332}{16a^2}+\frac{2.668(1-\nu)}{32b^2}\\
 & & & 0 & 0 & 0\\
 & & & & \frac{5.332}{16b^2}+\frac{5.332(1-\nu)}{32a^2} & \frac{-(1+\nu)}{8ab}\\
 & \textit{symmetric} & & & & \frac{5.332}{16a^2}+\frac{5.332(1-\nu)}{32b^2}
\end{bmatrix}$$

To fully utilize the Mindlin's plate theory, the stiffness contribution from transverse shear deformation should be evaluated in addition to bending stiffness of the plate. In order to meet this, the second part of Equation (3.20) shall be used. The shear strains in Equation (3.20) are obtained from Equations (3.16) and (3.17). Finally, after applying Equation (3.29), the quation for plate element stiffness in response to shear deformation is found as below:

$$k_{sh}=\frac{Ehk_f ab}{2(1+\nu)}\int_{-1}^{+1}\int_{-1}^{+1} {}_{¥}{}^{T}C_s{}^{m}\ {}_{¥}\,drds \tag{3.35}$$

Where: k_{sh} is plate element shear stiffness equation which results 12x12 matrix.

$$C_s{}^{m}=\begin{bmatrix}1 & 0\\ 0 & 1\end{bmatrix} \tag{3.36}$$

$$_{¥} = \begin{bmatrix} C_{¥1} & C_{¥2} \end{bmatrix} \tag{3.37}$$

and;

$$C_{¥1} = \begin{bmatrix} \frac{(1+s)}{4a} & 0 & \frac{(1+s)}{4} & \frac{-(1+s)}{4a} & 0 & \frac{(1+s)}{4} \\ \frac{(1+r)}{4b} & \frac{(1+r)}{4} & 0 & \frac{(1-r)}{4b} & \frac{(1-r)}{4} & 0 \end{bmatrix} \tag{3.38}$$

$$C_{¥2} = \begin{bmatrix} \frac{-(1-s)}{4a} & 0 & \frac{(1-s)}{4} & \frac{(1-s)}{4a} & 0 & \frac{(1-s)}{4} \\ \frac{-(1-r)}{4b} & \frac{(1-r)}{4} & 0 & \frac{-(1+r)}{4b} & \frac{(1+r)}{4} & 0 \end{bmatrix} \tag{3.39}$$

After applying the numerical integration given by Equation (3.33) and the sampling points given in Figure 3.3 and its respective weight integration, the plate element given in Figure 3.2 has the following shear stiffness:

$$k_{sh} = \frac{Ehk_f ab}{2(1+v)} \begin{bmatrix} k_{sh1} & k_{sh2} \\ & k_{sh3} \end{bmatrix} \tag{3.40}$$

Where: the values of k_{sh1}, k_{sh2} and k_{sh3} are 6x6 matrix as given below:

$$k_{sh1} = \begin{bmatrix} \frac{5.332}{16a^2} + \frac{5.332}{16b^2} & \frac{5.332}{16b} & \frac{5.332}{16a} & \frac{-5.332}{16a^2} + \frac{2.668}{16b^2} & \frac{2.668}{16b} & \frac{5.332}{16a} \\ & \frac{5.332}{16} & 0 & \frac{2.668}{16b} & \frac{2.668}{16} & 0 \\ & & \frac{5.332}{16} & \frac{-5.332}{16a} & 0 & \frac{5.332}{16} \\ & & & \frac{5.332}{16a^2} + \frac{5.332}{16b^2} & \frac{5.332}{16b} & \frac{5.332}{16a} \\ & & & & \frac{5.332}{16} & 0 \\ \textit{symmetric} & & & & & \frac{5.332}{16} \end{bmatrix}$$

$$k_{sh2}=\begin{bmatrix}
\frac{-2.668}{16a^2}-\frac{2.668}{16b^2} & \frac{2.668}{16b} & \frac{2.668}{16a} & \frac{2.668}{16a^2}-\frac{5.332}{16b^2} & \frac{5.332}{16b} & \frac{2.668}{16a} \\
\frac{-2.668}{16b} & \frac{2.668}{16} & 0 & \frac{-5.332}{16b} & \frac{5.332}{16} & 0 \\
\frac{-2.668}{16a} & 0 & \frac{2.668}{16} & \frac{2.668}{16a} & 0 & \frac{2.668}{16} \\
\frac{2.668}{16a^2}-\frac{5.332}{16b^2} & \frac{5.332}{16b} & \frac{-2.668}{16a} & \frac{-2.668}{16a^2}-\frac{2.668}{16b^2} & \frac{2.668}{16b} & \frac{-2.668}{16a} \\
\frac{-5.332}{16b} & \frac{5.332}{16} & 0 & \frac{-2.668}{16b} & \frac{2.668}{16} & 0 \\
\frac{-2.668}{16a} & 0 & \frac{2.668}{16} & \frac{2.668}{16a} & 0 & \frac{2.668}{16}
\end{bmatrix}$$

$$k_{sh3}=\begin{bmatrix}
\frac{5.332}{16a^2}+\frac{5.332}{16b^2} & \frac{-5.332}{16b} & \frac{-5.332}{16a} & \frac{-5.332}{16a^2}+\frac{2.668}{16b^2} & \frac{-2.668}{16b} & \frac{-5.332}{16a} \\
 & \frac{5.332}{16} & 0 & \frac{-2.668}{16b} & \frac{2.668}{16} & 0 \\
 & & \frac{5.332}{16} & \frac{5.332}{16a} & 0 & \frac{5.332}{16} \\
 & & & \frac{5.332}{16a^2}+\frac{5.332}{16b^2} & \frac{-5.332}{16b} & \frac{5.332}{16a} \\
 & & & & \frac{5.332}{16} & 0 \\
\textit{symmetric} & & & & & \frac{5.332}{16}
\end{bmatrix}$$

3.3. Development of Soil Element Stiffness Matrix

To evaluate soil element stiffness matrix, choosing a soil model is a critical step. It is understood that advanced constitutive soil models, which have good accuracy are available. However, applying such models is not quite easy. Therefore, the intention of this research is to use a model

that is found below the threshold of strong form of soil models, and then taking possible adjustments by comparing with better finite element based software.

In this research, the soil behavior is captured by using the two-parameter mechanical model of Pasternak. The major assumptions of this model are: a) the model parameters k_p and G_p are fully elastic, and b) only transverse stresses exist.

As mentioned in the previous Section 3.2, the approach used in the finite element formulation is variational/energy method. For this purpose, by considering Pasternak model shown in Figure 3.4, the shear stress of assumed isotropic shear layer is given by [13, 24]:

$$²_{xz} = G_p ¥_{xz}; ²_{yz} = G_p ¥_{yz} \tag{3.41}$$

Where: $²_{xz}$ and $²_{yz}$ are shear stresses on Pasternak shear layer, G_p is shear modulii of Pasternak shear layer, and $¥_{xz}$ and $¥_{yz}$ are shear strains in the Pasternak shear layer.

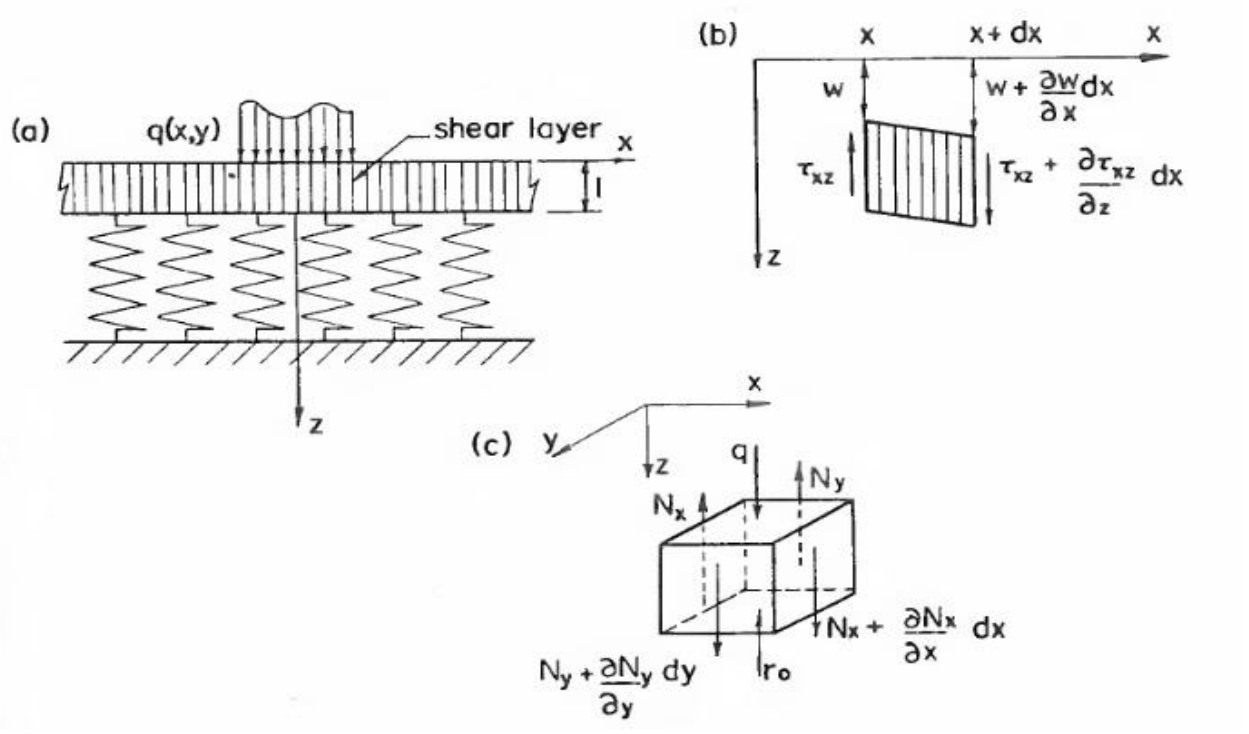

Figure 3. 4: Pasternak model. a) The basic model b) Shear stresses acting on the shear layer c) Forces acting on the shear layer [24].

The shear parameter of Pasternak model, G_p, is a function of the soil stratum thickness; and has the same unit as shear modulii of a plate, and the plate shear modulii is a function the plate thickness as it is shown in the second part of Equation (3.20), which is indicated by C_s. The equation of C_s is given by Equation (3.23).

Focusing only on the strain energy of the soil stratum, the strain energy of the spring and shear parameter contribution is [28, 29]:

$$\prod_s = \frac{1}{2}\int_A k_p w^2 dA + \frac{1}{2}\int_A \begin{bmatrix} ¥_{xz} & ¥_{yz} \end{bmatrix} G_p \begin{bmatrix} ¥_{xz} \\ ¥_{yz} \end{bmatrix} dA \tag{3.42}$$

Where: $w, ¥_{xz}$ and $¥_{yz}$ are as given by Equations (3.12), (3.16), and (3.17) respectively, and k_p is Pasternak model's vertical spring reaction modulus.

After applying the first variational theorem as given by Equation (3.29), the soil element stiffness equation (spring and shear parameter contribution) is:

$$k_s = k_p \int_A N^T N dA + G_p \left(\int_A ¥'_{xz}{}^T ¥'_{xz} dA + \int_A ¥'_{yz}{}^T ¥'_{yz} dA \right) \tag{3.43}$$

Where:

$$N = \begin{bmatrix} h_1 & h_2 & h_3 & h_4 \end{bmatrix} \tag{3.44}$$

and the value of h_1, h_2, h_3 and h_4 are the interpolation functions as given in Equation (3.11).

$$¥'_{xz} = \begin{bmatrix} \frac{1+s}{4a} & 0 & \frac{1+s}{4} & \frac{-(1+s)}{4a} & 0 & \frac{1+s}{4} & \frac{-(1-s)}{4a} & 0 & \frac{1-s}{4} & \frac{1-s}{4a} & 0 & \frac{1-s}{4} \end{bmatrix} \tag{3.45}$$

$$¥'_{yz} = \begin{bmatrix} \frac{1+r}{4b} & \frac{1+r}{4} & 0 & \frac{1-r}{4b} & \frac{1-r}{4} & 0 & \frac{-(1-r)}{4b} & \frac{1-r}{4} & 0 & \frac{-(1+r)}{4b} & \frac{1+r}{4} & 0 \end{bmatrix} \tag{3.46}$$

The first and second part of Equation (3.43) results in soil element matrices from the spring and shear parameter contributions, respectively. The soil element stiffness equation obtained from the spring parameter deformation can be written as:

$$k_{sv} = abk_p \int_{-1}^{+1}\int_{-1}^{+1} N^T N drds \tag{3.47}$$

After applying the numerical integration given by Equation (3.33) and the sampling points given in Figure 3.3 and its respective weight integration, the soil element that has equal finite element considerations as given in Figure 3.2 has the following vertical stiffness matrix:

$$k_{sv} = abk_p \begin{bmatrix} \frac{7.108}{16} & \frac{3.556}{16} & \frac{1.78}{16} & \frac{3.556}{16} \\ \frac{3.556}{16} & \frac{7.108}{16} & \frac{3.556}{16} & \frac{1.78}{16} \\ \frac{1.78}{16} & \frac{3.556}{16} & \frac{7.108}{16} & \frac{3.556}{16} \\ \frac{3.556}{16} & \frac{1.78}{16} & \frac{3.556}{16} & \frac{7.108}{16} \end{bmatrix} \tag{3.48}$$

As per the notation given in Figure 3.2, the respective nodal displacement vector attached with Equation (3.48) is:

$$w_i = \begin{bmatrix} w_1 & w_2 & w_3 & w_4 \end{bmatrix} \tag{3.49}$$

The soil element stiffness equation in response to the shear parameter deformation, which is the second part of Equation (3.43), is simplified as follows:

$$k_{ss} = G_p ab \left(\int_{-1}^{+1}\int_{-1}^{+1} ¥_{xz}^{\ T} ¥_{xz} drds + \int_{-1}^{+1}\int_{-1}^{+1} ¥_{yz}^{\ T} ¥_{yz} drds \right) \tag{3.50}$$

After applying the numerical integration given by Equation (3.33) and the sampling points given in Figure 3.3 and its respective weight integration, the soil element that has equal finite element considerations as given in Figure 3.2 has the following 12x12 shear stiffness matrix :

$$k_{ss} = \frac{G_p ab}{16} \begin{bmatrix} k_{ss1} & k_{ss2} \\ & k_{ss3} \end{bmatrix} \tag{3.51}$$

Where:

$$k_{ss1} = \begin{bmatrix} \frac{5.332}{a^2}+\frac{5.332}{b^2} & \frac{5.332}{b} & \frac{5.332}{a} & \frac{2.668}{b^2}-\frac{5.332}{a^2} & \frac{2.668}{b} & \frac{5.332}{a} \\ & 5.332 & 0 & \frac{2.668}{b} & 2.668 & 0 \\ & & 5.332 & \frac{-5.332}{a} & 0 & 5.332 \\ & & & \frac{5.332}{a^2}+\frac{5.332}{b^2} & \frac{5.332}{b} & \frac{5.332}{a} \\ & & & & 5.332 & 0 \\ \textit{symmetric} & & & & & 5.332 \end{bmatrix}$$

$$k_{ss2} = \begin{bmatrix} \frac{-2.668}{a^2}-\frac{2.668}{b^2} & \frac{2.668}{b} & \frac{2.668}{a} & \frac{-5.332}{b^2}+\frac{2.668}{a^2} & \frac{5.332}{b} & \frac{2.668}{a} \\ \frac{-2.668}{b} & 2.668 & 0 & \frac{-5.332}{b} & 5.332 & 0 \\ \frac{-2.668}{a} & 0 & 2.668 & \frac{2.668}{a} & 0 & 2.668 \\ \frac{-5.332}{b^2}+\frac{2.668}{a^2} & \frac{5.332}{b} & \frac{-2.668}{a} & \frac{-2.668}{a^2}-\frac{2.668}{b^2} & \frac{2.668}{b} & \frac{-2.668}{a} \\ \frac{5.332}{b} & 5.332 & 0 & \frac{2.668}{b} & 2.668 & 0 \\ \frac{-2.668}{a} & 0 & 2.668 & \frac{2.668}{a} & 0 & 2.668 \end{bmatrix}$$

$$k_{ss3}=\begin{bmatrix} \frac{5.332}{a^2}+\frac{5.332}{b^2} & \frac{-5.332}{b} & \frac{-5.332}{a} & \frac{-5.332}{b^2}+\frac{2.668}{a^2} & \frac{-2.668}{b} & \frac{-5.332}{a} \\ & 5.332 & 0 & \frac{-2.668}{b} & 2.668 & 0 \\ & & 5.332 & \frac{5.332}{a} & 0 & 5.332 \\ & & & \frac{5.332}{a^2}+\frac{5.332}{b^2} & \frac{-5.332}{b} & \frac{5.332}{a} \\ & & & & 5.332 & 0 \\ \textit{symmetric} & & & & & 5.332 \end{bmatrix}$$

3.4. Determination of the Plate-Soil Element Stiffness Matrix

As discussed in the above Section 3.2 and 3.3, the element stiffness matrix of the plate and the soil are evaluated independently. However, the equilibrium of the loaded plate-soil system is formulated by minimization of the total potential energy, which is given by Equation (3.18). Minimization of this equation, that is, applying Equation (3.29), results in the following equilibrium equation of an element plate-soil system. The finite element notations are as defined in Figure 3.2.

$$[k_{ps}]\{u\}=\{f_l\} \tag{3.52}$$

Where: $[k_{ps}]$ is the 12x12 element stiffness matrix of plate-soil system. f_l is nodal load vector for single element of plate-soil system given by:

$$f_l^T=\left\{F_1 \quad m_{x1} \quad m_{y1} \quad F_2 \quad m_{x2} \quad m_{y2} \quad F_3 \quad m_{x3} \quad m_{y3} \quad F_4 \quad m_{x4} \quad m_{y4}\right\} \tag{3.53}$$

and F_i, m_{xi} and m_{yi} are the applied nodal force, moment about x and moment about y for node i, respectively. The displacement-rotation vector is given by:

$$u^T=\left\{w_1 \quad \__{x1} \quad \__{y1} \quad w_2 \quad \__{x2} \quad \__{y2} \quad w_3 \quad \__{x3} \quad \__{y3} \quad w_4 \quad \__{x4} \quad \__{y4}\right\} \tag{3.54}$$

The element stiffness matrix of plate-soil system is the summation of the element stiffness of matrices given by Equations (3.34), (3.40), (3.48), and (3.51).

$$[k_{ps}] = [k_b] + [k_{sh}] + [k_{sv}] + [k_{ss}] \tag{3.55}$$

The Equations (3.48) and (3.51) involve the Pasternak's model parameters, which are, spring and shear parameters, respectively. These parameters are evaluated from the recommendation of Worku (2014) for Kerr-equivalent Pasternak model. In this recommendation, the Pasternak model is adjusted to the three-parameter Kerr model so that equivalent results can be obtained. To achieve this, the following two conditions have to be satisfied [33]: a) shear parameter of Kerr model is equal to the shear parameter of Pasternak model (G_K=G_P), and b) the surface deflection of Kerr model and Pasternak model are equal.

After applying the above two criteria, the Pasternak model parameters used in this research are given by the following equations [33], where the adjustment factor in the original work is excluded. Nevertheless, this does not mean applying an adjustment factor is totally excluded, see Chapter 5 for detail discussion of the adjustment factor.

$$k_p = \left(\frac{(0.4\nu_s + 0.67)E_s}{H} \right); G_p = (1.36\nu_s + 2.28)G_s H \tag{3.56}$$

Where: H is depth of homogenous soil stratum and ν_s, E_s and G_s are the soil Poisson's ratio, Young's modulus and shear modulus, respectively.

3.5. Development of Boundary Conditions

Assembling the element stiffness matrix and nodal loading of the plate-soil system results in the same form as Equation (3.52). Attempting to directly solve such an equation does not give unique solution, because the global stiffness matrix becomes singular. To obtain a solution, boundary conditions have to be applied, that implies, the stiffness matrix of the elements at the plate edges have to be modified.

Modeling the soil stratum by Pasternak model leads to a dish shaped deformation, continuing to beyond the plate edges. Therefore, this section is aimed at determining equivalent stiffness

parameters of the deformed soil outside the plate. This is achieved by computing the equivalent forces due to the surrounding soil as function of the deformations on the boundary of the plate.

The general differential equation of loaded bending plate resting on Pasternak soil model is given by:

$$D\nabla^2\nabla^2 w(x,y) + k_p w(x,y) - G_p\nabla^2 w(x,y) = p(x,y) \tag{3.57}$$

Where: D and p(x, y) are plate bending rigidity and applied load respectively.

For the region outside of the plate, which is the surrounding soil, Equation (3.57) is reduced to the below equation:

$$k_p w(x,y) - G_p\nabla^2 w(x,y) = 0 \tag{3.58}$$

Now, the major task of evaluating boundary conditions lies on solving deflection of the surrounding soil from Equation (3.58). The major assumption considered to solve the homogenous differential Equation of (3.58) is, displacement of the surrounding soil can be expressed by exponentially decaying function. The discretization concept of the finite element is helpful in defining the solution regionally rather than finding a single function that satisfies the whole surrounding soil surface displacement. A similar assumption was attempted by Vlasov and Leont'ev to solve the surrounding soil surface displacement of symmetrically loaded plate [30].

After dividing the surrounding soil into regions as shown in Figure 3.5, soil surface displacement functions of each region that satisfy Equation (3.58) are selected. The functions have to satisfy the following criteria: a) the function has to be decaying function, b) the function should satisfy the plate edge nodal displacements, and c) the functions have to give continuous displacement at the region's boundary.

Considering the right hand side (RH) middle region of Figure 3.5, and then taking small strip in x-direction with its width as shown in Figure 3.6, the soil surface displacement of this strip can be defined by the following equation:

$$w(x) = w_a e^{-a(x-a)} \tag{3.59}$$

Where: w_a is nodal displacement at the plate edge as indicated in Figure 3.5, α is constant with a unit one per unit length, and x is measured from the element center as shown in Figure 3.5.

After inserting Equation (3.59) into Equation (3.58), the value of α is:

$$\alpha = \sqrt{\frac{k_p}{G_P}} \tag{3.60}$$

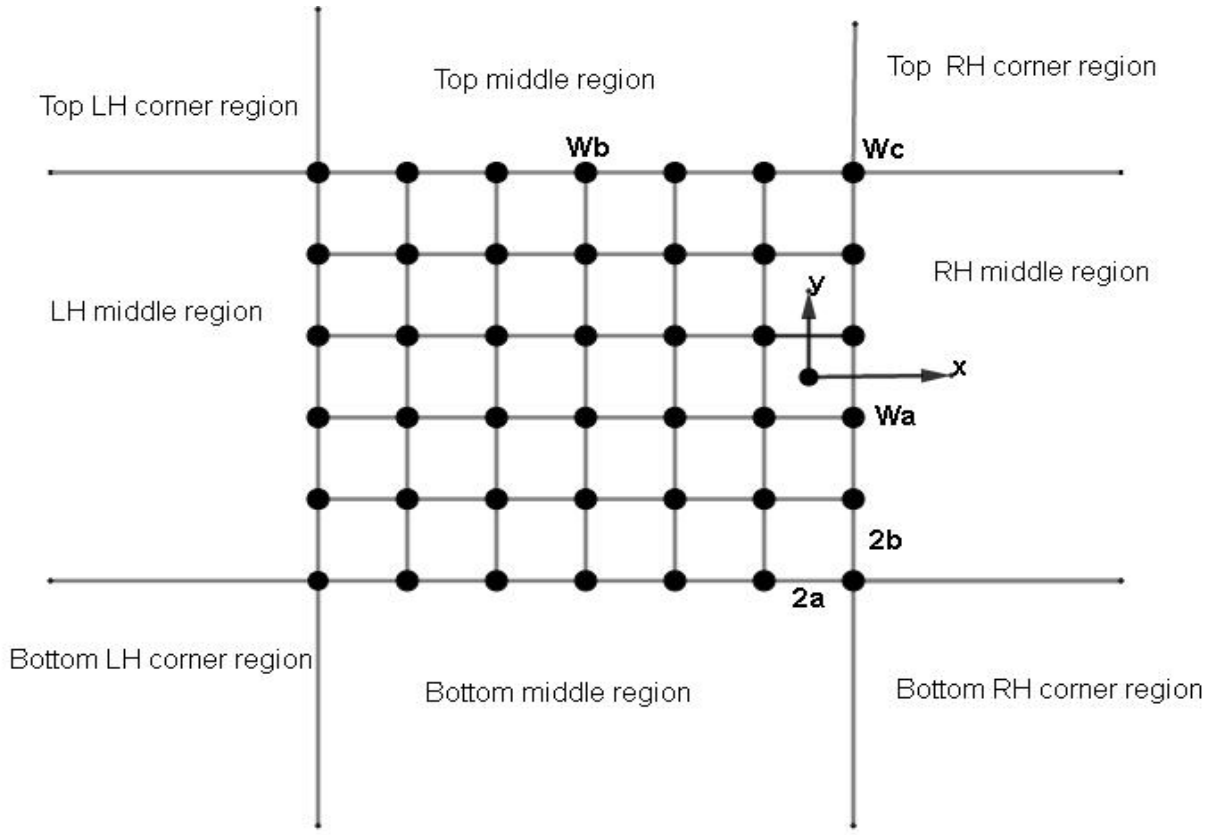

Figure 3. 5: Typical discretized plate, divided regions of surrounding soils, plate edge nodal displacement, and element size and element local axis.

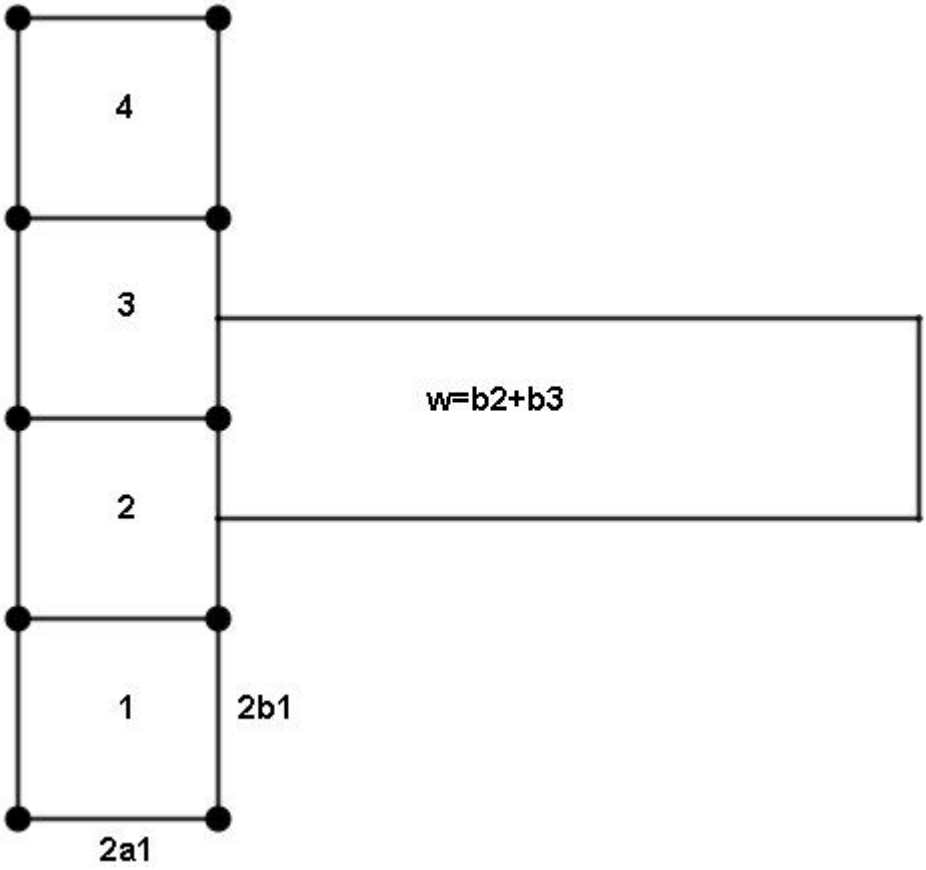

Figure 3. 6: Typical edge plate elements and a strip of surrounding soil with width W=b2+b3.

Again, considering the top RH corner region as shown in Figure 3.5, the soil surface displacement that satisfies Equation (3.58) is given by :

$$w(x,y) = w_c e^{-(x-a)} e^{-(y-b)} \tag{3.61}$$

Where: w_c is the plate element nodal displacement as shown in Figure 3.5, is constant with unit of one per unit length and x and y are measured from center of the plate corner element.

After inserting Equation (3.61) into Equation (3.58), and performing the necessary mathematical manipulations, is found as below:

$$= \sqrt{\frac{k_p}{2G_P}} \tag{3.62}$$

The soil surface displacements of the remaining regions of Figure 3.5 are evaluated in a similar way as the above approaches.

Once the soil surface displacement is estimated, the boundary forces at the plate edge are determined in terms of this displacement. For the RH middle region of Figure 3.5, the strain energy of the soil strip in Figure 3.6 is given by:

$$\prod_{ss} = \frac{1}{2}\int_A \left(k_p w(x)^2 + G_p \left(\frac{\partial w(x)}{\partial x} \right)^2 + G_p \left(\frac{\partial w(x)}{\partial y} \right)^2 \right) dA \tag{3.63}$$

After inserting Equation (3.59) in to Equation (3.63), and applying the required derivation gives :

$$\prod_{ss} = \frac{1}{2} \int_0^{b_2+b_3} \int_a^{\infty} \left(k_p w_a^{\,2} e^{-2\mathrm{a}(x-a)} + G_p \mathrm{a}^2 w_a^{\,2} e^{-2\mathrm{a}(x-a)} \right) dxdy \tag{3.64}$$

Where: b_2 and b_3 are as indicated in Figure 3.6, which are half of the length of Element 2 and 3 respectively.

Evaluating Equation (3.64) and then applying the first variational principle gives the following nodal force at x=a:

$$F_a = \sqrt{\left(k_p G_p\right)} \left(b_2 + b_3\right) w_a \tag{3.65}$$

Note that, the values of b_2 and b_3 depend on the finite element mesh size at the plate edges. The nodal displacement at plate edge, w_a, is not constant throughout the plate edge. This implies, the nodal force given by Equation (3.65) is a function of the finite element mesh size and nodal displacements. Note also that Equation (3.65) has the same form as the left hand side of Equation (3.52), which implies, the element stiffness matrix of the edge plate-soil system is modified by adding the appropriate stiffness of Equation (3.65). All the middle regions of Figure 3.5 have similar form of nodal force as Equation (3.65).

The boundary force contribution of the top RH corner region of Figure 3.5 is estimated after expressing its strain energy as follows:

$$\prod_{scr} = \frac{1}{2}\int_b^\infty \int_a^\infty \left(k_p w(x,y)^2 + G_P \left(\frac{\partial w(x,y)}{\partial x} \right)^2 + G_p \left(\frac{\partial w(x,y)}{\partial y} \right)^2 \right) dxdy \tag{3.66}$$

Inserting the displacement given by Equation (3.61) into Equation (3.66), and then performing the integration and applying the first variation principle gives the following nodal force, which is the contribution from the top RH corner region of Figure 3.5.

$$F_{cr} = \frac{1}{2}\left(\frac{1}{2^{\,2}} k_p + G_p \right) w_c \tag{3.67}$$

Now, the nodal force at the corner of a plate is a summation of the nodal force given by Equation (3.67) and the contributions from the middle regions. For example, the nodal force for Element 4 in Figure 3.6 is evaluated as follows:

$$F_c = \left(G_P + \sqrt{\left(k_p G_P \right)} \left(a_4 + b_4 \right) \right) w_c \tag{3.68}$$

Where: a_4 and b_4 are half of the width and length of Element 4, respectively (refer to Figure 3.6).

Again, Equation (3.68) has a similar form as left hand side of Equation (3.52).Therefore, the element stiffness matrix of the corner plate-soil system is modified by adding the appropriate stiffness of Equation (3.68).All the remaining corner regions of Figure 3.5 have similar form of nodal force as Equation (3.68).

3.6. Determination of Equivalent Nodal Loading

The previous sections of this chapter deal with estimation of element stiffness matrix including the boundary conditions. Thus, at this stage, the assembling of the element stiffness matrices gives non-singular global stiffness matrix. In order to solve the global deformation, assembled global nodal loading is required. This section deals with the determination the element nodal loading, which gives input for the assembling of the nodal loading.

The potential energy for a single element of a loaded plate-soil system is given by Equation (3.18). However, the potential energy formula of the loads is not given in this equation. Now, considering only uniformly distributed load, its work done on single element is given by:

$$\prod_l = -\int_{-1}^{1}\int_{-1}^{1} pw(r,s)\det J dr ds \tag{3.69}$$

Where: p is the uniformly distributed load and w(r, s) is the element displacement as given by Equation (3.12).

After applying the first variation principle, Equation (3.69) gives the following equivalent concentrated nodal load equation:

$$F_p = -ab\int_{-1}^{1}\int_{-1}^{1} N^T p dr ds \tag{3.70}$$

Evaluating Equation (3.70) results in:

$$F_p = -4abp\begin{Bmatrix} \frac{1}{4} \\ \frac{1}{4} \\ \frac{1}{4} \\ \frac{1}{4} \end{Bmatrix} \tag{3.71}$$

An important observation from Equation (3.71) is, the applied uniformly distributed load on an element is divided among the four nodes equally. This approach is used for applied concentrated force and bending moment.

3.7. Determination of Internal Shear Force and Bending Moment

As it is shown in the previous sections of this chapter, deformation based finite element formulation is used. That is, the only unknown variables obtained after formulation of the global equilibrium are displacements and section rotations. Therefore, if post processing results such as shear force and bending moment are required, constitutive relationships have to be applied.

Internal bending moments per unit length are calculated by integrating the elementary in-plane stress couples through the thickness of the plate as follow:

$$\left.\begin{aligned} M_{yy} &= -\int_{-h/2}^{h/2} \pm_{xx} z dz \\ M_{xx} &= -\int_{-h/2}^{h/2} \pm_{yy} z dz \end{aligned}\right\} \tag{3.72}$$

Where: M_{yy} and M_{xx} are the internal bending moments per unit length about y-axis and x-axis, respectively.

If the internal bending moment about y-axis per unit length is considered, replacing the value of $\pm_{xx}$ from Equation (3.4) into the first part of Equation (3.72) and then performing the integration gives:

$$M_{yy} = \frac{Eh^3}{12(1-\nu^2)}\left(\frac{\partial}{\partial x} + \nu\frac{\partial}{\partial y}\right) \tag{3.73}$$

An important observation from Equation (3.73) is, the internal bending moment about y-axis (per unit length) is a function of the section rotation of an element (refer to Figure 3.2). Equation (3.73) is used to calculate the internal bending moment about the y-axis per unit length within an element. The variables $_x$ and $_y$ are the section rotations within an element, which are functions of the element interpolation function and nodal section rotations (refer to Equation (3.12)).

In a similar manner, the internal bending moment about the x-axis (per unit length) within an element is evaluated as follows:

$$M_{xx} = \frac{Eh^3}{12(1-\nu^2)}\left(\frac{\partial}{\partial y} + \nu\frac{\partial}{\partial x}\right) \tag{3.74}$$

The transverse shear force in the xz-plane per unit length of the plate is determined as follows:

$$Q_{xz} = \int_{-h/2}^{h/2} \text{²}_{xz} dz \tag{3.75}$$

Where: $²_{xz}$ is given by Equation (3.5), which is written as follow after applying correction factor to account for non uniformity of the shear stress across the thickness of the plate.

$$²_{xz} = \frac{Ek_f}{2(1+v)}¥_{xz} \tag{3.76}$$

Combining Equation (3.75) and Equation (3.76) and then performing integration results in:

$$Q_{xz} = \frac{Ehk_f}{2(1+v)}¥_{xz} \tag{3.77}$$

The shear strain ($¥_{xz}$) in Equation (3.77) is a function of element interpolation functions and nodal displacements and section rotations which is given by Equation (3.16). Therefore, the shear force given by Equation (3.77) defines the shear force within an element.

Similarly, the shear force in yz-plane per unit length of the plate within the element is given by:

$$Q_{yz} = \frac{Ehk_f}{2(1+v)}¥_{yz} \tag{3.78}$$

Where: $¥_{yz}$ is as given by Equation (3.17).

Both the shear strains $¥_{xz}$ and $¥_{yz}$ are functions of the interpolation function, nodal displacement and section rotations within the element (refer to Equations (3.16) and (3.17)). A clear difference is observed between the equations of the shear forces and bending moments. That is, the shear forces are functions of the plate properties, displacement and section rotations of the element, where as the bending moments are only a function of the plate properties and section rotations of the element. This is due to the effect of Mindlin's plate theory (refer to Equations (3.2) and (3.3)).

4. Computer Implementation of Finite Element Model

4.1. General Introduction

The finite element method has become a very powerful computing tool in engineering fields. This is only possible, if the computing techniques are implemented on computing machines, i.e. digital computers have to be used. Normally, it seems possible, by using many elements, to virtually approximate any continuum with complex boundary and loading conditions to such a degree that an accurate analysis can be carried out. However, the limitations of the computer and the program employed may prevent the use of a sufficiently fine discretization to obtain accurate results. Hence, it is clearly desirable to use efficient finite element programs.

The type of element, mesh generation algorithm, element stiffness matrix and vector assembling algorithms, interpolation functions and solution methods are some of the factors that control the efficiency of a finite element program. The main purpose of applying effective finite element methods is to reduce the cost of computing, generally resources and time. Hence, the aim of this research is to produce an effective 3D equivalent finite element program that can be used easily in routine personal computers.

The major tasks involved in finite element method are, discretization of the problem domain, generating global node numbering, generating element connectives arrays, evaluating element stiffness matrix, calculating equivalent load vectors, assembling stiffness matrix, assembling load vectors and calculating post processing results. For all these purposes, programming is required. In this research, MATLAB is used as the programming tool/language.

No attempt is made to present the developed functions just by copy and paste. Instead, the techniques used in the development of the subroutines are described in the form of flow charts. This approach creates better visualization of the developed functions, especially when the numbers of code-lines are substantial amount such as in the finite element model.

4.2. Generating Finite Element Model Information

Assembling of stiffness matrix and load vector is not possible if there is no enough information about the finite element model. Such information includes, global node numbering, global element numbering, degree of freedom numbering, element size, identifying origin for xyz-coordinate and element connectivity array. Most of these data are generated automatically by algorithms, which mainly require model dimension.

Solution of any practical problem by finite element method involves a very large number of simultaneous equations and hence, computer memory needs to be effectively utilized. Storage space is saved typically by using symmetric matrix, small bandwidth and by avoiding storage of zero elements within a stiffness matrix. A sparser global stiffness matrix is obtained when the half bandwidth of the global stiffness matrix becomes small. Half bandwidth is given by the following formula [15, 16]:

$$B_{hw} = (A+1)*C \tag{4.1}$$

Where: A is maximum global node numbering difference of an element within a mesh, and C is the number of degree of freedom per node.

Equation (4.1) indicates that the size of half band width depends on the global node numbering scheme. Therefore, the selected global node numbering should give minimum half bandwidth. For this research, the global node numbering scheme shown in Figure 4.1 is used.

To generate global node numbering, the following fundamental problem parameters have to be supplied to the respective subroutines, a) plate size in the x and y-direction, b) location of the columns in the plate, c) element size in the x and y-direction.

In practice, the global stiffness matrix size is large. Therefore, if normal matrix addition rule is used, the element stiffness matrix should be in the same size as the global stiffness matrix. However, this approach demands substantial computer memory storage. A remedy for this is, adding matrices by using element connectivity array and one-dimensional array of element stiffness matrix or load vector.

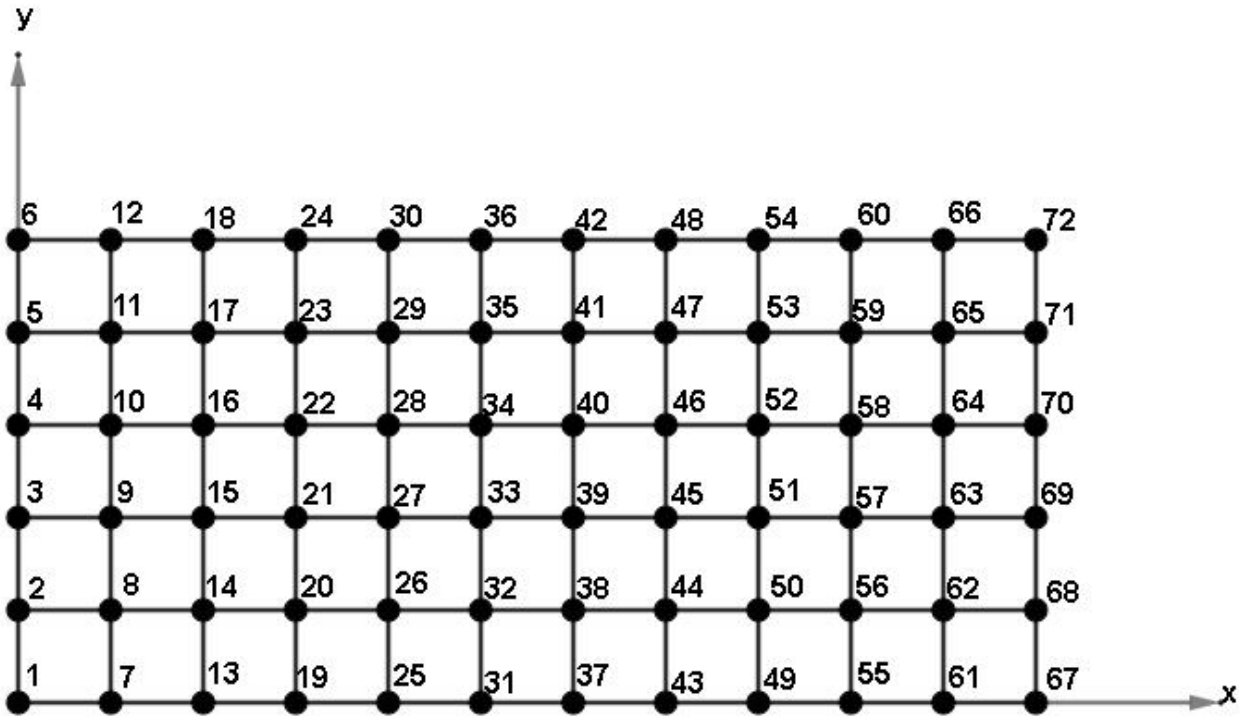

Figure 4. 1: Typical mesh and global node numbering for rectangular plate.

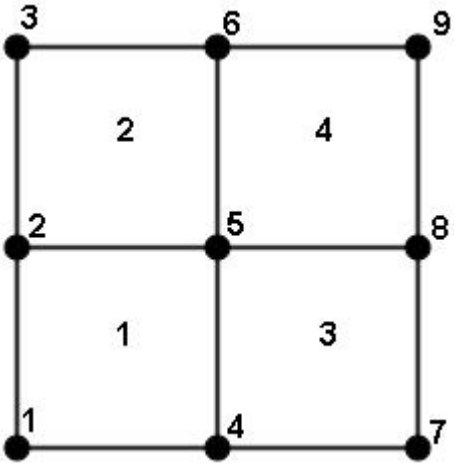

Figure 4.2: Typical plate with four elements, global element numbering and global node numbering.

Element connectivity array is read from identification array (ID). An identification array is defined by global node numbering and global degree of freedom. Example, considering a plate as in Figure 4.2 and taking three degree of freedom per a node, the identification array is given as follows:

$$ID = \begin{bmatrix} 1 & 4 & 7 & 10 & 13 & 16 & 19 & 22 & 25 \\ 2 & 5 & 8 & 11 & 14 & 17 & 20 & 23 & 26 \\ 3 & 6 & 9 & 12 & 15 & 18 & 21 & 24 & 27 \end{bmatrix}$$

Taking Element 1 from Figure 4.2, its global node numbering for the convention of local node numbering as shown in Figure 3.2 is given by:

$$\begin{bmatrix} 5 & 2 & 1 & 4 \end{bmatrix}$$

LM_1 and LM_2 are elements of the connectivity array for Element 1, which are read as follows:

$$LM_1 = \begin{bmatrix} ID(1,5) & ID(2,5) & ID(3,5) & ID(1,2) & ID(2,2) & ID(3,2) \end{bmatrix}$$

$$LM_2 = \begin{bmatrix} ID(1,1) & ID(2,1) & ID(3,1) & ID(1,4) & ID(2,4) & ID(3,4) \end{bmatrix}$$

Now, the connectivity array for Element 1 is as follows:

$$LM = \begin{bmatrix} LM_1 & LM_2 \end{bmatrix}$$

Then the result is:

$$LM = \begin{bmatrix} 13 & 14 & 15 & 4 & 5 & 6 & 1 & 2 & 3 & 10 & 11 & 12 \end{bmatrix}$$

This example shows, the connectivity array of an element is determined from the global nodal points to which the element is connected and the global equation numbers that have been assigned to those nodal points.

In this research, a subroutine that works like the above example is provided. The subroutine generates each element's connectives for any structured rectangular mesh size. Structured rectangular elements with low aspect ratio produces accurate and convergent solution compared

with the unstructured and high aspect ratio elements [9]. Thus, emphasis is put on using structured and low aspect ratio of rectangular elements.

In order to obtain the connectivity array of each element, six subroutines are used. Applications of all the six subroutines achieve the following six objectives:

1) To store plate dimension and column position
2) To generate and store element size in x and y-direction,
3) To generate and store global node numbering of each element,
4) To generate and store global node numbering of the whole plate,
5) To generate and store global degree freedom of each element,
6) To generate and store connectivity array of each element.

An easy way of understanding the programming up to the element connectivity array is to show it with simple presentation. This can be done by using a flowchart or a pseudo code. Figure 4.3 shows flowchart representation of the programming up to element connectivity array.

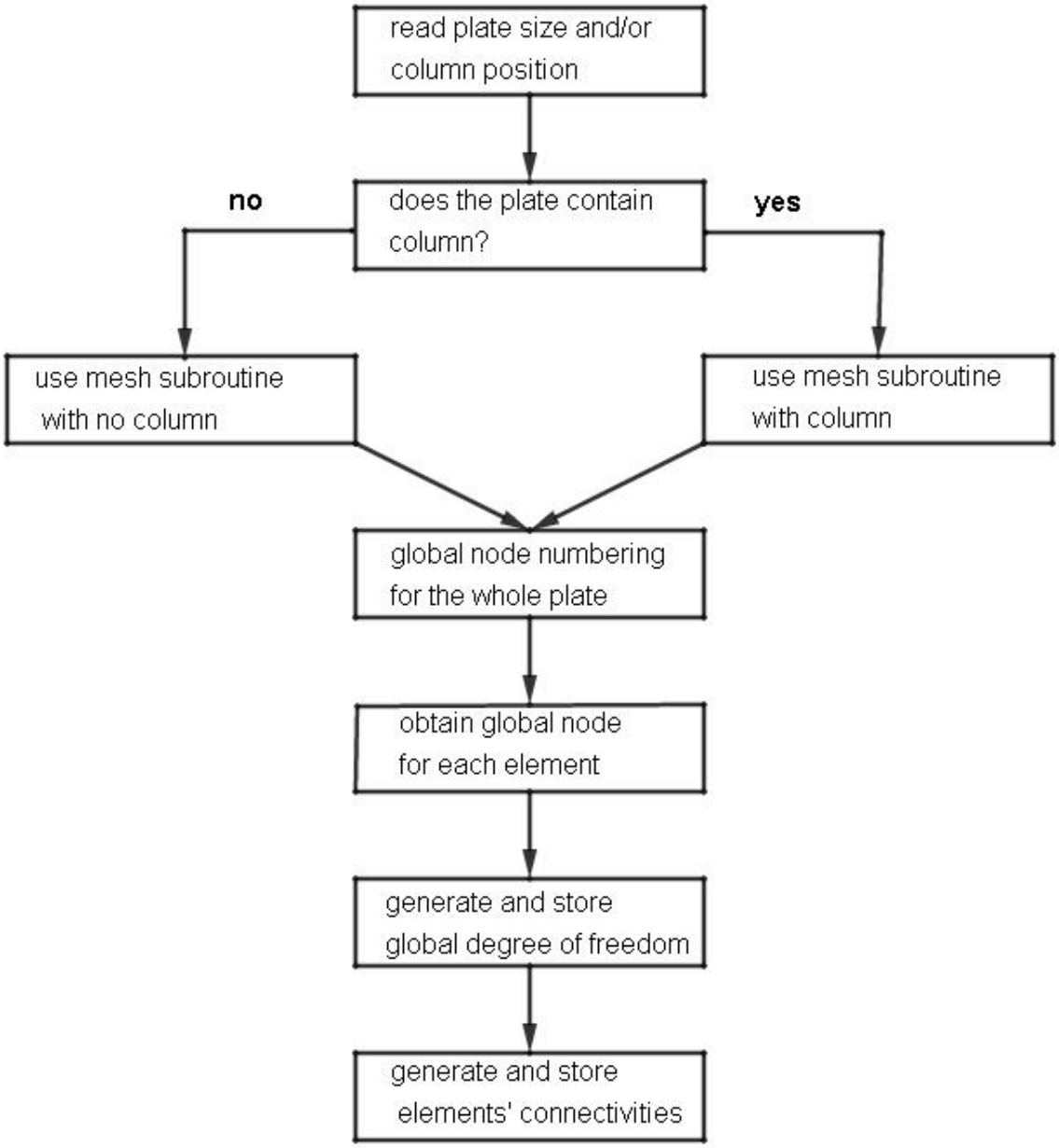

Figure 4.3: Flow chart of the element connectivity array.

4.3. Assembling of Element Stiffness Matrix and Load Vector

The procedure of assembling the element matrices and vectors is based on the requirement of compatibility at the element nodes. This means that at the nodes where elements are connected, the values of the unknown nodal degrees of freedom or variables are the same for all the elements linked at that node.

The assemblage process for obtaining global stiffness matrix of finite element model without the application of element connectivity array is symbolically written as follows:

$$K = \sum_{1}^{i} k_{ps}{}^{i} \tag{4.2}$$

Where: K global stiffness matrix of typical finite element model, and $k_{ps}{}^{i}$ is the stiffness matrix of the ith element.

It should be noted that the element stiffness matrices in Equation (4.2) are of the same order as the global stiffness matrix, K. However, considering the internal structure of the element stiffness matrices nonzero elements are in only those rows and columns that correspond to element degrees of freedom. Therefore, in practice, it is only needed to store the compacted element stiffness matrix, which is of order equal to the number of element degrees of freedom, together with an element connectivity array that relates to each element degree of freedom the corresponding assemblage degree of freedom. Note that element connectivity arrays for the whole plate-soil system are formulated as in the example given in Section 4.2.

To make the element stiffness matrix assembling procedure easily understandable, an example is employed in this section. Consider a simple mesh that is given in Figure 4.2, and the intention in this example is to identify the position of the element stiffness matrix for Element 1 in the global stiffness matrix. To do this, each element of the stiffness matrix of Element 1 is indexed using the element connectivity array of Element 1. The element connectivity array for Element 1 is given in the example of Section 4.2. Therefore, the indexing of each element of the stiffness matrix of Element 1 is as shown in Table 4.1.

Table 4.1: Addressing element stiffness matrix for Element 1 of the mesh in Figure 4.2.

Column index=element connectivity array (LM) →

Row index=element connectivity array (LM) ↓

k(13,13)	k(13,14)	k(13,15)	k(13,4)	k(13,5)	k(13,6)	k(13,1)	k(13,2)	k(13,3)	k(13,10)	k(13,11)	k(13,12)
k(14,13)	k(14,14)	k(14,15)	k(14,4)	k(14,5)	k(14,6)	k(14,1)	k(14,2)	k(14,3)	k(14,10)	k(14,11)	k(14,12)
k(15,13)	k(15,14)	k(15,15)	k(15,4)	k(15,5)	k(15,6)	k(15,1)	k(15,2)	k(15,3)	k(15,10)	k(15,11)	k(15,12)
k(4,13)	k(4,14)	k(4,15)	k(4,4)	k(4,5)	k(4,6)	k(4,1)	k(4,2)	k(4,3)	k(4,10)	k(4,11)	k(4,12)
k(5,13)	k(5,14)	k(5,15)	k(5,4)	k(5,5)	k(5,6)	k(5,1)	k(5,2)	k(5,3)	k(5,10)	k(5,11)	k(5,12)
k(6,13)	k(6,14)	k(6,15)	k(6,4)	k(6,5)	k(6,6)	k(6,1)	k(6,2)	k(6,3)	k(6,10)	k(6,11)	k(6,12)
k(1,13)	k(1,14)	k(1,15)	k(1,4)	k(1,5)	k(1,6)	k(1,1)	k(1,2)	k(1,3)	k(1,10)	k(1,11)	k(1,12)
k(2,13)	k(2,14)	k(2,15)	k(2,4)	k(2,5)	k(2,6)	k(2,1)	k(2,2)	k(2,3)	k(2,10)	k(2,11)	k(2,12)
k(3,13)	k(3,14)	k(3,15)	k(3,4)	k(3,5)	k(3,6)	k(3,1)	k(3,2)	k(3,3)	k(3,10)	k(3,11)	k(3,12)
k(10,13)	k(10,14)	k(10,15)	k(10,4)	k(10,5)	k(10,6)	k(10,1)	k(10,2)	k(10,3)	k(10,10)	k(10,11)	k(10,12)
k(11,13)	k(11,14)	k(11,15)	k(11,4)	k(11,5)	k(11,6)	k(11,1)	k(11,2)	k(11,3)	k(11,10)	k(11,11)	k(11,12)
k(12,13)	k(12,14)	k(12,15)	k(12,4)	k(12,5)	k(12,6)	k(12,1)	k(12,2)	k(12,3)	k(12,10)	k(12,11)	k(12,12)

It is clearly shown in Table 4.1 that each element of the stiffness matrix of Element 1 is indexed in terms of element connectivity of Element1. The connectivity arrays are shown at the top and left hand side of Table 4.1. An element of stiffness matrix of Element 1 is located in the global stiffness matrix by index expressed in terms of the element connectivity array. Example, the top right hand corner element of Table 4.1 is expressed as k (13, 12). This means, the location of this element on the global stiffness matrix is on Row 13 and Column 12.

An important observation from the above example is, element stiffness matrix is added to global stiffness matrix by storing 12 elements of connectivity array and 12x12 element stiffness matrix. However, if normal matrix addition rule is used, the element stiffness matrix is stored as 27x27 matrix (refer to Figure 4.2). This method becomes more beneficial when the number of global degree of freedom is large or when the finite element mesh is very fine.

A similar procedure is used to assemble element load vector into global load vector. During the assembling of both element stiffness matrix and load vector, a null global stiffness matrix and load vector should be created first. This minimizes the memory relocation time during each iteration /looping. The flowcharts for computing the element stiffness matrix and load assembling are given in Figures 4.4 and 4.5, respectively. Dimensional

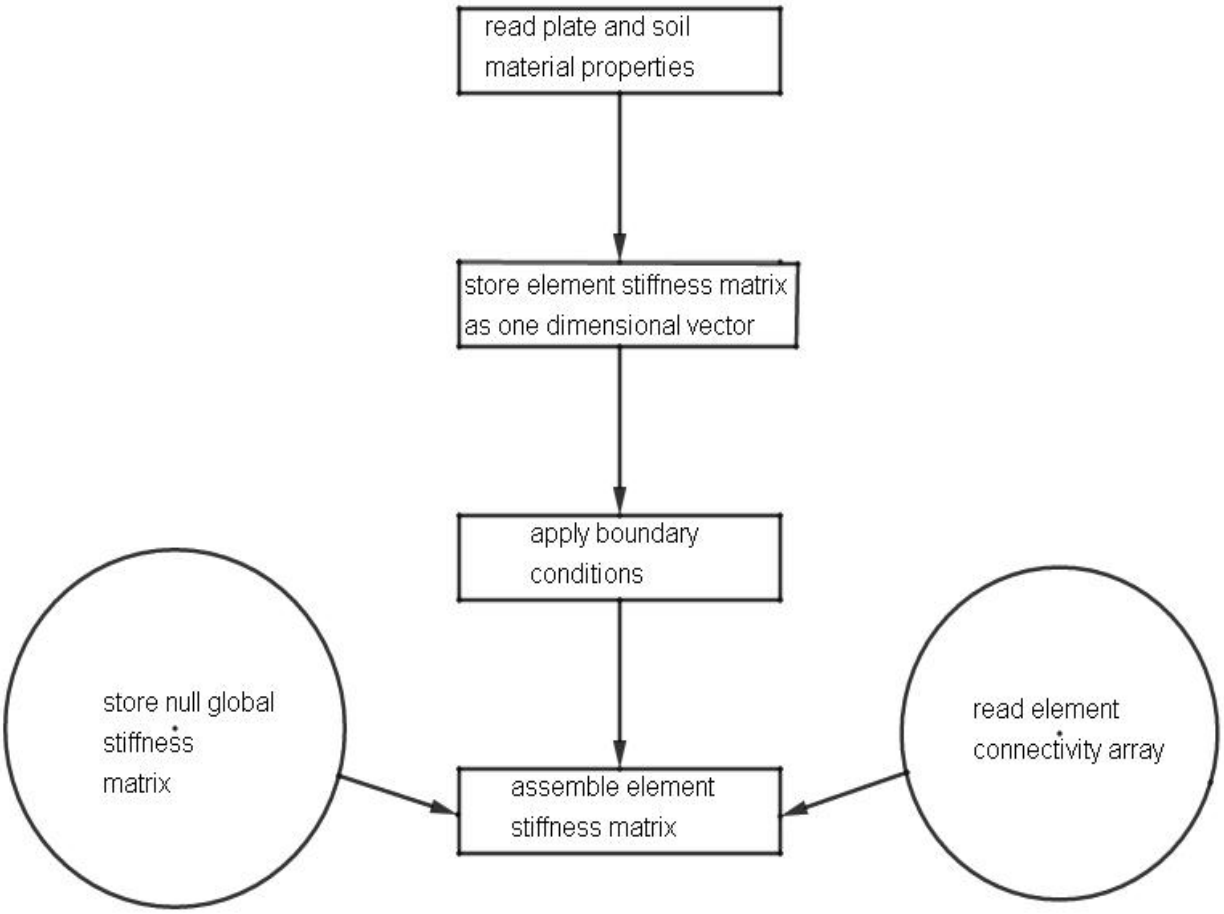

Figure 4. 4: Flow chart for the element stiffness matrix assembling.

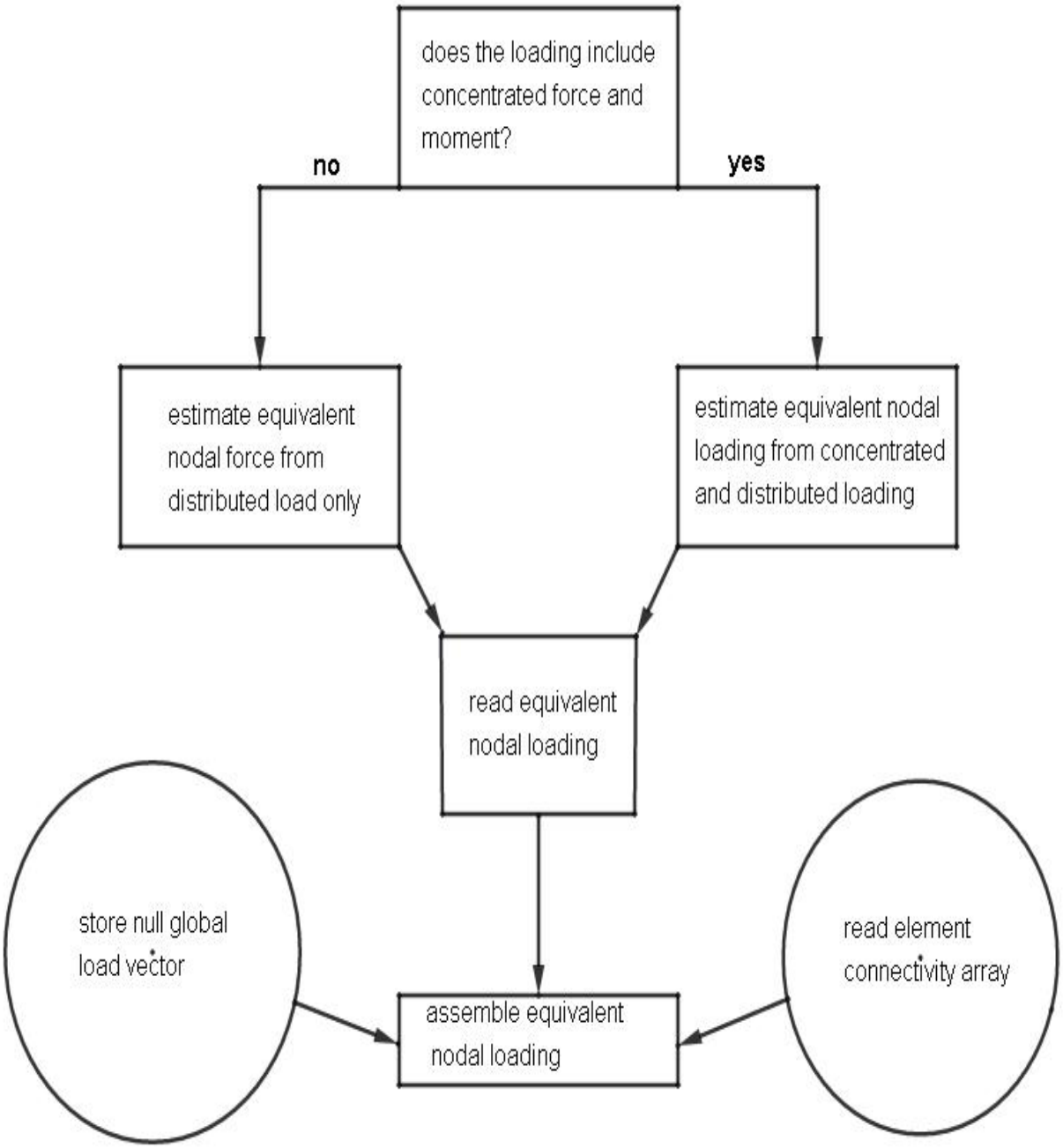

Figure 4. 5: Flow chart to assemble element nodal loading.

4.4. Solution Method and Evaluation of Post-processing Results

The practical applications of finite element method lead to large systems of simultaneous algebraic equations. If the size of the problem is large or the finite element mesh size is small, storing the whole global stiffness matrix needs considerable computer memory space. In such cases, finite element equation systems possess some properties that allow reduction of storage and computing time. Symmetry and sparsity are the major important properties of global stiffness matrix. Symmetric property aids in storing only half of the global stiffness matrix including the diagonal elements. Furthermore, the global stiffness matrix contains zero elements, that is, a sparse matrix contains more zero entries than nonzero entries. Therefore, storing only non- zero entries economizes the storage and the computation time [15].

After assembling the element stiffness matrix and the load vector of the plate-soil system, the following global simultaneous equation is obtained:

$$KU = R \tag{4.3}$$

Where: K is the global stiffness matrix as defined in Equation (4.2),U is the global deformation vector which has a similar form as in Equation (3.54) and R is the global load vector which has similar form as in Equation (3.53).

The overall effectiveness of a finite element analysis depends largely on the numerical procedures used for the solution of the system of equilibrium equations. In general, the accuracy of a finite element analysis can be improved if a more refined finite element mesh is used. This means the cost of analysis and its practical feasibility depends to a considerable degree on the solution algorithms used [3].

Essentially, there are two different classes of methods for the solution of Equation (4.3): a) direct solution techniques, b) iterative solution methods. In a direct solution, the Equations in (4.3) are solved using a number of steps and operations that are predetermined in an exact manner, whereas iteration is used when an iterative solution method is employed. Direct solution methods are usually used for problems of small to moderate size. For large problems, iterative methods are preferable, because they require less computing time [15].

The most effective direct solution techniques currently used are applications of Gauss elimination. Although, Gaussian elimination can be applied to any set of simultaneous linear equations, it becomes more effective in the finite element analysis. Because, finite element analysis has the following important properties: a) symmetry, b) positive definiteness, c) bandedness [3].

In this research, the cost of analysis is minimized by avoiding storage of zero elements in the element stiffness matrix, global stiffness matrix, and global load vector. Solution is obtained using MATLAB built-in functions. A typical solution result of MATLAB built-in solution method is compared to a solution that is obtained using Gaussian elimination based subroutine; the same results are obtained in both methods. The solution vector contains nodal displacements and section rotations only. The flowchart for the solution of nodal displacement and section rotations is shown in Figure 4.6.

In this research, the post-processing results of a plate are, bending moment about x-axis, bending moment about y-axis, shear force in the xz-plane, and shear force in the yz-plane. Considering first the bending about the y-axis, which is given by Equation (3.73), it is further simplified after inserting Equation (3.12) into it as follows:

$$M_{yy} = \frac{Eh^3}{12(1-\nu^2)}\left(\tilde{\kappa}_x + \nu\,\tilde{\kappa}_y\right) \tag{4.4}$$

Where:

$$\tilde{\kappa}_x = \begin{bmatrix} \frac{1+s}{4a} & \frac{-(1+s)}{4a} & \frac{-(1-s)}{4a} & \frac{1-s}{4a} \end{bmatrix} \begin{Bmatrix} \theta_{y1} \\ \theta_{y2} \\ \theta_{y3} \\ \theta_{y4} \end{Bmatrix} \tag{4.5}$$

$$\tilde{\kappa}_y = \begin{bmatrix} \frac{1+r}{4b} & \frac{1-r}{4b} & \frac{-(1-r)}{4b} & \frac{-(1+r)}{4b} \end{bmatrix} \begin{Bmatrix} \theta_{x1} \\ \theta_{x2} \\ \theta_{x3} \\ \theta_{x4} \end{Bmatrix} \tag{4.6}$$

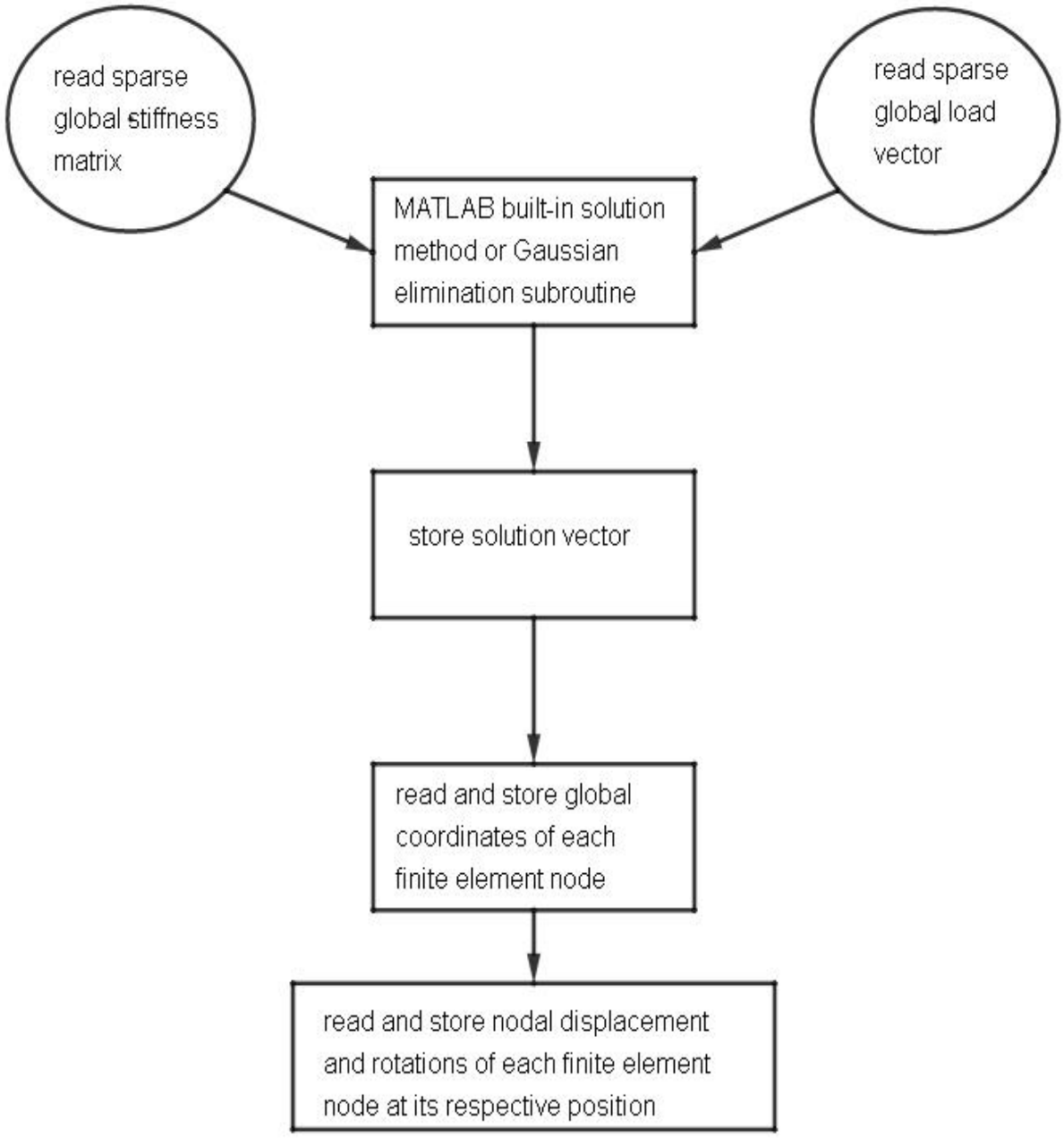

Figure 4. 6: Flow chart for the solution of the displacements and section rotations.

Note that Equation (4.4) is used for a single element and the conventions given in Figure 3.2 are used to derive Equations (4.5) and (4.6).

Similarly, the bending moment about the x-axis is given by:

$$M_{xx} = \frac{Eh^3}{12(1-v^2)}\left(\tilde{}_{y} + v\,\tilde{}_{x} \right) \tag{4.7}$$

The shear force in the xz-plane is obtained by direct substitution of Equation (3.16) into Equation (3.77). Likewise, shear force in the yz-plane is obtained by direct substitution of Equation (3.17) into Equation (3.78).

As it is clearly shown by Equations (3.16), (3.17), (4.5), and (4.6), the element shear forces and bending moments per unit length are obtained at the desired location of the element by specifying the values of r and s. However, in this research the shear forces and bending moments per unit length are estimated only at the node of finite element mesh.

The local system coordinate axes, the positive bending moments, and shear forces of an element are as shown on Figures 4.7 and 4.8.

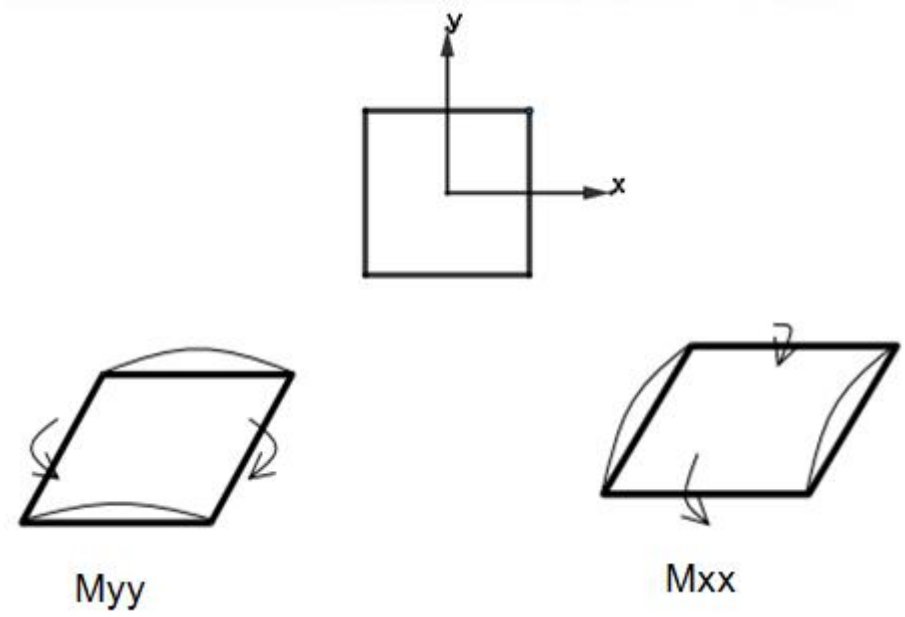

Figure 4.7: Definitions of positive bending moments and local axes for a typical element.

Figure 4. 8: Definitions of positive shear forces per the local axes given in Figure 4.7.

In this research, the post-processing results are estimated using four subroutines. The general flowchart of the post-processing results is given in Figure 4.9.

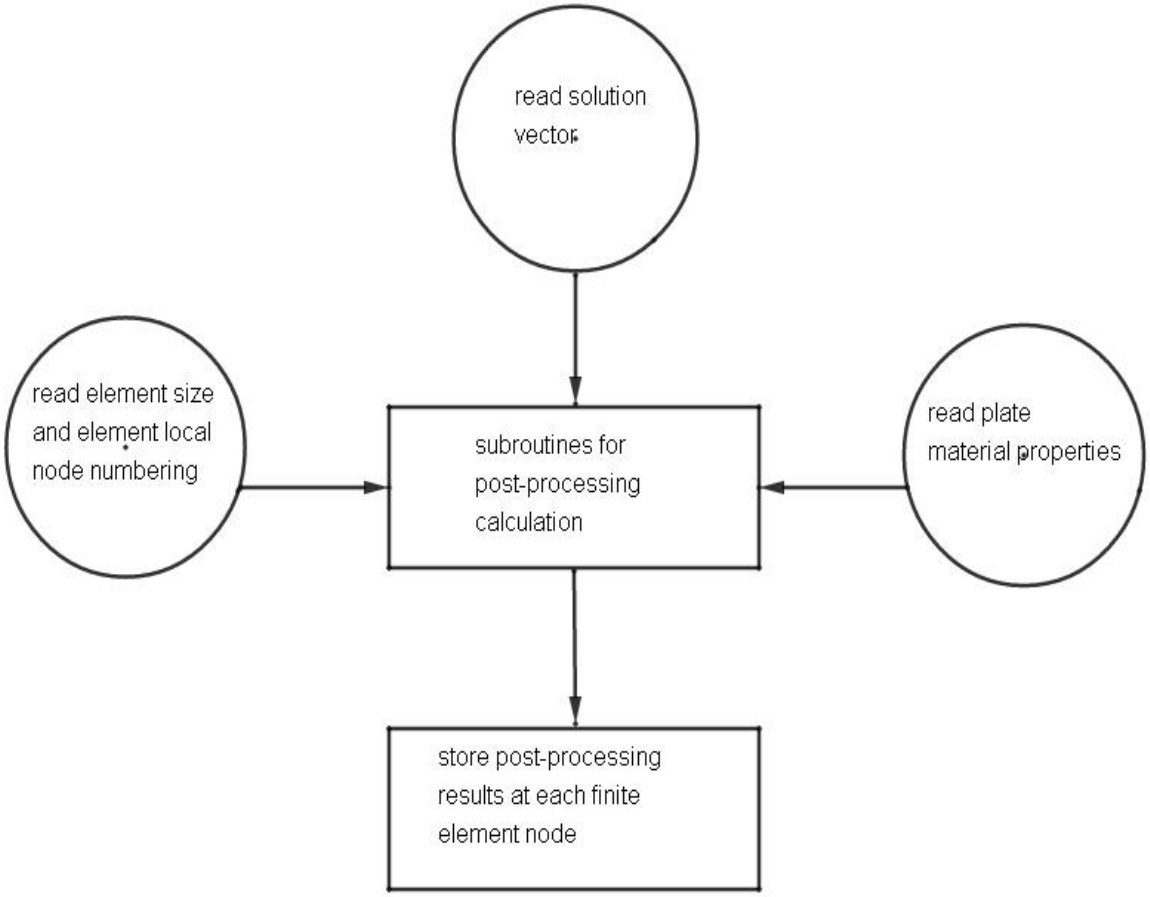

Figure4.9: General flow chart for the post-processing result.

5. Verification, Adjustment and Convergence of the Model

5.1. General Introduction

Applying all the methods presented in the previous chapters give approximate solution to the exact response of the mathematical model. This solution is proper if it converges to the analytical solution of the differential equations that govern the response of the mathematical model. For this reason, convergence analysis has to be performed. If the exact solution of the governing differential equation is not known, the convergence of the finite element solutions can be measured only on the fact that all basic kinematic, static, and constitutive conditions contained in the mathematical model must ultimately (at convergence) be satisfied. Furthermore, the finite element solution error should be small as the finite element mesh size is decreased successively.

Finite element analysis is a powerful tool for evaluating complex engineering problems. Like in all analytical software, the principle bad output stem from bad input (garbage in garbage out) applies for finite element software. There are many ways that the finite element analysis can take a wrong turn. Some of the common sources of wrong solution include: a) unstable finite element formulation, b) bad mesh, c) poorly applied boundary conditions, d) programming error. Therefore, validation and verification processes are required to check the correctness of the solution. Validation of a finite element solution involves experimental test of the prototype of the mathematical model. On the other hand, verification involves checking the finite element solution against an analytical solution of the mathematical model or against a validated and verified finite element software. Generally, validation of the finite element software demands extensive cost and expertise. Thus, only verification of the developed finite element program will be discussed.

In this research, PLAXIS 3D FOUNDATION is used as benchmark for the assessment of the developed finite element program. It is obvious that the developed finite element program will not give identical solution as PLAXIS 3D FOUNDATION. The main reason for this is, the developed finite element program does not include the full 3D effect of both the plate and the soil medium. As a result, the assembled stiffness matrix is underestimated, which leads to overestimation of deformation as compared with PLAXIS 3D FOUNDATION.

Generally, this scenario is clearly observed in all practical range of plate and soil types. Therefore, in order to get similar solutions adjustment factor has to be applied.

In the forthcoming sections, the convergence analysis, verification, and adjustment of the developed finite element program are presented sequentially.

5.2. Convergence Analysis of the Model

The accuracy or efficiency of the approximate solution depends on the choice of shape functions (blending functions). Accuracy is captured by a quality called convergence. By convergence, it means that as we add more nodes and elements into the mesh that replaces the original mesh structure, the sequence of trial solutions must approach to the exact solution. Thus, it is essential that the quantities such as displacements, stresses and strain energies are exactly recovered, surely, and if possible, quickly. Hence, the shape functions have to meet the following major convergence requirements [25]:

1) Continuity within the element,
2) Continuity in the element boundaries,
3) Rigid body motions,
4) Ability to represent constant curvatures.

Generally, the convergence characteristics of finite elements are evaluated by patch test. Patch is a small assembly of finite elements. In the patch test, the patch is subjected to a certain set of displacement and boundary forces. If a constant-curvature is attained under these conditions, then the patch test is passed and the finite element model solution is convergent [25]. If the convergence behavior of the finite element is not identified early, the finite element model solution obtained after successive mesh refinement may: a) converge to the exact solution, b) converge to wrong number, c) diverge entirely. Therefore, if patch test is applied properly, it is a necessary and sufficient condition for convergence [16].

In this research, rectangular four node finite elements (refer to Figure 3.2) are used. Based on the study by Bathe and N.Dvorkin, the following important properties of such a finite element are found [2]:

1) The element is able to represent three rigid body modes,
2) The element does not contain spurious zero energy modes,
3) The element passes patch test,
4) The element can be applied for the analysis of very thin plates (it has no locking behavior).

From the above results, the type of finite element implemented in this research is convergent and the convergence of the developed finite element model is checked as discussed subsequently.

The finite element model (refined model) solution error is contributed from discretization, numerical integration, and round off. The discretization error has the most pronounced influence on the convergence of the finite element model solution. Thus, only the discretization error is discussed next.

After successive mesh refinement, the strain energy of the finite element model solution approaches the exact solution's strain energy. The mesh is refined in such a manner that the nodes of the coarser mesh exist in the finer mesh and the size of the next finer element is half of the pervious coarser element size [3], see Figure 5.1.

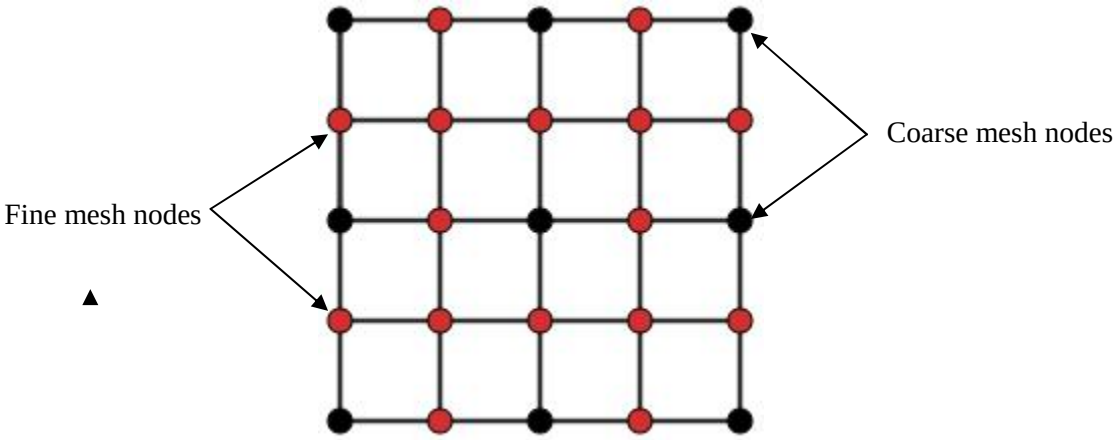

Figure 5.1: Typical mesh refinement, the red colored nodes are added after applying the first mesh refinement.

The total potential energy for a given mesh is defined as follows [3]:

$$\Pi\Big|_{U_{any}} = \frac{1}{2}U_{any}^{T}KU_{any} - U_{any}^{T}R \tag{5.1}$$

Where: U_{any} is global deformation vector for the given mesh.

Inserting Equation (4.3) into Equation (5.1), and noting that the first part of Equation (5.1) is strain energy and the second part is energy due to external loads, then the potential energy and strain energy of the finite element model are given as follow:

$$\left.\begin{aligned}\Pi &= -\frac{1}{2}U^{T}R,\\ \text{¦} &= \frac{1}{2}U^{T}R\end{aligned}\right\} \tag{5.2}$$

where: ¦ is the strain energy of the finite element model

Therefore, to evaluate the strain energy of the finite element model, it is only needed vector multiplication of the global deformation vector and applied external load vector. In this research, a subroutine is written for this purpose.

The finite element model is said to be convergent, if the strain energy difference (error) between the finite element model solution and the governing differential equation solution (exact solution) decreases continuously, but this happens when the mesh refinement strategy in Figure 5.1 is applied. However, if the exact solution is not known, the strain energy error is estimated by subtracting the current strain energy of the finite element model from the limiting strain energy of the same finite element model [3].

In the finite element solution, the deformations are underestimated, and hence the stiffness of the mathematical model is overestimated. “This overestimation of the stiffness is (physically) a result of the "internal displacement constraints" that are implicitly imposed on the solution as a result of the displacement assumptions”. However, as the mesh is refined, the finite element solution/stiffness converges to the exact solution/stiffness of the mathematical model [3].

In this research, the strain energy convergence analysis of the finite element model is presented in Figure 5.2.

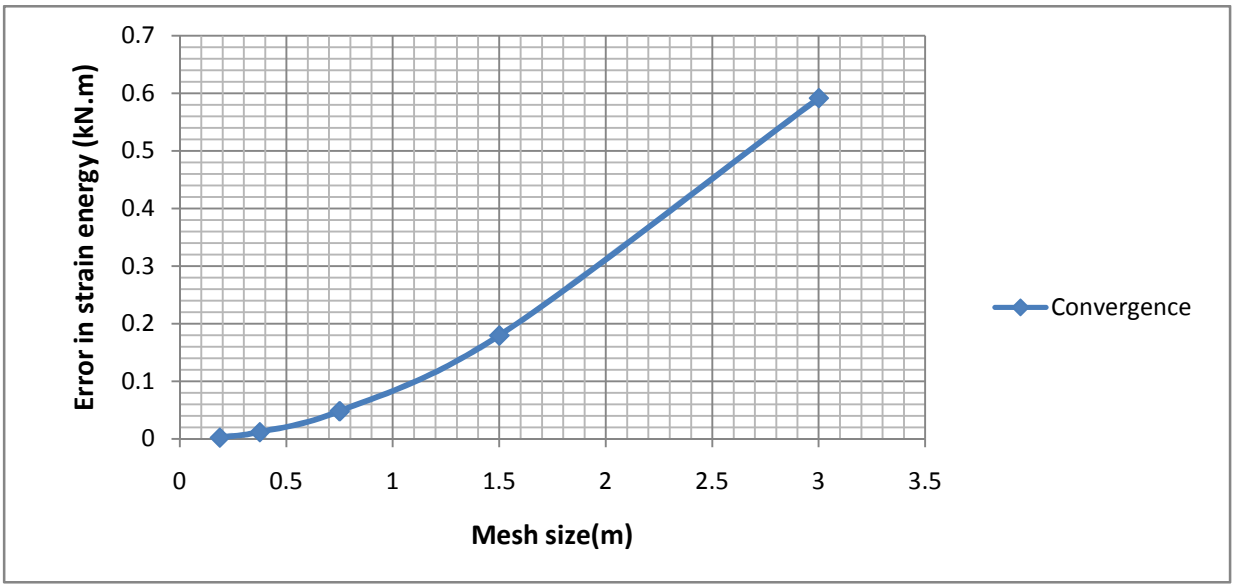

Figure 5.2: Convergence of strain energy for the developed finite element model.

As is already noted, the finite element that is used in this research passes the patch test, and thus the finite element model's solution has to converge to the solution of the governing differential equation/limiting solution. The strain energy convergence analysis of the developed finite model that is shown in Figure 5.2 clearly demonstrates this fact.

The convergence analysis of strain energy for the developed finite element shows that the strain energy error decreases continuously, as the mesh size is refined as per Figure 5.1. A typical check indicates that the difference in strain energy between mesh size of 1m and 0.5m is around 0.12kN.m. Again, the maximum deflection of the plate remains constant for mesh size of equal or less than 0.75m. Therefore, if the only applied external load is uniformly distributed load, then using a mesh size starting from 1m doesn't result significant discretization error. However, when the applied external load contains concentrated column loads, finer mesh size should be used in these regions. In this case, care has to be exercised not to use large aspect ratio finite elements. This is because using larger aspect ratio introduces computational error. To mitigate this problem, the user can refine the mesh size in the concentrated load regions, but the mesh size in the other regions is limited automatically not to be larger than the column size.

5.3. Verification of the Model (Simple Checks)

The solution of a numerical simulation is completely dependent on the quality and accuracy of the model. To investigate the quality and accuracy of a model, the numerical solution of the model is compared against the analytical solution of the governing mathematical model and /or experimental test result of a physical model, if available. Therefore, verification is a quantitative comparison of solution of a numerical model with the analytical solution of the governing mathematical model, and validation is a quantitative comparison of solution of a numerical model with experimental test results of the physical model.

Most likely, application of finite element methods means that it is not possible to get closed solution to the mathematical model or it is not easy to solve the mathematical model analytically. Thus, the finite element method is very important in situations where obtaining solution by other means is impossible or at least hard. This means, verification of the finite element model is not possible or it is not an easy task. However, the mathematical model can be solved after applying some simplifications, and this result is compared with the finite element model result. Obviously, these two results will not be the same. But a general decision is made if the finite element model solution makes sense or not.

In this research, the verification of the developed finite element model is made mainly against PLAXIS 3D FOUNDATION. In this section, rough deflection comparison of the developed finite element model and PLAXIS 3D FOUNDATION are presented. The detailed comparison (detailed verification) on deflection, shear force, and bending moment are discussed in Chapter 6. Other simple checks of the developed finite element model are discussed in the current section. Note that in this section, the developed finite element model does not consider an adjustment factor. Because, the intention in this section is to check the developed finite element model by using simple known facts.

One of the simple checks is, if the shear parameter is included and the plate is subjected to uniformly distributed load, then according to two-parameter subgrade model, the deformation of the plate should have bowl shape. The developed finite element model confirms that this deformation behavior is achieved, refer to Figure 5.3 for the 3D view of the deformation.

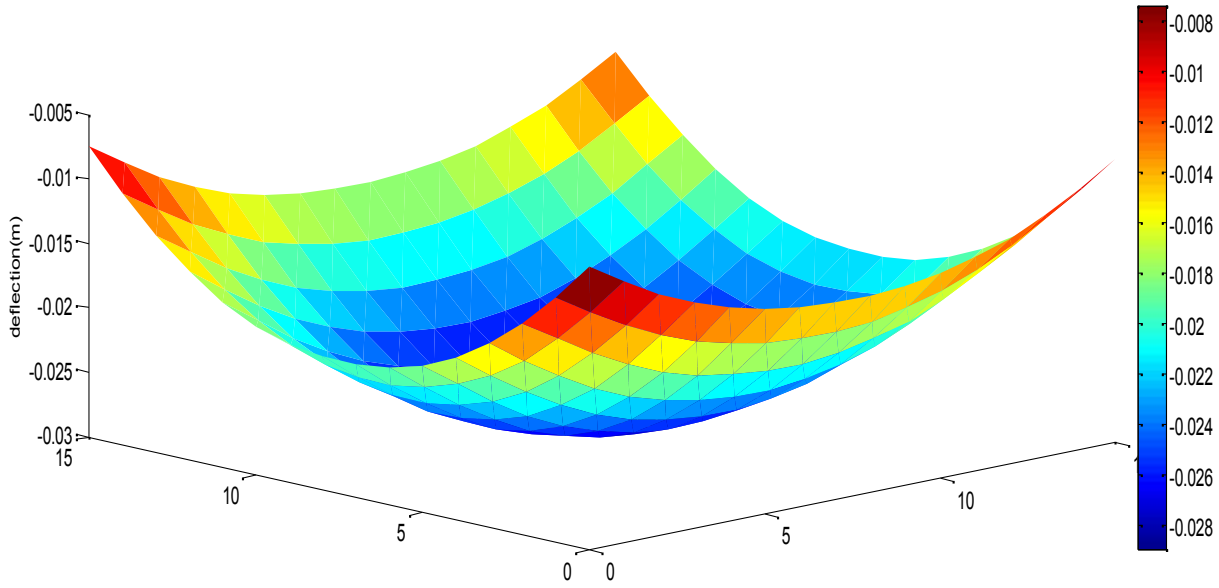

Figure 5.3: Deflection simulation of the developed finite element model for Pasternak model.

Both the Young's modulus (E_s) of a soil medium and applied load on the plate have significant impact on the magnitude of the plate's deflection. Hence, as a 2nd check the maximum deflection of the plate should decrease as the Young's modulus (E_s) of a soil medium is increased. On the other hand, the maximum deflection of the plate should increase as the loading is increased. The results of the developed finite element model validates these properties, refer to Figure 5.4 and 5.5, respectively.

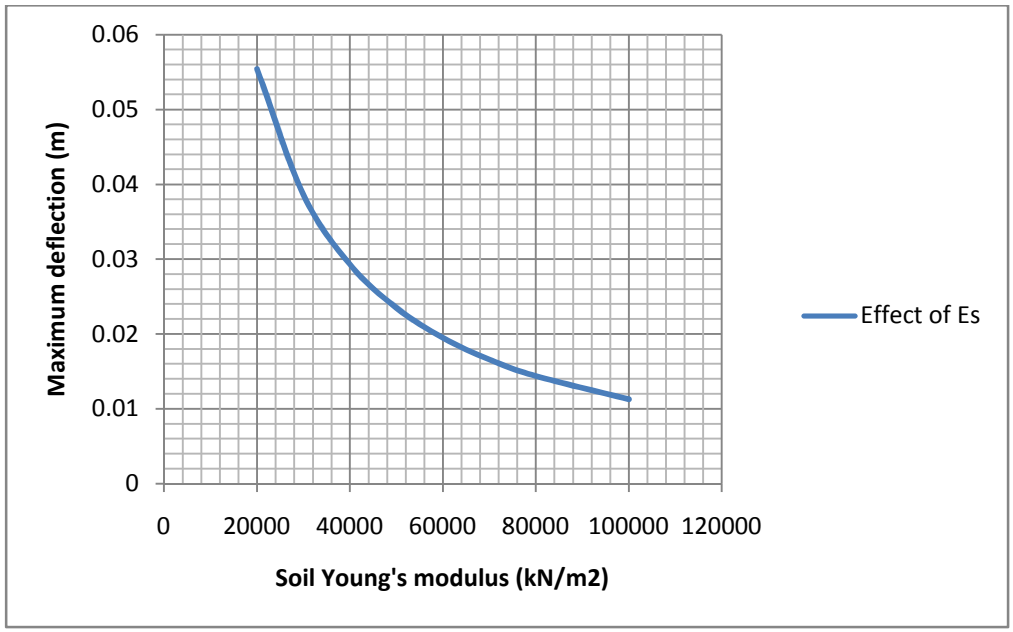

Figure 5. 4: Effect of soil Young's modulus variation on the maximum deflection of a plate.

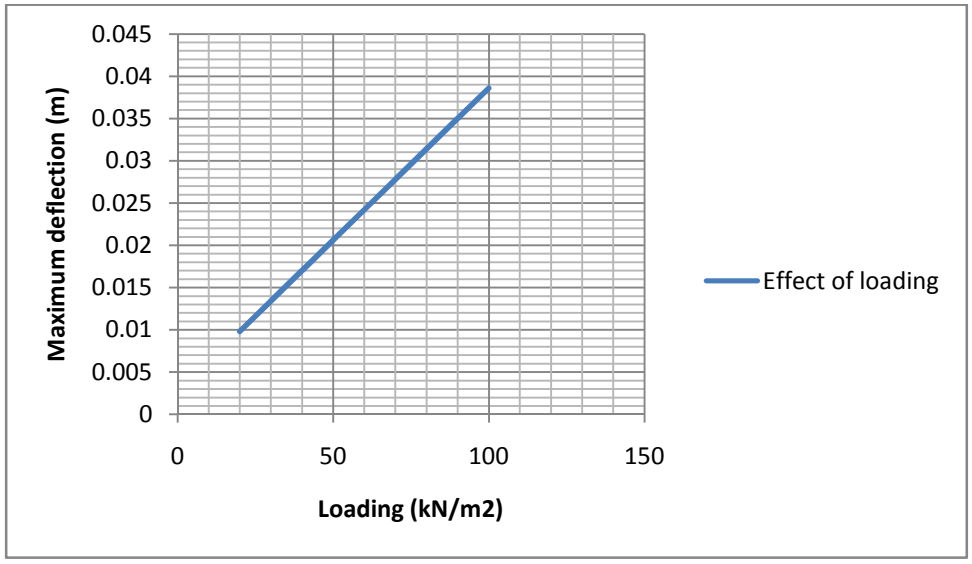

Figure 5.5: Effect of load variation on the maximum deflection of a plate.

Even though there is a difference in the formulation of the PLAXIS 3D FOUNDATION and the developed finite element model, generally the significant discrepancy between the solutions of the two models is expected to be only in terms of magnitude. Taking this idea as a benchmark, if

the two models use the same material properties and loading, then the 3D deflection of the two models should be similar in shape.

Throughout this research, whenever PLAXIS 3D FOUNDATION is used, both the soil and the concrete are represented by linear-elastic material model. Note also that the developed finite element model is applicable only for linear-elastic material model.

In the rough deflection comparison two types of loading are considered. These are a uniformly distributed load and four concentrated column forces. The deflection of a plate for a uniformly distributed load that is evaluated using both the developed finite element model and PLAXIS 3D FOUNDATION is shown in Figure 5.6 (the upper two figures). Again, the deflection of a plate due to the four concentrated column forces evaluated by both the developed finite element model and PLAXIS 3D FOUNDATION is shown in Figure 5.6 (the lower two figures).

Although it is not presented here, the effects of the spacing and number of concentrated load on the deflection pattern of a plate are investigated. It is confirmed that both the developed finite element model and the PLAXIS 3D FOUNDATION results in a similar deflection pattern.

Note that the number on the legend bar of the developed finite element model on Figure 5.6 explains the deflection in unit of m; and the word MIPFE (Mindlin-Pasternak Finite Element) in the figure definition is the abbreviation for the developed finite element model. Therefore, if the word MIPFE is used in any part of this document it is to mean the developed finite element model.

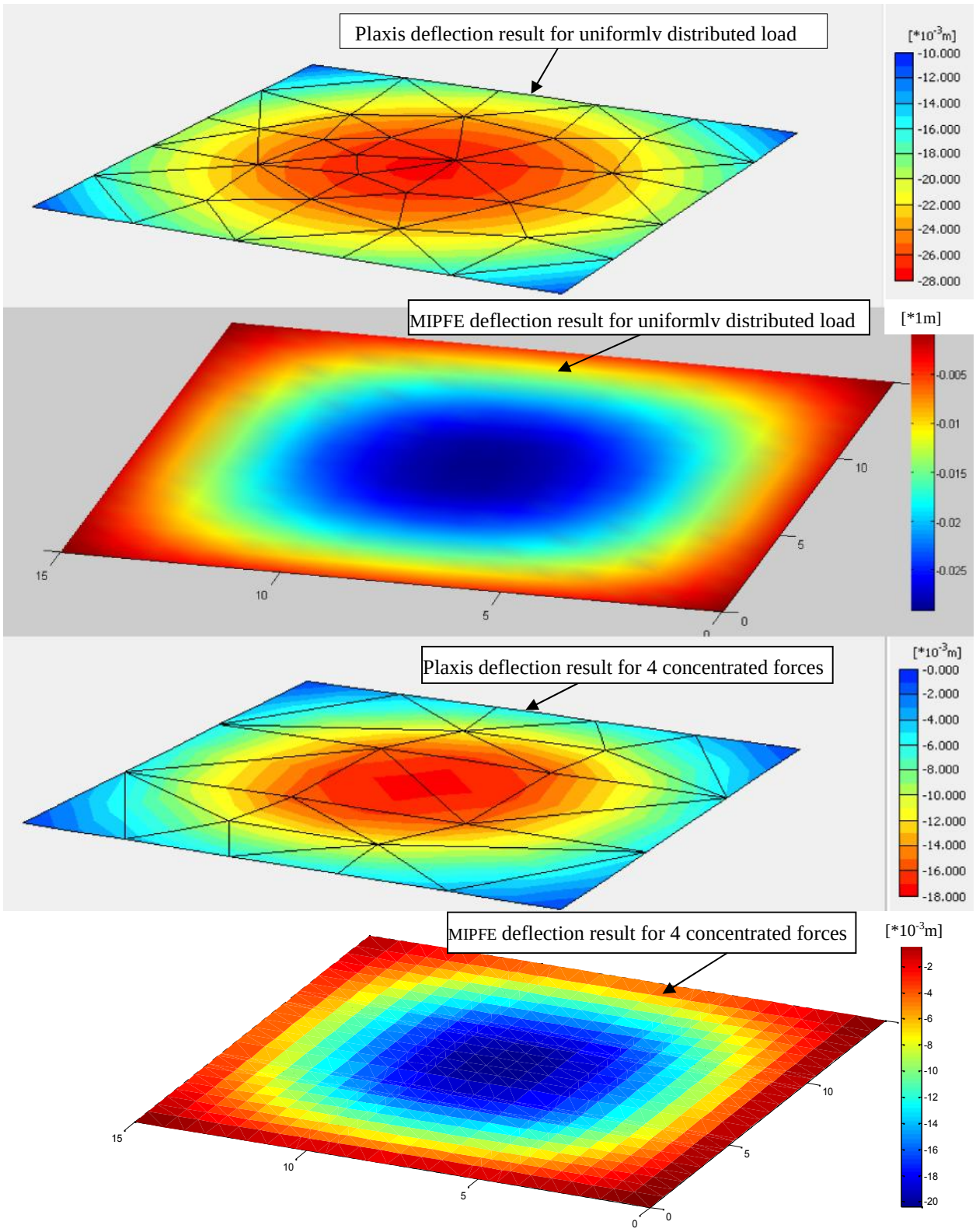

Figure 5.6: 3D deflection for uniformly distributed load and four concentrated forces.

5.4. Adjustment of the Model

As it is presented in Figure 5.6, both the developed finite model and PLAXIS 3D FOUNDATION show a similar deflection pattern. However, attention shall be given to the assessment of a deflection variation with respect to the variation of the soil stratum thickness, H. This is necessary, because the analytical subgrade employed is sensitive to H. For this reason, the difference in maximum deflection of the plate-soil model that is evaluated by the developed finite element and PLAXIS 3D FOUNDATION has to be investigated.

The maximum deflection of the plate-soil model is calculated by both the developed finite element model and PLAXIS 3D FOUNDATION. The comparison of maximum deflection of the plate for various thickness of soil stratum, thickness of plate, soil type, and area of plate shows that the maximum deflection evaluated by the developed finite element model is higher than the PLAXIS 3D FOUNDATION. It is observed that the difference in the maximum deflection between the two models has a close relationship to the thickness of the soil medium. Accordingly, the difference in maximum deflection increases as the thickness of the soil medium is increased.

As it is already discussed, the maximum deflection evaluated by MIPFE is higher than the maximum deflection evaluated by PLAXIS 3D FOUNDATION. This means, the stiffness of the plate-soil model calculated by MIPFE is underestimated as compared to the stiffness of plate-soil model evaluated by PLAXIS 3D FOUNADTION. This discrepancy is continuously magnified as the soil thickness is successively increased. This implies, the developed finite element model is suffering from the weakness of the employed soil subgrade model.

To understand the source of this discrepancy, it is helpful to assess the behavior of the first part of Equation (3.56). From this equation, the magnitude of the spring parameter of Pasternak's subgrade model continuously decreases as the soil thickness is increased. On the other hand, the shear parameter increases as the soil thickness is increased. However, the net effect of increasing the soil thickness is decreasing the soil stiffness, which makes the developed finite model sensitive to a soil thickness as compared with the PLAXIS 3D FOUNDATION. The typical Figure 5.7 is sketched for: uniformly distributed load=100kN/m^2, plate thickness=0.3m, soil Young's modulus=30MPa and plate aspect ratio=1. From this figure, the developed finite model is sensitive to soil thickness as compared with PLAXIS 3D FOUNDATION.

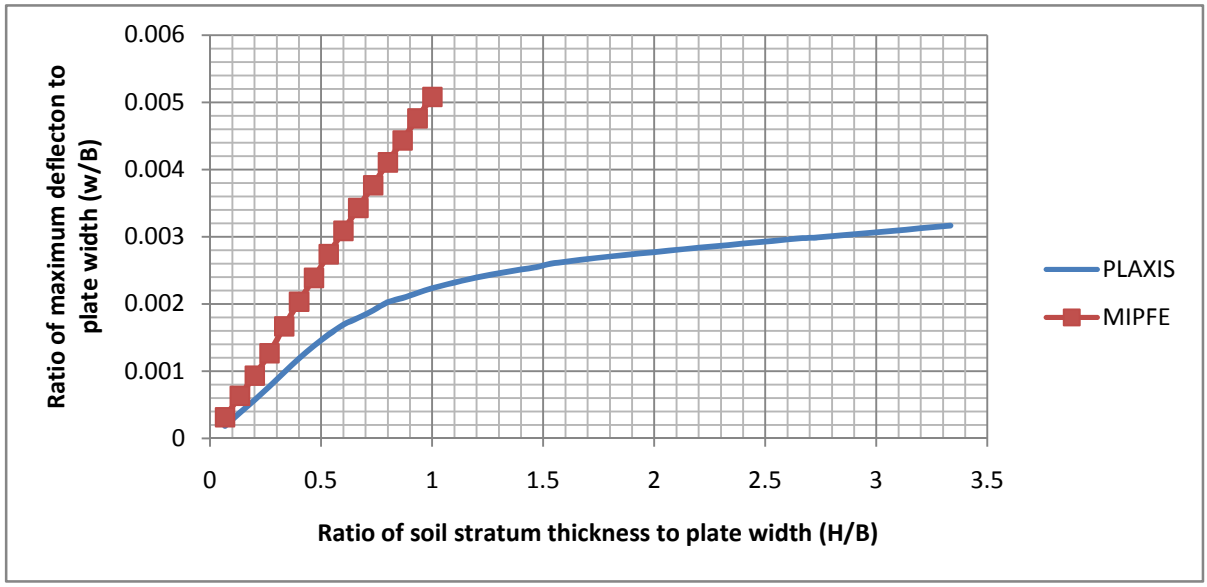

Figure 5. 7: Typical variation of maximum deflection with respect to soil stratum thickness.

As it is shown in Figure 5.7, the maximum deflection calculated by MIPFE does not show convergence behavior. From this observation and the above discussion, the sensitiveness of the developed finite element model can be limited by controlling the soil thickness.

The study of Worku has identified the above divergence behavior (refer to Figure 5.7) of a two-parameter subgrade model. Furthermore, this study recommends a method that brings the maximum deflection to a limiting value. This is performed by limiting the thickness of the soil stratum to certain maximum value. This value is obtained by equating the maximum deflection of a model that accounts a two-parameter with better finite element model [33]. In this research, this approach is used as benchmark, and then further modifications are done by observing the behavior of the maximum deflection for a different plate and soil properties (see the forthcoming pages for detail).

Adjustment factors are determined for different case of soil type, soil stratum thickness, plate thickness, plate size and load types. To determine a typical adjustment factor, the first step is to select soil type, plate thickness, plate size and load type, and then the soil stratum thickness is increased successively starting from small value. For each of these cases the maximum deflection is determined by both MIPFE and PLAXIS 3D FOUNDATION. Finally, the adjustment

factor is determined from the normalized graph of maximum deflection versus thickness of soil stratum (refer to Figure 5.8).

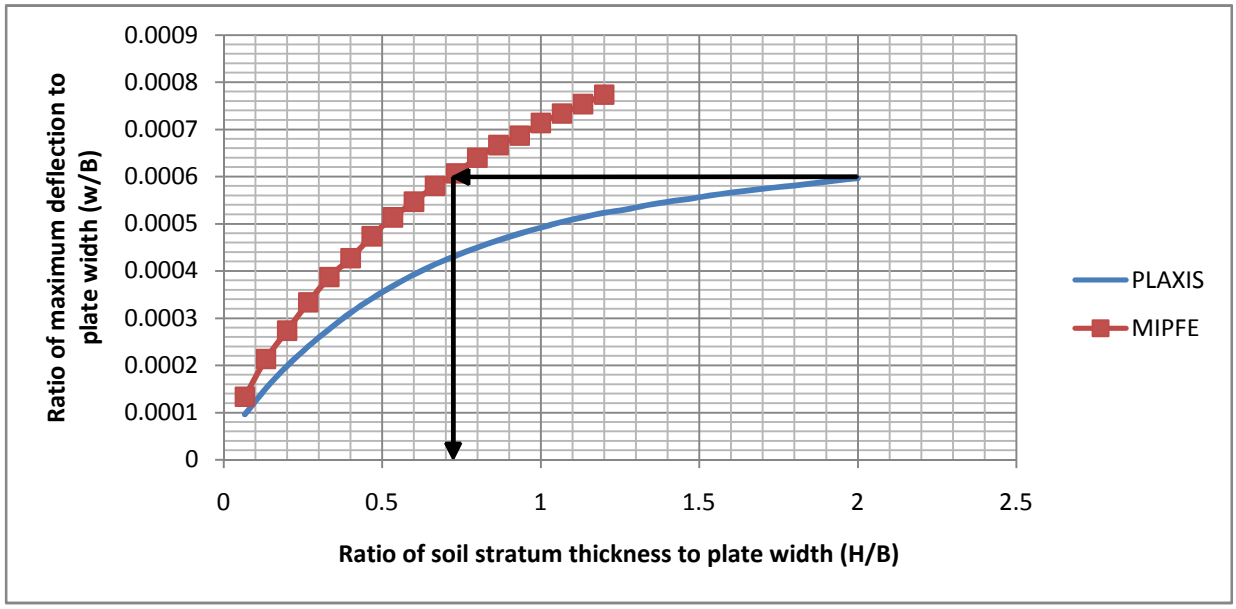

Figure 5. 8: Estimation of typical adjustment factor for concentrated load.

Following the same procedure schematically shown in Figure 5.8, adjustment factors are determined for concentrated forces, uniformly distributed load and mixed loading (concentrated loads and uniformly distributed load). Table 5.1 shows typical adjustment factors for mixed loading.

If it is required to determine the exact adjustment factors for all types of soil, plate thickness, plate size and loads types, then a lot of operations are needed, which is not practical. Therefore, typical adjustment factors have to be determined for selected types of soil, plate thickness, plate size and load types, and then the properties of these results have to be studied if it is possible to identify an approximate relationship.

The properties of the adjustment factors have to be identified with respect to soil Young's modulus, plate thickness, and plate aspect ratio for each load type. Figures 5.9, 5.10 and 5.11 show variations of the adjustment factor with respect to the soil Young's modulus (Es), plate thickness (h), and plate aspect ratio (L/B), respectively for a uniformly distributed load. A similar trend is observed for a concentrated and mixed loading type.

Table 5.1: Typical adjustment factors for mixed loading.

Soil Young's modulus (kN/m2)	Plate thickness (m)	Ratio of plate length to width (L/B)	Convergence adjustment factor(H/B)
30000	0.4	2	0.6
	0.6		0.7
	0.8		0.94
	1.2		1.2
	0.4	3	0.7
	0.6		0.95
	0.8		1.2
	1.2		1.5
60000	0.4	1	0.45
	0.6		0.52
	0.8		0.62
	1.2		0.8
	0.4	2	0.55
	0.6		0.65
	0.8		0.78
	1.2		1
	0.4	3	0.6
	0.6		0.7
	0.8		0.9
	1.2		1.3
	0.4	4	0.7
	0.6		0.8
	0.8		1
	1.2		1.6

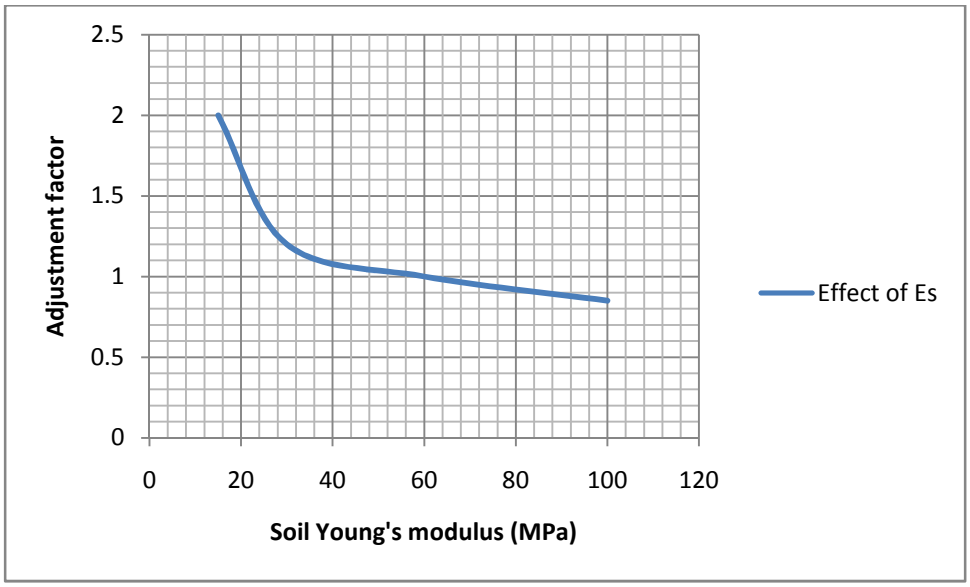

Figure 5. 9: Effect of soil Young's modulus on adjustment factor.

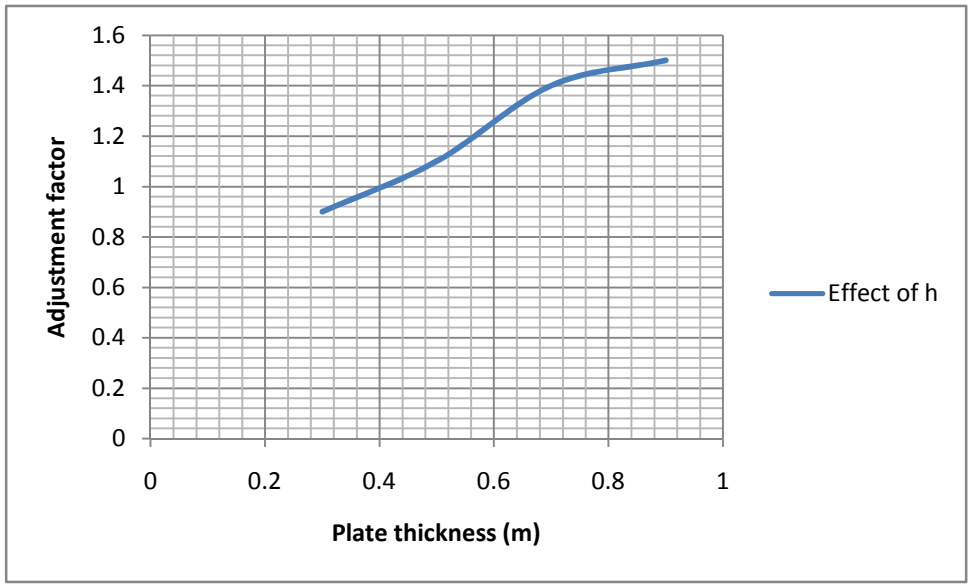

Figure 5.10: Effect of plate thickness on adjustment factor.

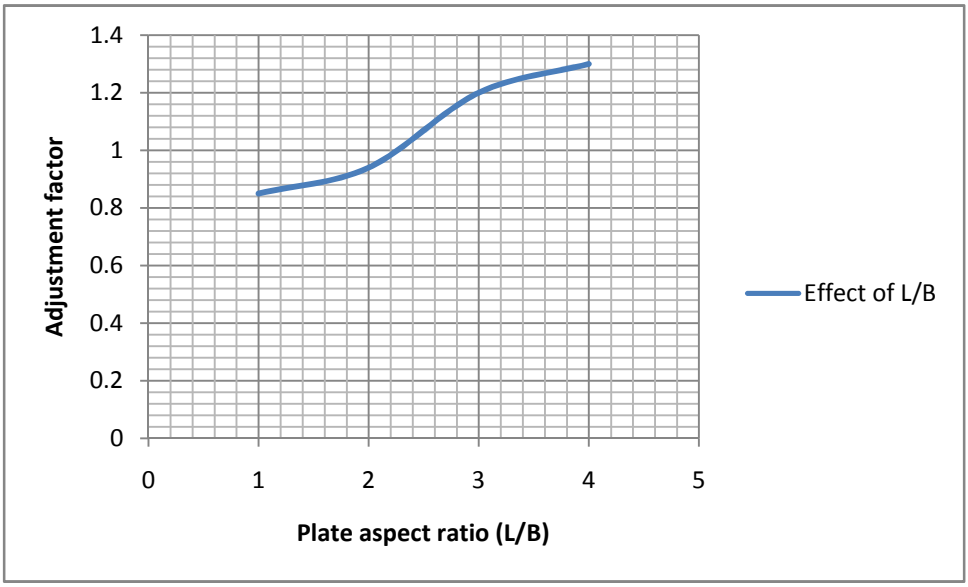

Figure 5. 11: Effect of plate aspect ratio on adjustment factor.

A vital observation from Figures 5.9, 5.10 and 5.11 is, if we have discrete set of adjustment factors for wide range of a soil type, plate thickness, and plate aspect ratio, then interpolation can be used to determine the unknown intermediate adjustment factors (see the Example at the end of this section). This implies, if a user provides input data of a soil type, plate thickness, and plate aspect ratio, then the respective adjustment factors are evaluated by interpolating between the known adjustment factors. Clearly, this approach has an advantage over a single adjustment factor that is obtained by curve fitting.

In this research, all the discrete adjustment factors and the interpolation operations are included in the developed computer program. Therefore, there is no user intervention for this purpose. Note that the adjustment factors are applied if the actual soil stratum thickness is greater than or equal to the plate width multiplied by the adjustment factor. On the other hand, if this value is greater than the given soil stratum thickness, then the actual soil stratum thickness is used.

Generally, a loaded plate that rests on an elastic foundation has greater depth of influence as compared with a beam under the same conditions. The depth of influence of a loaded plate is

radically increased as the loaded plate size is increased and the soil stiffness is decreased. A typical observation in this research indicates that the depth of influence reaches up to 88m. This is observed for a plate size of 15mx60m, a soil Young's modulus of 15MPa and a load of $100kN/m^2$.

As the depth of influence becomes large, using an adjustment factor that is determined by the above approach has a flaw. This can be further elaborated by referring to Figure 5.8. From this figure, the adjustment factor is around 0.73. According to the previous discussion, if the actual soil thickness is less than 0.73*B, then the actual soil thickness is used. However, as it is observed from this figure, a difference (error) in maximum deflection of the two models (MIPFE and PLAXIS 3D FOUNDATION) is also observed for soil thickness of less than 0.73*B. Hence, in order to decrease the difference in maximum deflection of the two models, the adjustment factor needs to be varied depth-wise. Thus, if we consider the typical adjustment factors in Table 5.1, they have to be replaced by adjustment factors that are a function of an actual soil stratum thickness (see Table 5.2a & 5.2b).

The depth-wise variation of an adjustment factor is determined from the relationships of the soil thickness required for MIPFE and PLAXIS 3D FOUNDATION such that both of them give equivalent maximum deflection. This implies, the adjusted soil thickness required for MIPFE is determined such that its maximum deflection is equivalent with the maximum deflection for the actual soil thickness obtained by using PLAXIS 3D FOUNDATION. In order to determine the exact depth-wise variation of an adjustment factor a lot operations are required for different soil types, plate thickness, plate size and load types, but this is difficult. Thus, an approximate depth-wise variation of adjustment factor is determined from discrete set of soil types, plate thickness, plate size and load types.

Figure 5.12 shows discrete points and fitted curve of the relationship between the actual soil stratum thickness (Ha) and the soil stratum thickness required for MIPFE (Hm) so that it gives equal maximum deflection as compared with PLAXIS 3D FOUNDATION. This figure is obtained for: concentrated load=4000kN, soil Young's modulus=30MPa, plate thickness=0.4m and plate aspect ratio (L/B)=1. If the soil stratum thickness required for MIPFE (Hm) is determined, then the adjustment factor is evaluated by dividing Hm to B.

As it is shown in Figure 5.12, the discrete points can be fitted by two independent curves, which are from **a** to **b** and from **b** to **c**. Accordingly, the relationship of Ha and Hm in between **a** and **b** is approximated by: Hm=(-0.0064*(Ha-4)+0.15)*(Ha-22)+5+0.06*(Ha-4). Similarly, the relationship of Ha and Hm in between **b** and **c** is given by: Hm=0.048*(Ha-22)+5. By following the same procedure, the depth-wise variation of adjustment factor is determined for discrete set of soil types, plate thickness, plate size and load types. Table 5.2a & 5.2b show a typical depth-wise variation adjustment factors for mixed loading, which replace the adjustment factors given in Table 5.1. Note that the limiting/maximum value of adjustment factor does not exceed the adjustment factor obtained by using the method in Figure 5.8.

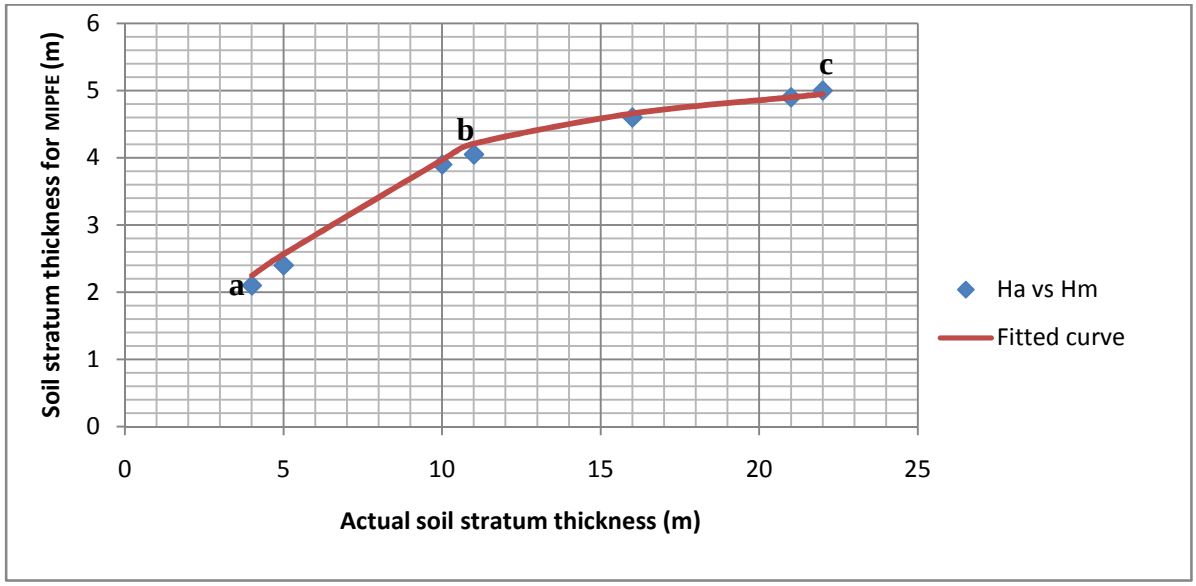

Figure 5.12: Typical relationship between the actual soil thickness (Ha) and the soil thickness required for MIPFE (Hm).

Finally, the user of the developed finite element model is required to provide the actual inputs for the soil thickness, soil material properties, plate material properties, plate dimensions and loading type and magnitude. The developed computer program performs all the operations required to determine the adjustment factor automatically. Refer the next example for illustration of the operations/series of interpolation.

Table 5.2a: Typical depth-wise variation of adjustment factors for mixed loading.

Soil Young's modulus (kN/m2)	Plate thickness (m)	Plate aspect ratio (L/B)	Adjustment factor (Hm/B) Note: C1=-0.00043*(Ha-4), C2=0.004*(Ha-4)
30000	0.4	2	(C1+0.011)*(Ha-41)+0.6+C2, Ha=<20
			0.0027*(Ha-41)+0.6, Ha>20
	0.6		(C1+0.014)*(Ha-41)+0.7+C2, Ha=<19
			0.006*(Ha-41)+0.7, Ha>19
	0.8		(C1+0.019)*(Ha-41)+0.94+C2, Ha=<20
			0.012*(Ha-41)+0.94, Ha>20
	1.2		(C1+0.024)*(Ha-41)+1.2+C2, Ha=<19
			0.016*(Ha-41)+1.2, Ha>19
	0.4	3	(C1+0.01)*(Ha-50)+0.7+C2, Ha=<19
			0.0036*(Ha-50)+0.7, Ha>19
	0.6		(C1+0.015)*(Ha-50)+0.87+C2, Ha=<19
			0.0072*(Ha-50)+0.87+C2, Ha>19
	0.8		(C1+0.021)*(Ha-50)+1.2+C2, Ha=<21
			0.013*(Ha-50)+1.2, Ha>21
	1.2		(C1+0.027)*(Ha-50)+1.5+C2, Ha=<21
			0.021*(Ha-50)+1.5, Ha>21
60000	0.4	1	(C1+0.0087)*(Ha-36)+0.47+C2, Ha=<15
			0.0027*(Ha-36)+0.47, Ha>15
	0.6		(C1+0.01)*(Ha-36)+0.53+C2, Ha=<15
			0.0038*(Ha-36)+0.53, Ha>15
	0.8		(C1+0.012)*(Ha-36)+0.61+C2, Ha=<14
			0.0063*(Ha-36)+0.61, Ha>14
	1.2		(C1+0.017)*(Ha-36)+0.8+C2, Ha=<14
			0.012*(Ha-36)+0.8, Ha>14

Table 5.2b: Typical depth-wise variation of adjustment factors for mixed loading.

Soil Young's modulus (kN/m2)	Plate thickness (m)	Plate aspect ratio (L/B)	Adjustment factor (Hm/B) Note: C1=-0.00043*(Ha-4), C2=0.004*(Ha-4)
60000	0.4	2	(C1+0.01)*(Ha-41)+0.55+C2, Ha=<17
			0.0031*(Ha-41)+0.55, Ha>17
	0.6		(C1+0.012)*(Ha-41)+0.63+C2, Ha=<18
			0.0047*(Ha-41)+0.63, Ha>18
	0.8		(C1+0.014)*(Ha-41)+0.73+C2, Ha=<18
			0.0067*(Ha-41)+0.73, Ha>18
	1.2		(C1+0.02)*(Ha-41)+1+C2, Ha=<17
			0.013*(Ha-41)+1, Ha>17
	0.4	3	(C1+0.0093)*(Ha-50)+0.61+C2, Ha=<16
			0.0034*(Ha-50)+0.61, Ha>16
	0.6		(C1+0.011)*(Ha-50)+0.73+C2, Ha=<16
			0.0055*(Ha-50)+0.73, Ha>16
	0.8		(C1+0.014)*(Ha-50)+0.87+C2, Ha=<16
			0.008*(Ha-50)+0.87, Ha>16
	1.2		(C1+0.022)*(Ha-50)+1.26+C2, Ha=<19
			0.015*(Ha-50)+1.26, Ha>19
	0.4	4	(C1+0.0087)*(Ha-60)+0.67+C2, Ha=<15
			0.0036*(Ha-60)+0.67, Ha>15
	0.6		(C1+0.011)*(Ha-60)+0.8+C2, Ha=<16
			0.0053*(Ha-60)+0.8, Ha>16
	0.8		(C1+0.014)*(Ha-60)+1.02+C2, Ha=<15
			0.0093*(Ha-60)+1.02, Ha>15
	1.2		(C1+0.023)*(Ha-60)+1.55+C2, Ha=<11
			0.02*(Ha-60)+1.55, Ha>11

After determining discrete adjustment factors by the above discussed approaches, showing the steps to determine an adjustment factor for any given problem creates a clear visualization of the way an adjustment factor is evaluated.

Consider an Example with the following input parameters: soil Young's modulus (Es)=40MPa, actual soil stratum thickness (Ha)=30m, plate thickness (h)=0.9m, plate aspect ratio (L/B)=2.5 and the loading contains both distributed load and concentrated forces. The adjustment factor (AF) is determined as follows:

1. The given load type is distributed load and concentrated forces (mixed loading), hence the adjustment factor is found by interpolation from the discrete adjustment factors of Table 5.2a & 5.2b.
2. The interpolation with respect of the plate thickness for L/B=2, Es=30MPa & 60MPa is performed as follows:
   2.1. Go to Table 5.2a, then for Es=30MPa, L/B=2 and h=0.8m, the adjustment factor obtained for Ha=30m is **0.808**. Similarly, the adjustment factor for Es=30MPa, L/B=2 and h=1.2m is **1.02**. Therefore, the adjustment factor for Es=30MPa, L/B=2 and h=0.9m is found by linear interpolation as follows:

$$AF_{302} = \frac{1.02 - 0.808}{1.2 - 0.8}(0.9 - 0.8) + 0.808 = 0.861$$

   2.2. Go to Table 5.2b, then for Es=60MPa, L/B=2 and h=0.8m, the adjustment factor obtained for Ha=30m is **0.6563**. Similarly, the adjustment factor for Es=60MPa, L/B=2 and h=1.2m is **0.857**. Thus, the adjustment factor for Es=60MPa, L/B=2 and h=0.9m is found by linear interpolation as follows:

$$AF_{602} = \frac{0.857 - 0.6563}{1.2 - 0.8}(0.9 - 0.8) + 0.6563 = 0.706$$

3. The interpolation with respect to soil Young's modulus for L/B=2 is performed as follows:

   For Es=40MPa, L/B=2 and h=0.9m, the adjustment factor is obtained by linear interpolation as follows:

$$AF_{402} = \frac{AF_{602} - AF_{302}}{60 - 30}(40 - 30) + AF_{302} = 0.809$$

4. The interpolation with respect to plate thickness for L/B=3, Es=30MPa & 60MPa is performed as follows:

   4.1. Go to Table 5.2a, then for Es=30MPa, L/B=3 and h=0.8m, the adjustment factor obtained for Ha=30m is **0.94**. Similarly, the adjustment factor for Es=30MPa, L/B=3 and h=1.2m is **1.08**. Therefore, the adjustment factor for Es=30MPa, L/B=3 and h=0.9m is found by linear interpolation as follows:

$$AF_{303} = \frac{1.08 - 0.94}{1.2 - 0.8}(0.9 - 0.8) + 0.94 = 0.975$$

   4.2. Go to Table 5.2b, then for Es=60MPa, L/B=3 and h=0.8m, the adjustment factor obtained for Ha=30m is **0.71**. Similarly, the adjustment factor for Es=60MPa, L/B=3 and h=1.2m is **0.96**. Thus, the adjustment factor for Es=60MPa, L/B=3 and h=0.9m is found by linear interpolation as follows:

$$AF_{603} = \frac{0.96 - 0.71}{1.2 - 0.8}(0.9 - 0.8) + 0.71 = 0.7725$$

5. The interpolation with respect to soil Young's modulus for L/B=3 is performed as follows:

   For Es=40MPa, L/B=3 and h=0.9m, the adjustment factor is obtained by linear interpolation as follows:

$$AF_{403} = \frac{AF_{603} - AF_{303}}{60 - 30}(40 - 30) + AF_{303} = 0.9075$$

6. Finally, the interpolation with respect to plate aspect ratio is performed as follows:

   For Es=40MPa, L/B=2.5 and h=0.9m, the adjustment factor is obtained by linear interpolation as follows:

$$AF = \frac{AF_{403} - AF_{402}}{3 - 2}(2.5 - 2) + AF_{402} = 0.858$$

6. Numerical Examples and Comparisons

6.1. General Introduction

Simple and general verifications of the developed finite element model are already discussed in Section 5.3; however, these verifications do not fully indicate the degree of accuracy of the developed finite element model as compared to 3D finite element model. Hence, refined verifications of the developed finite element model are presented in this chapter. These verifications are performed by comparing the results of the developed finite element model with PLAXIS 3D FOUNDATION.

In order to identify the prediction capacity of PLAXIS 3D FOUNDATION, documents of validation and verification of the implemented version of PLAXIS 3D FOUNDATION are reviewed. There is a manual titled "PLAXIS 3D FOUNDATION Validation Manual" that discusses about verification of the software. The verification of PLAXIS 3D FOUNDATION is done by comparing with known theoretical solution of simple problems. For example, the solution of a plate with a fixed displacement boundary condition and uniform distributed load is determined by both PLAXIS 3D FOUNDATION and theoretical solution method. It is indicated that the error is below 2.5% for both the displacement and bending moment [18]. Therefore, it has to be understood that the simulation performance of PLAXIS 3D FOUNDATION for all plate problems is measured by this typical verification method. This implies that a refined verification method such as validation is not used. Hence, there might be a deviation of the PLAXIS 3D FOUNDATION's solution from its respective physical /prototype model's solution.

In the following sections, numerical examples are given for different types of loadings, soils, and plates. The examples are selected such that the effect of a soil Young's modulus, soil thickness, plate thickness, plate aspect ratio, and loading type are considered. Each example is solved by both the developed finite element model and PLAXIS 3D FOUNDATION. Graphical comparisons are presented for displacement, shear force, and bending moment.

6.2. Plates Subjected to Uniformly Distributed Loads

Two examples are discussed for uniformly distributed type of load. The only difference between the two examples is the type of soil. The comparison with respect to deflection, shear force, and bending moment is presented by considering the same mesh line for both the PLAXIS 3D FOUNDATION and developed finite element model. However, the mesh design in PLAXIS 3D FOUNDATION is unstructured. For this reason, it is not possible to get exact straight mesh line as compared with the developed finite element model's mesh orientation. Such difference contributes to the discrepancy of results, because the solutions of the PLAXIS 3D FOUNDATION and developed finite element model do not exactly lie at the same mesh line.

Tables 6.1 and 6.2 show the material properties and loading for the two examples, respectively. The graphical comparisons of deflection, shear force, and bending moment are presented in Figures 6.2 and 6.3.

Table 6.1: Material properties and loading for the first example of uniformly distributed load.

Loose Sand Properties		**Plate Properties**		**Loading**
Young's modulus	30000kN/m^2	Young's modulus	25000000kN/m^2	70kN/m^2
Poisson's ratio	0.3	Poisson's ratio	0.2	
Saturated density	20kN/m^2	Plate density	24kN/m^2	
Unsaturated density	18kN/m^2	Plate length (L)	15m	
Friction angle	Not required	Plate width (B)	15m	
Soil thickness	10m	Plate thickness (h)	0.4m	

Table 2.2: Material properties and loading for the second example of uniformly distributed load.

Stiff Clay Properties		**Plate Properties**		**Loading**
Young's modulus	100000kN/m^2	Young's modulus	25000000kN/m^2	70kN/m^2
Poisson's ratio	0.3	Poisson's ratio	0.2	
Saturated density	22kN/m^2	Plate density	24kN/m^2	
Unsaturated density	18kN/m^2	Plate length (L)	15m	
Cohesive strength	Not required	Plate width (B)	15m	
Soil thickness	10m	Plate thickness(h)	0.4m	

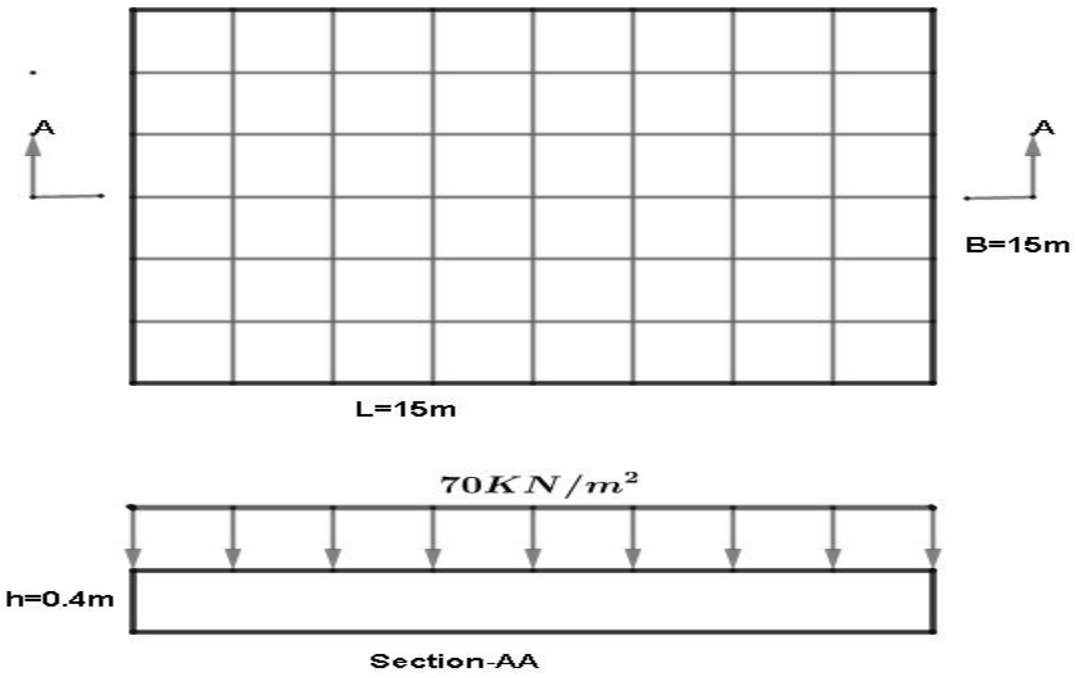

Figure 6.1: Plate dimensions and applied load magnitude for uniformly distributed load case.

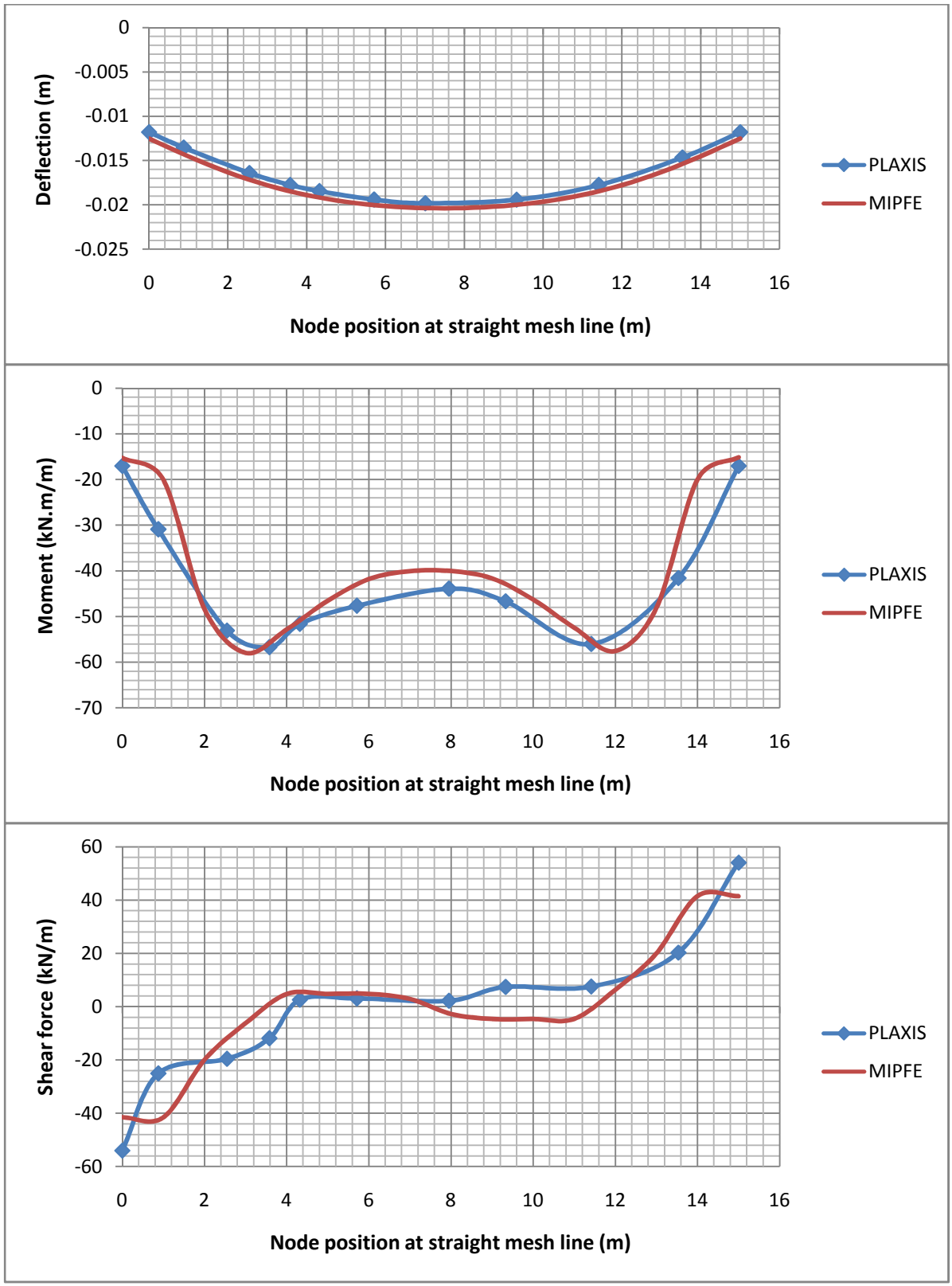

Figure 6. 2: Solution comparisons for the material properties and loading in Table 6.1.

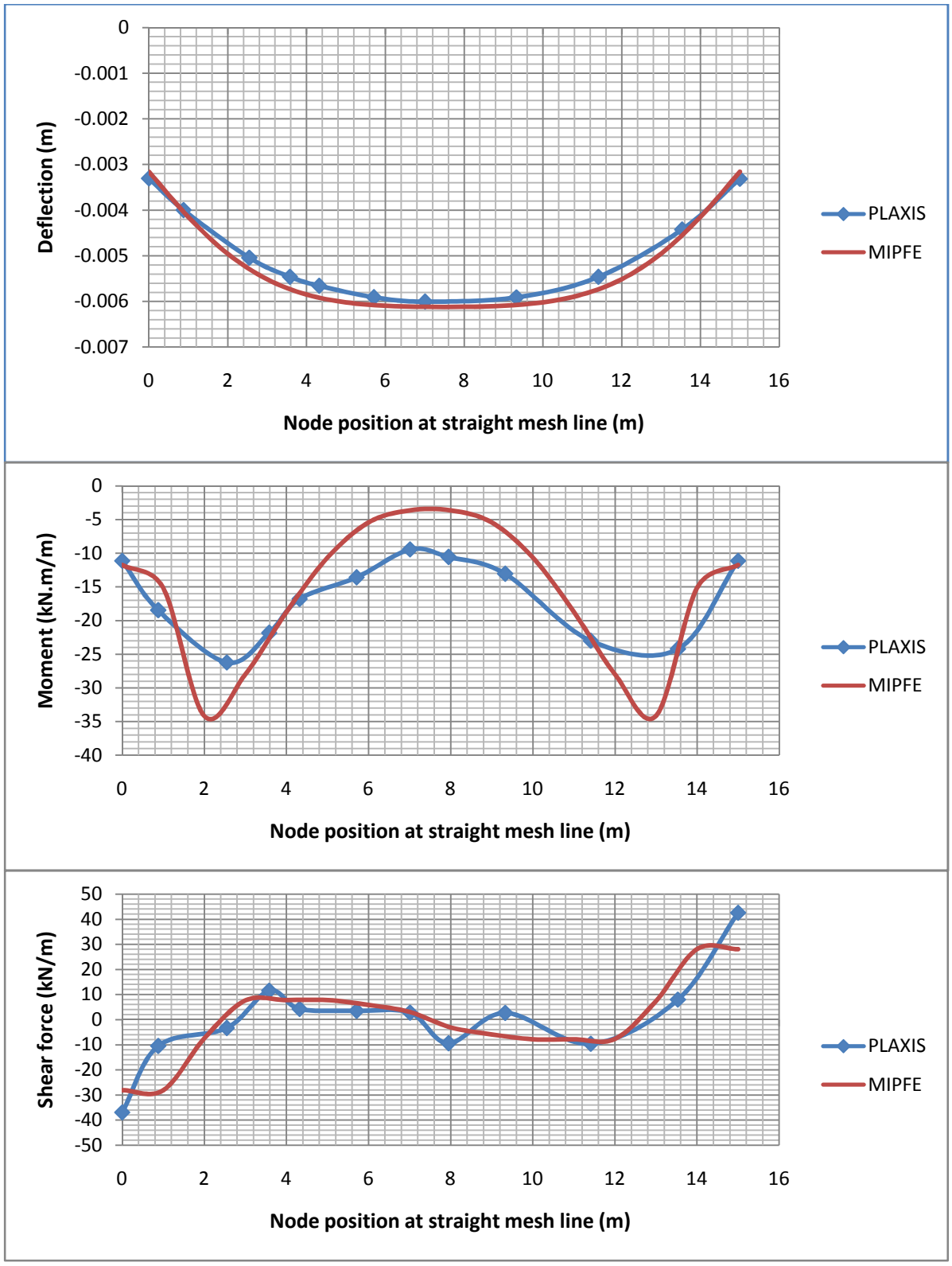

Figure 6. 3: Solution and comparisons for the material properties and loading in Table 6.2.

In the above two examples for distributed load, the influence of varying the soil type is observed. Accordingly, the magnitude of maximum deflection, maximum shear force, and maximum bending moment decrease as the soil Young's modulus is increased. Both PLAXIS 3D FOUNDATION and MIPFE reflect this trend. Regarding the maximum bending moment, PLAXIS 3D FOUNDATION becomes sensitive to the soil Young's change as compared with MIPFE.

6.3. Plates Subjected to Concentrated Forces

In order to demonstrate the behavior of deflection, shear force and bending moment after the application of concentrated loads, four concentrated forces with separation distance of 5m in x-direction and 3m in y-direction are used. Four types of examples are implemented. The only difference between these examples is the soil thickness and the soil type. The detail material properties and loading are shown in Tables 6.3 and 6.4, respectively. The graphical comparisons of the deflection, shear force, and bending moment are presented on Figure 6.5 to Figure 6.8. Note that the plate contains four columns and it is symmetric with respect to the loading and the geometry (refer to Figure 6.4).

Table 6.3: Material properties, concentrated forces, shallow thickness of soil and loose soil.

Loose Sand Properties		**Plate Properties**		**Loading**
Young's modulus	30000kN/m^2	Young's modulus	25000000kN/m^2	2000kN per each column
Poisson's ratio	0.3	Poisson's ratio	0.2	
Saturated density	20kN/m^2	Plate density	24kN/m^2	
Unsaturated density	18kN/m^2	Plate size (BxL)	12mx20m	
Friction angle	Not required	Plate thickness (h)	0.7m	
Soil thickness	5m	Column spacing (x,y)	(5m,3m)	

Table 6.4: Material properties, concentrated forces, shallow thickness of soil and stiff soil.

Stiff Clay Properties		**Plate Properties**		**Loading**
Young's modulus	100000kN/m^2	Young's modulus	25000000kN/m^2	2000kN per each column
Poisson's ratio	0.3	Poisson's ratio	0.2	
Saturated density	22kN/m^2	Plate density	24kN/m^2	
Unsaturated density	18kN/m^2	Plate size (BxL)	12mx20m	
Cohesive strength	Not required	Plate thickness (h)	0.7m	
Soil thickness	5m	Column spacing (x,y)	(5m,3m)	

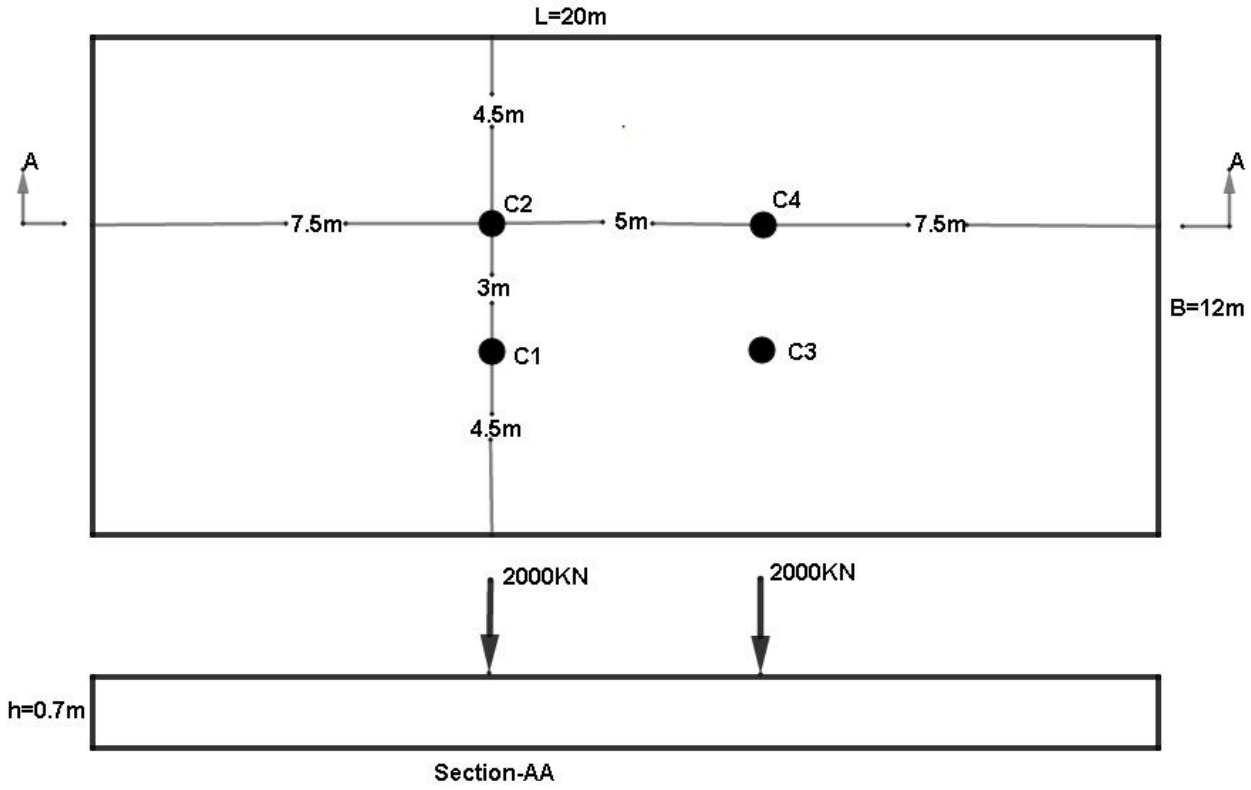

Figure 6.4: Plate dimensions and positions of applied concentrated forces.

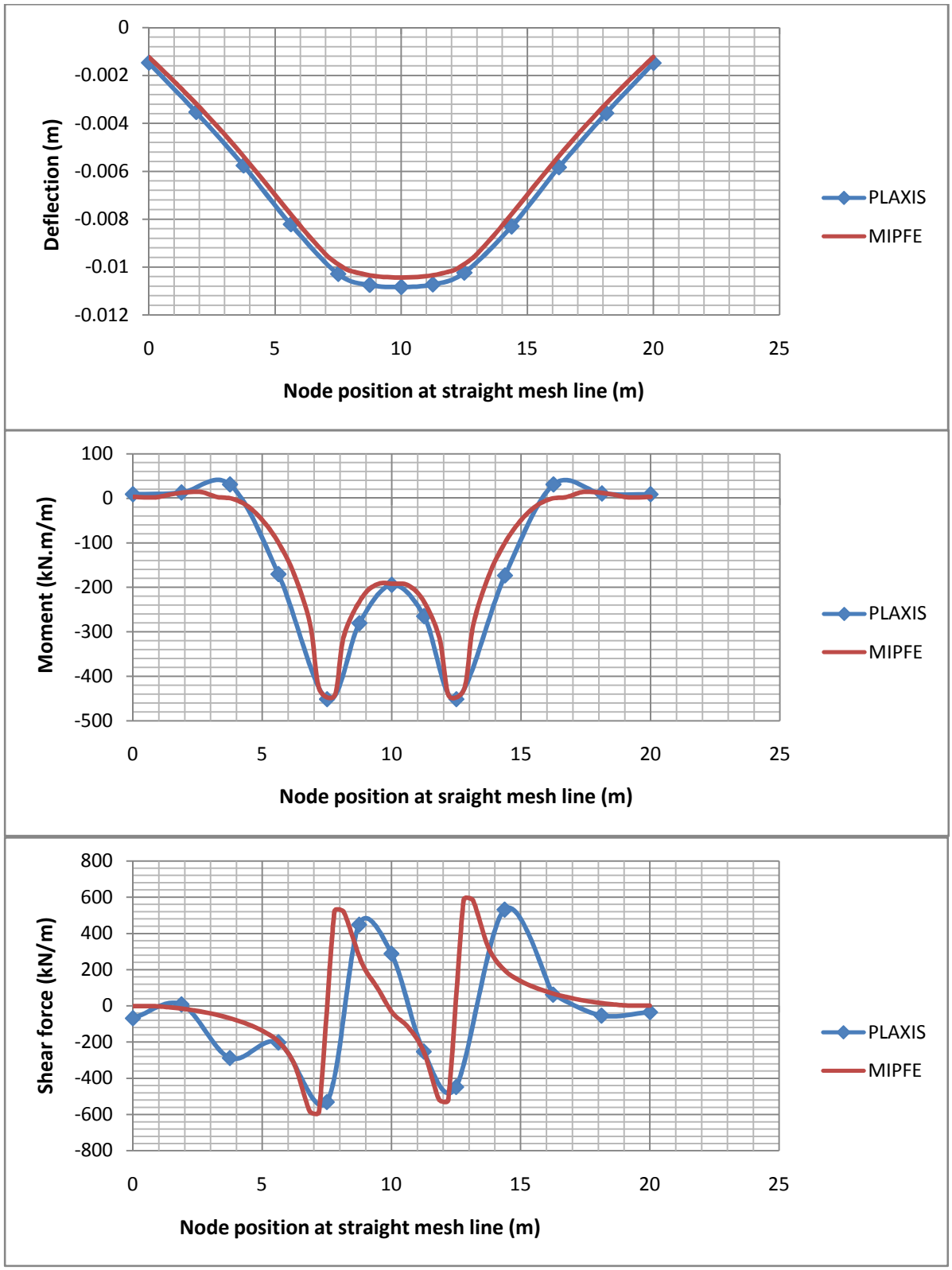

Figure 6. 5: Solution comparisons for material properties and loading in Table 6.3.

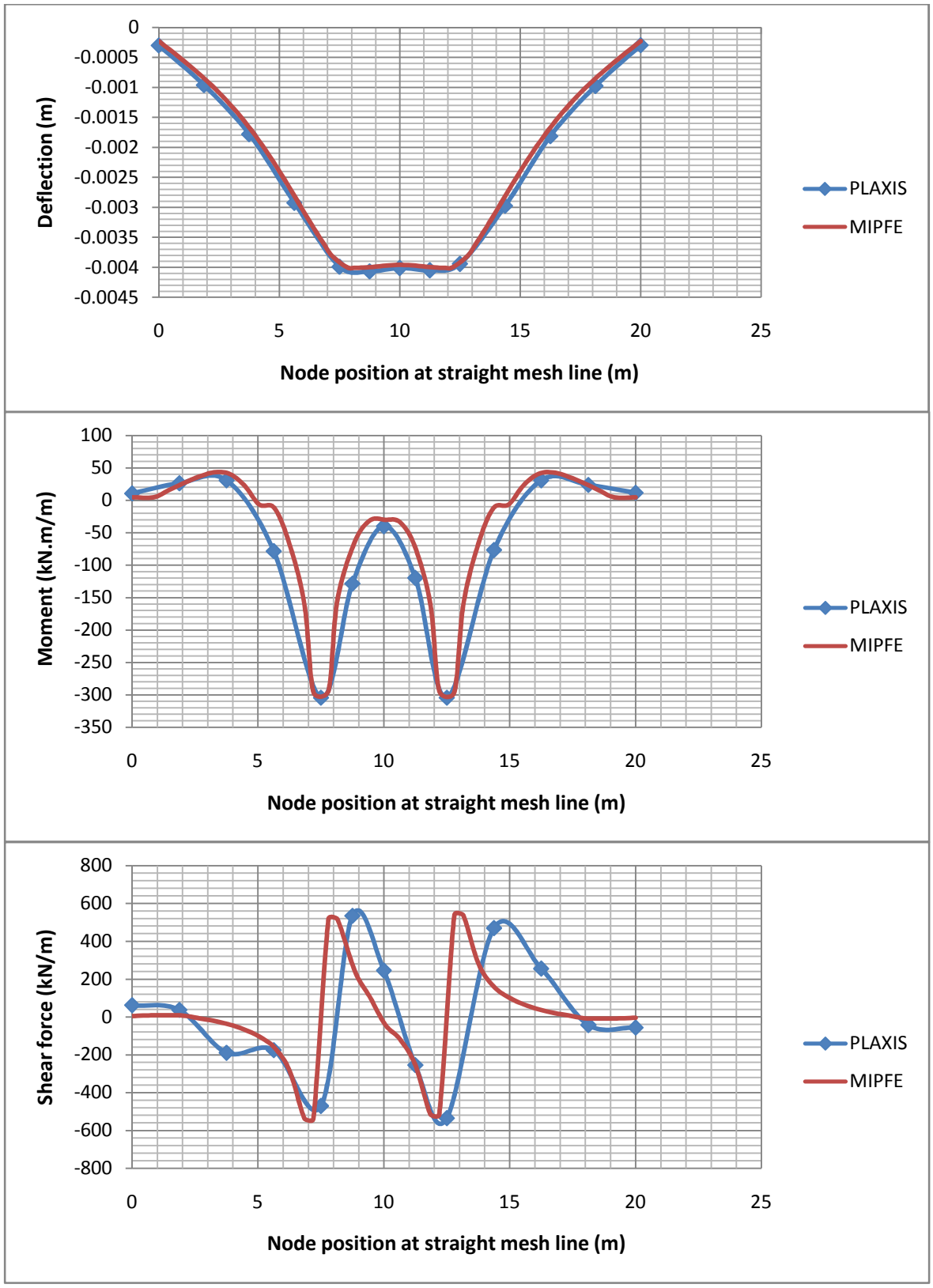

Figure 6.6: Solution comparisons for the material properties and loading in Table 6.4.

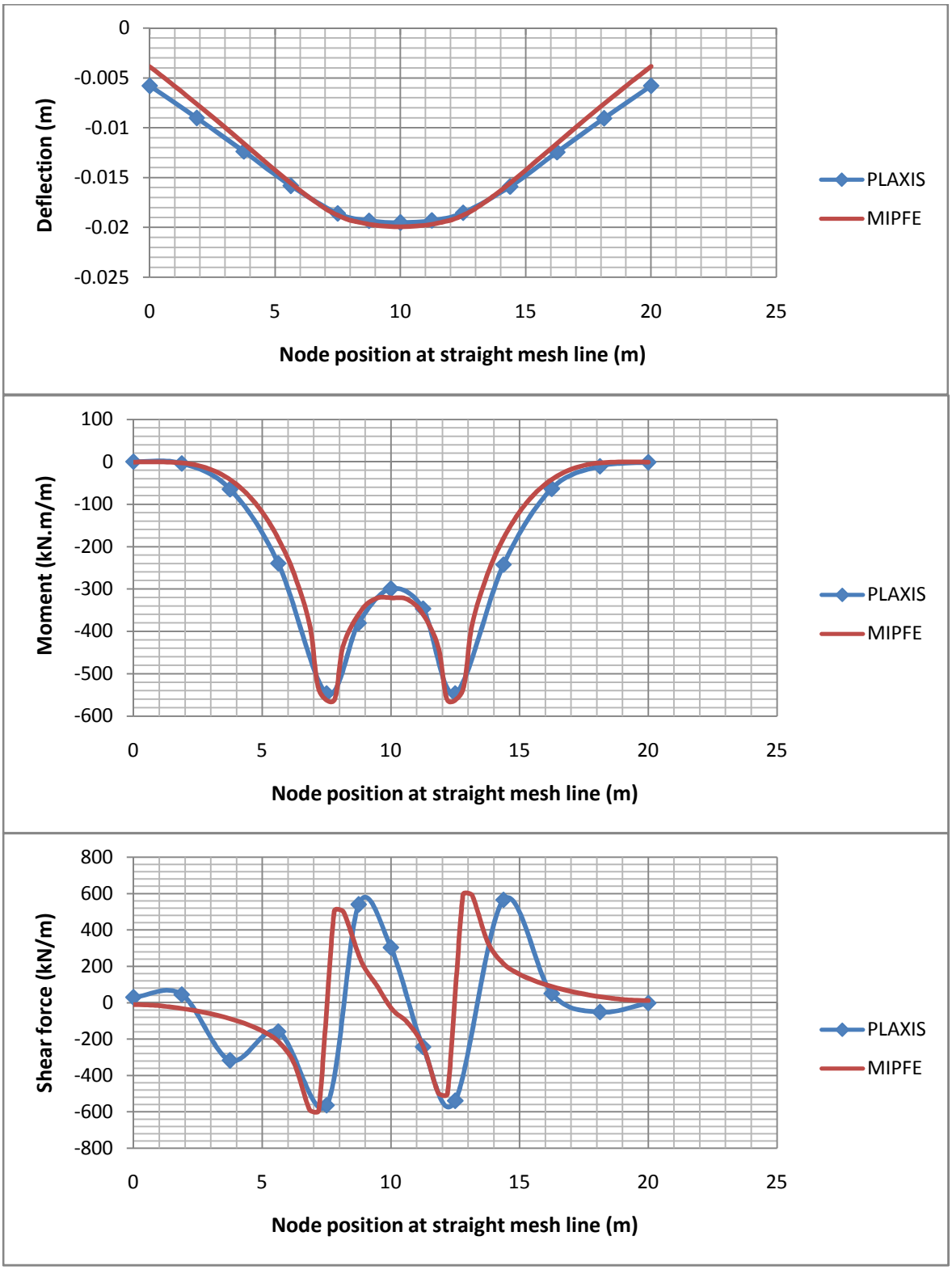

Figure 6.7: Solution comparisons for the material properties and loading in Table 6.3, but soil thickness is 15m.

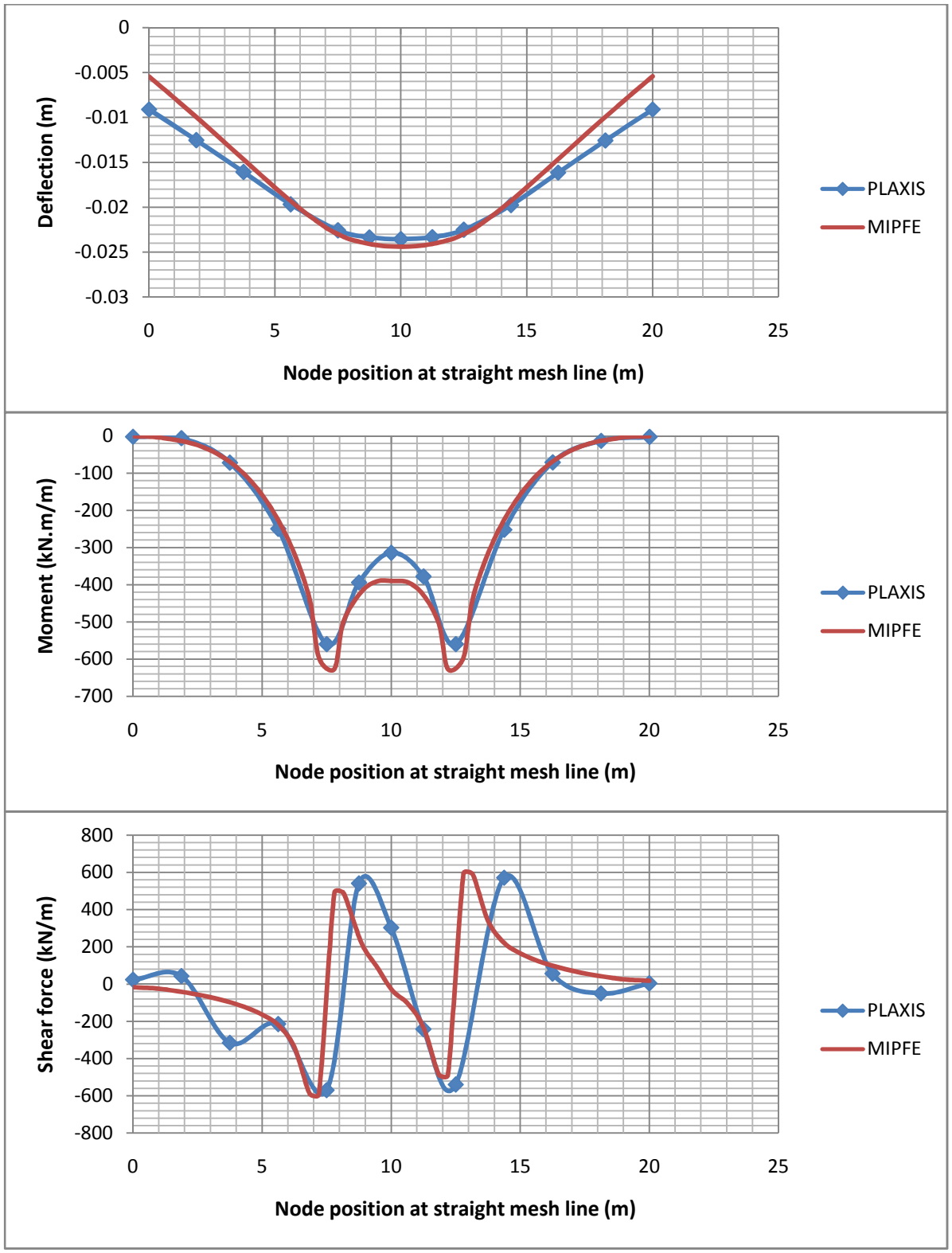

Figure 6.8: Solution comparisons for the material properties and loading in Table 6.3, but the soil thickness is 30m.

In the above four example for concentrated forces, the first two examples try to look the effect of varying in the soil Young's modulus and the remaining two are employed to check the effect of soil thickness. From these examples, the deflections and the bending moments estimated by MIPFE in all the four examples are generally in good agreement with the results of PLAXIS 3D FOUNDATION. The shear forces of both models are generally in fairly good agreement except indicating the maximum shear force at closer locations rather being at same location.

6.4. Plates Subjected to Mixed Loading

The examples given in this section are for mixed loading. The mixed loading consists of only uniformly distributed load and concentrated forces. Bending moment is excluded from the mixed loading, because bending moment is not included in the PLAXIS 3D FOUNDATION's input load category. However, the developed finite element model supports bending moment input. The accuracy of finite element model solution is mainly controlled by the global stiffness matrix and boundary condition. Therefore, if the bending moment is assembled to the right position of the global load vector, then including the bending moment in the mixed loading will not be a major accuracy problem but this has to be proved by comparing the result of MIPFE with other full-fledged finite element software that supports bending moment as input load.

In the following four examples for mixed loading, four concentrated forces and a uniformly distributed load are used. The intention of the examples is to identify the effect of variation in plate aspect ratio and plate thickness. The detail material properties and loadings for the four examples are shown in Table 6.5. The graphical comparisons for deflection, shear force, and bending moment are shown in Figure 6.10 to Figure 6.13. The plates are symmetrical with respect to loading and geometry (refer to Figure 6.9). Figure 6.9 shows the plate dimensions in terms of the plate thickness (h), plate length (L), plate width (B) and column spacing (x,y). The values of these variables are obtained from Table 6.5.

Table 6.5: Material properties and mixed loading values.

Loose Sand Properties		**Plate Properties**		**Loading**
Young's modulus	60000kN/m^2	Young's modulus	25000000kN/m^2	1000kN per each column **and** 30kN/m^2
Poisson's ratio	0.3	Poisson's ratio	0.2	
Saturated density	20kN/m^2	Plate density	24kN/m^2	
Unsaturated density	18kN/m^2	The plate size, plate thickness and column spacing for different cases are:		
Soil thickness	15m			
Case	**Plate size (BxL)**	**Plate thickness (h)**		**Column spacing**
1	15mx15m	0.8m		(5m,5m)
2	15mx30m	0.8m		(10m,5m)
3	15mx45m	0.8m		(10m,5m)
4	15mx30m	0.6m		(10m,5m)

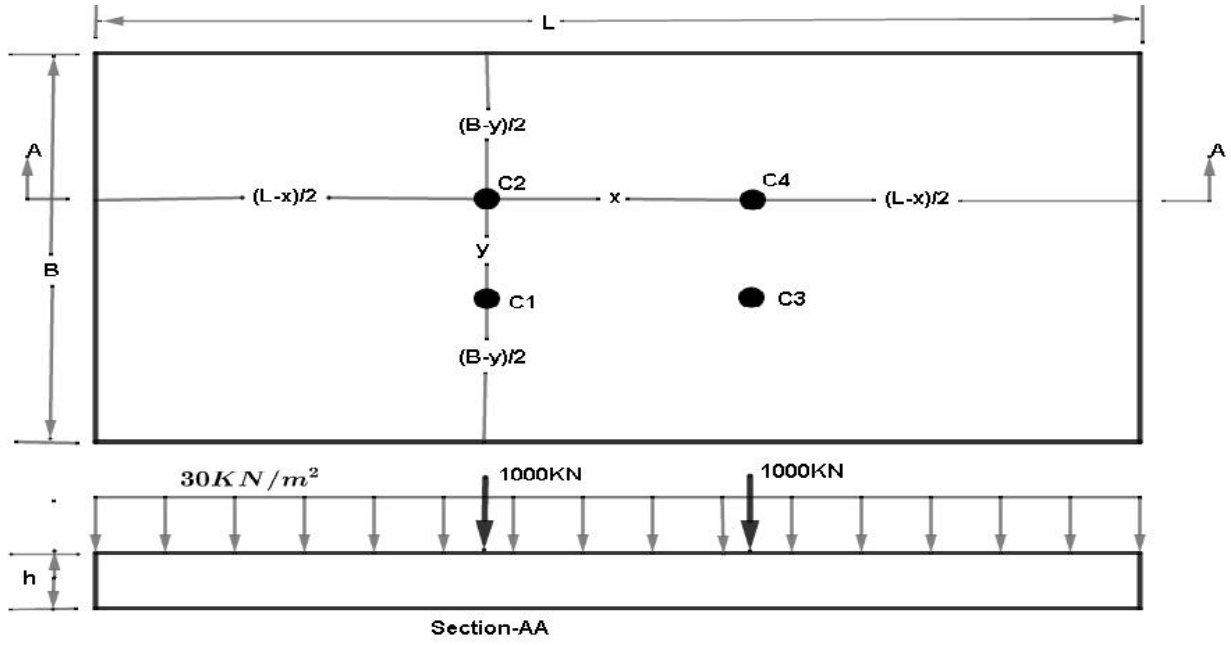

Figure 6.9: Plate dimensions and load positions for mixed loading case.

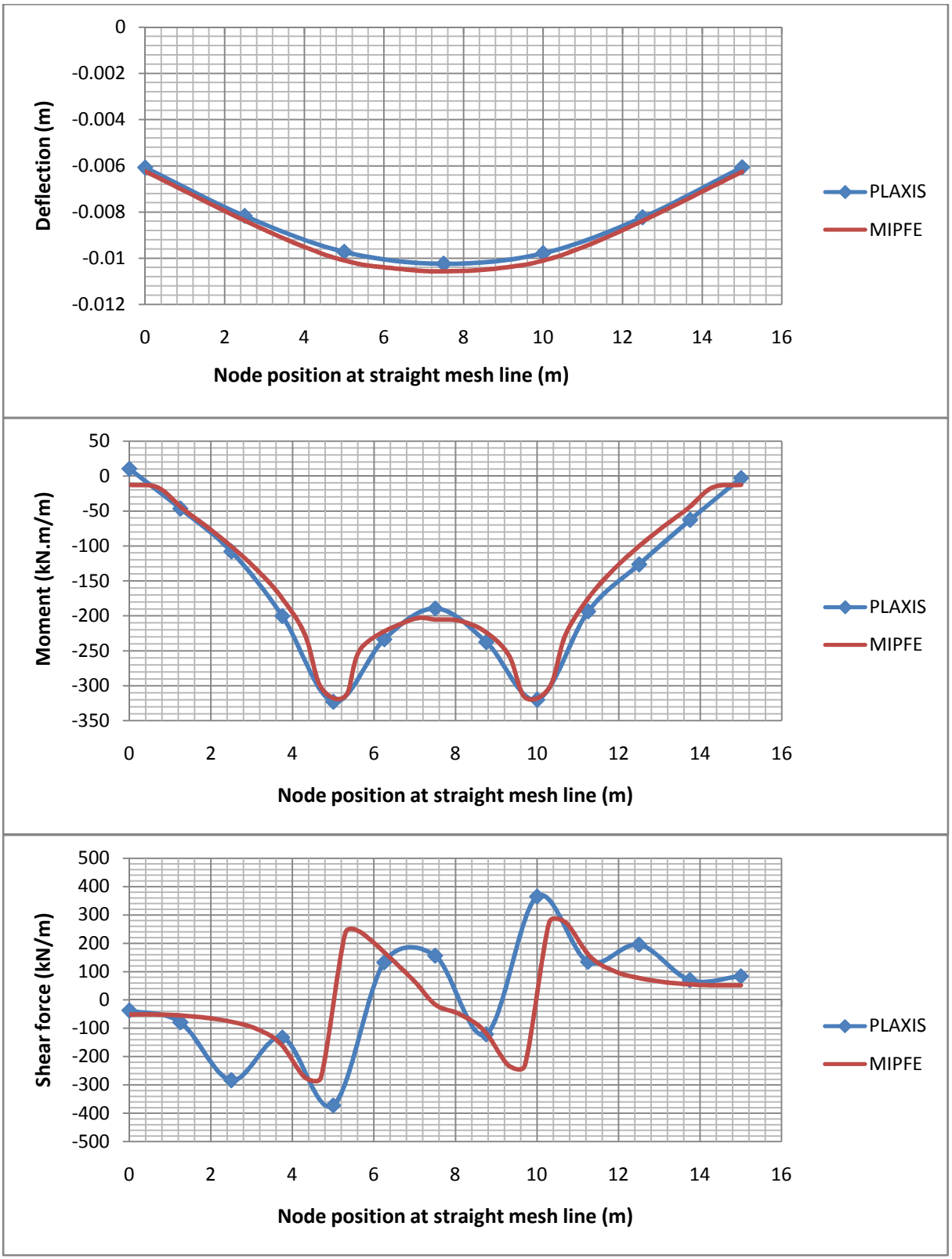

Figure 6.10: Solution comparisons for the material properties, loading and case 1 of Table 6.5.

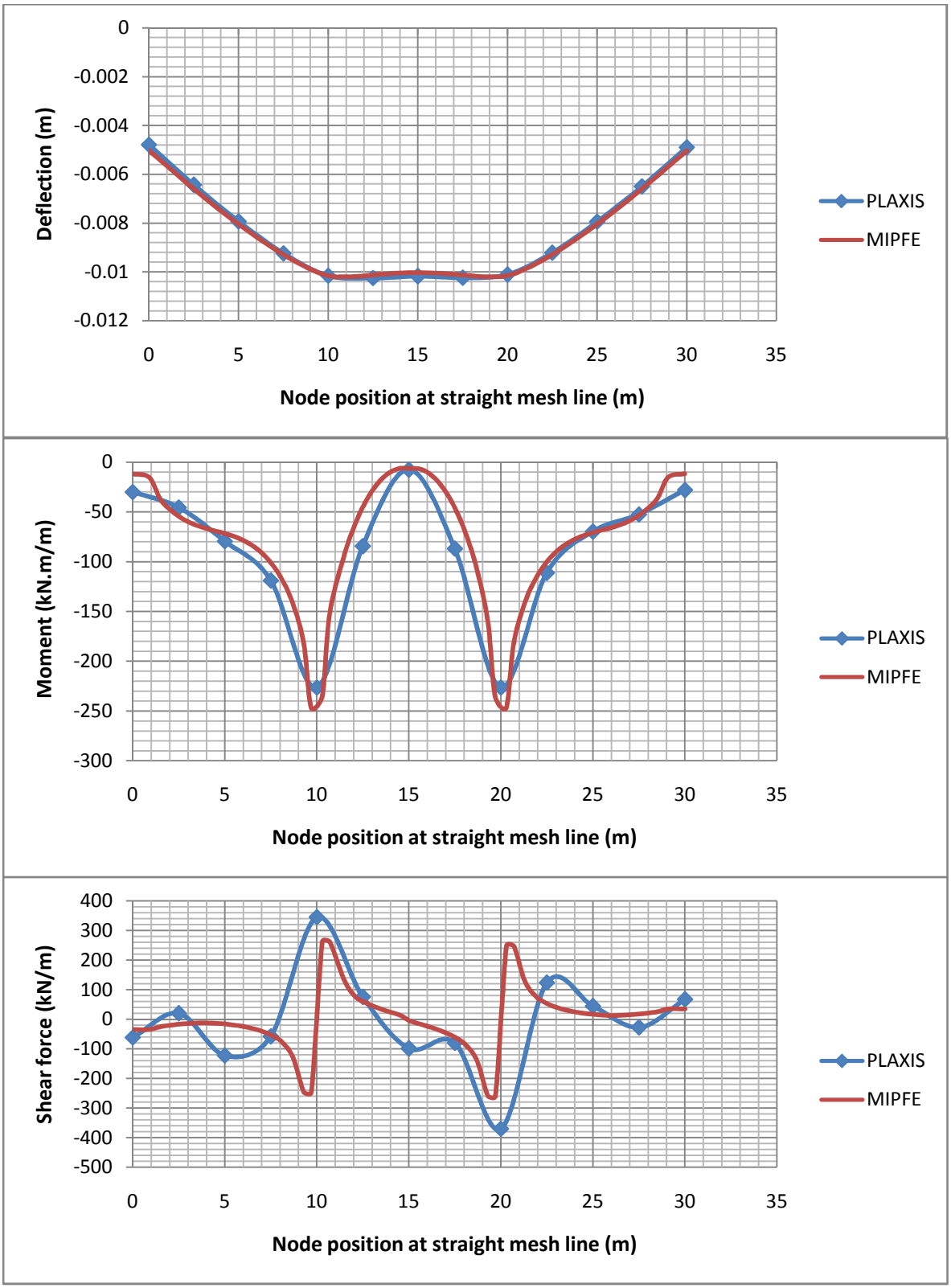

Figure 6.11: Solution comparisons for the material properties, loading and case 2 of Table 6.5.

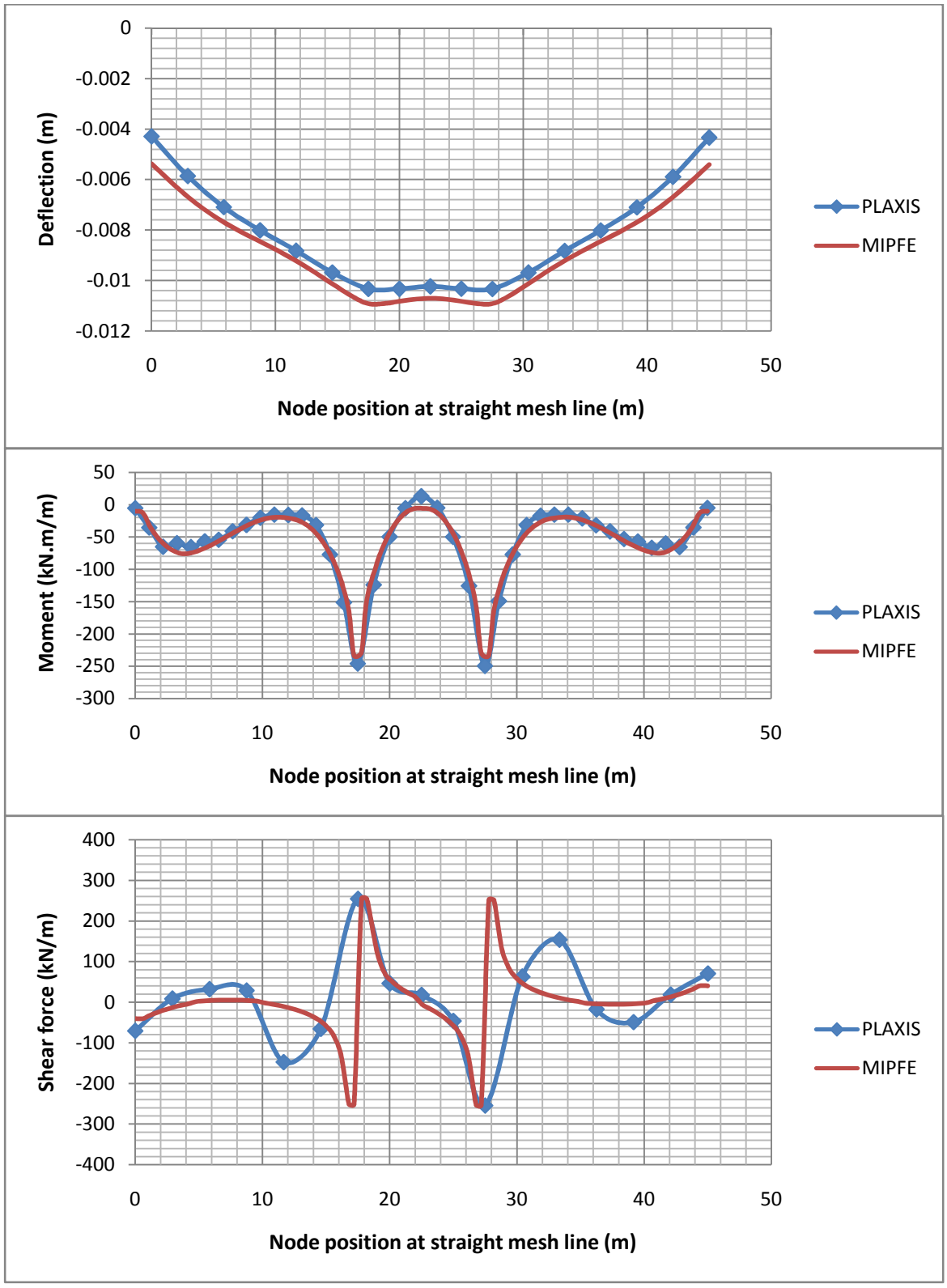

Figure 6.12: Solution comparisons for the material properties, loading and case 3 of Table 6.5.

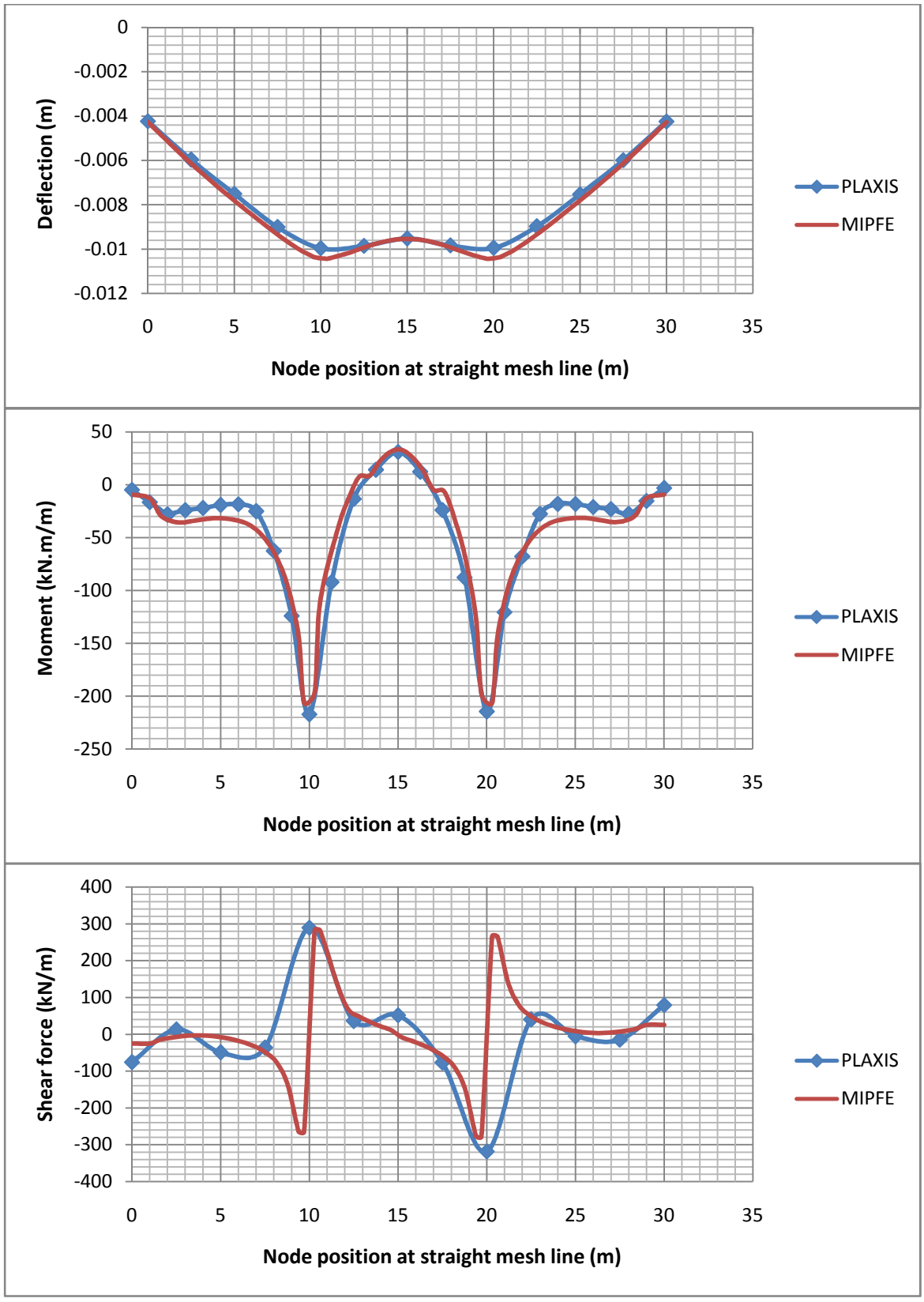

Figure 6. 13: Solution comparisons for the material properties, loading and case 4 of Table 6.5.

In this section four different examples have been presented for mixed loading case, the three examples try to illustrate the effect of plate aspect ratio and the last example shows the effect of plate thickness. Generally, the deflections and bending moments evaluated by both models are in good agreement. Some discrepancies are observed on the shear forces estimated by PLAXIS 3D FOUNDATION (see Section 6.5 for the detail discussion).

6.5. Discussion of Results

Generally, the deflection of both models is in good convergence. According to the above figures of deflection due to concentrated forces, discrepancy is observed as the soil thickness is varied. For lower thickness of soil, good convergence of deflection is observed around the edge and center of the plate (refer to Figures 6.5 and 6.6). However, as the soil thickness is increased, better convergence of deflection is observed around the center of the plate than around the edge of the plate (refer to Figures 6.7 and 6.8).

Generally, as it is observed from the above figures of bending moment, both models show a closer agreement of bending moment diagram for concentrated forces and mixed loading. An important observation is, if the loading contains columns with concentrated force, then maximum bending moment reinforcement bars are required just under the columns. Both PLAXIS 3D FOUNDATION and the developed finite element model evidently show this fact (refer to the figures of bending moment).

In general, as it can be observed from the above figures of deflection and bending moments, both models are in good agreement. However, the shear forces are not in closer agreement. In order to identify the sources of the discrepancies, independent study of the shear force diagrams of each model is important. The shear force diagrams of each model are assessed based on the following properties of shear force diagram: a) If the plate is symmetrical with respect to both loading and geometry, then the shear force diagram should be symmetrical. b) The shear force diagram is discontinuous at the locations of concentrated forces, if not it should be varied smoothly. c) Maximum shear force occurs at the locations of concentrated forces. The developed finite model satisfies all these properties. On the other hand, PLAXIS 3D FOUNDATION does not fully satisfy these properties (refer to the figures of shear force in Section 6.4).

In order to investigate the flaws of PLAXIS 3D FOUNDATION associated with shear force prediction, it is important to assess the efficiency and reliability of the implemented finite element type. According to the details in the PLAXIS 3D FOUNDATION scientific manual, PLAXIS 3D FOUNDATION is formulated based on pure displacement finite element formulation, specifically, the plate is formulated by 6-node triangular element [17]. However, pure displacement finite element is valuable only when higher order finite elements are employed. Indeed, the least order of interpolation that should be applied is a cubic interpolation function, which results in a 16-node quadrilateral element and a 10-node triangular element. If not, spurious shear stresses are predicted with the pure displacement-based finite elements [3]. Hence, the shear force evaluated by using PLAXIS 3D FOUNDATION has discrepancies, which is a result of the implementation of weak interpolation functions. An efficient and reliable remedy for this problem is to use mixed interpolation [3]. Note that the developed finite model in this research is based on mixed interpolation (refer to Section 3.2).

As it is shown by the above examples, both the developed finite element model and PLAXIS 3D FOUNDATION give non-zero shear force at the plate edge. However, the developed finite element model's shear force is less than the PLAXIS 3D FOUNDATION's shear force. As per the above examples, if the loads do not contain a uniformly distributed load, then both finite element models result in almost negligible bending moment at edge of the plate. This is clearly shown on the cases of concentrated load. Nevertheless, to arrive at definitive conclusions, further parametric studies have to be performed.

As it is already discussed in the previous chapter, generally the solutions of the developed finite model do not converge to the PLAXIS 3D FOUNDATION's solution with out adjustment. The major and critical sources of discrepancies for these divergences are differences in, a) mathematical modeling , b) finite element modeling , c) boundary condition modeling. In order to mitigate the effect of these differences on the solution, adjustment factors are provided in the previous chapter. Thus, as it is confirmed by the above examples, the degree of convergence of the developed finite element model's solution to the PLAXIS 3D FOUNDATION's solution is improved. In general, keeping the above mentioned modeling difference in mind, if the PLAXIS 3D FOUNDATION's solution is taken as benchmark solution (valid solution), then the developed finite element model's solution is safe and gives reasonably good results.

7. Conclusions and Recommendations

7.1. Conclusions

This research has presented a linear finite element model based on Mindlin plate theory and newly devised Kerr-equivalent Pasternak model. The implemented subgrade model is sensitive to the soil thickness. Thus, adjustment factors are used to bring the solution of the developed finite element model in agreement with the solution of PLAXIS 3D FOUNDATION. This finite element model is applicable for the analysis of flexible rectangular foundation structures for the range of parameters shown in Table 7.1.

Table 7.1: Range of parameters used in this research.

Parameter	Range of parameter
Plate length (L) in m	$5 \le L \le 70$
Plate width (B) in m	$5 \le B \le 70$
Plate thickness (h) in m	$0.3 \le h \le 1.2$
Uniformly distributed load (UDL) in kN/m^2	$40 \le UDL \le 400$
Plate aspect ratio (L/B)	$1 \le L/B \le 4$
Soil Young's modulus (E_s) in MPa	$15 \le E_s \le 100$
Concentrated load per column (CL) in kN	$100 \le CL \le 8000$
Number of columns (NC)	$1 \le NC \le 36$

The following conclusions are made for the range of the parameters alone:

- The developed finite element program implements 3D equivalent finite element and it is confirmed that the program can be used in routine personal computers for linear elastic cases effectively
- The developed finite element computer program is convergent.

- The solution of the developed finite element computer program is fairly in good agreement with the solution of PLAXIS 3D FOUNDATION.

7.2. Recommendations

The developed finite element model is limited only to linear elastic response of both a homogenous soil and a foundation structure. Furthermore, the foundation structure has to be rectangular raft foundation that does not contain cutouts, holes, beams and piles.

Hence, the application of the current study is possibly enhanced by including the following conditions in the future studies:

- Cutouts, holes, beams and piles.
- Triangular finite elements.
- Non-uniform thickness of soil below the region of a foundation structure.
- Layered soils.
- Plastic behavior of soils.

Bibliography

1. **Amlesu,T. (2018),** "Analysis of Strip Plates on Elastic Foundation Using Generalized Subgrade Model", A Thesis for Partial Fulfillment of the Degree of Master of Science in Geotechnical Engineering, Addis Ababa University.
2. **Bath, K.J., and Dvorkin, E.N. (1985),** "A four node plate bending element based on Mindlin/Reissner plate theory and a mixed interpolation", international journal for numerical methods in engineerings, Vol. 21, 367-383, John Wiley & Sons, Ltd.
3. **Bathe, K.J. (2014),** "Finite Element Procedures", Second Ed., K.J. Bathe, Watertown, MA,USA.
4. **Buczkowski, R., Taczala, M. and Kleiber, M. (2015),** "16-node locking-free Mindlin Plate Resting on Two-parameter Elastic Foundation"
5. **Coduto, D.P. (2001),** "Foundation Design Principles and Practices", Second Ed., Prentice Hall,USA
6. **Deyu, C.,** "Finite Element Method Engineering", Bihang University.
7. **Duncan, J.M. (1994),** "The Role of Advanced Constitutive Relations in Practical Applications", Proc,13thInt. Conf. Soil Mech. Found. Eng., New Delhi, India.
8. **Flugge, W. (1962),** "Hand book of Engineering Mechanics", McGraw-Hill Book Company, New York.
9. J**avidinejad, A. (2012),** "FEA Practical Illustration of Mesh-Quality-Results Differences between Structured Mesh and Unstructured Mesh", Department of Stress Engineering, Zodiac Aerospace, USA
10. **Kerr A.D. (1964),** "Elastic and Viscoelastic Foundation Models", Journal of Applied Mechanics, Transaction of ASME, pp. 491-498.
11. **Lade, P.V. (2005),** "Overview of Constitutive Models For Soils", Geotechnical Special Publication No.128, ASCE.
12. **Lanczos, C. (1952), "**The Variational Principles of Mechanics", University of Toronto Press, Toronto.
13. **Madhav, M., Abhishek, S.v., and Rajyalakshmi,K. (2015**), "Modelling Ground-Foundation Interaction", Conference paper.

14. **Meron, A. (2018),** "Application of aGeneralized Subgrade Model in the Analysis ofCircular Plates on Elastic Foundations", A Thesis for Partial Fulfillment of the Degree of Master of Science in Geotechnical Engineering, Addis Ababa University.
15. **Nikishkov, G. (2010),** "Programming finite elements in Java™",Springer-Verlag London Limited, London.
16. **O.C. Zienkiewicz, R.L. Taylor (2000),** "The Finite Element Method", Fifth edition, Butterworth-Heinemann.
17. "PLAXIS 3D FOUNDATION Scientific Manual" version 1.5.
18. "PLAXIS 3D FOUNDATION Validation Manual" Version 1.5.
19. **Potts, D. and Zdravkovic, L.(2001),** "Finite element analysis in geotechnical engineering (application)". Thomas Telford Ltd, London.
20. **Potts, D.M., and Zdravkovid, L. (1999),** "Finite element analysis in geotechnical engineering (theory)", Thomas Telford Ltd, London.
21. **Poulos, H.G.,(2018),"**Rational Assessment of Modulus of Subgrade Reaction ", Geotechnical Engineering Journal of the SEAGS & AGSEA, Sydney.
22. **Reissner, E. (1958),** "A Note on Deflection of Plates on Viscoelastic Foundation", journal of applied methatics, pp.144-155.
23. **Saad, M. (2009),** "Elasticity: Theory, Application, and Numerics", Second Ed., Elsevier Inc.
24. **Selvadurai, A.P.S. (1979),** "Elastic Analysis of Soil-Foundation Interaction", Elsevier Scientific Publishing Company, Amsterdam, Netherlands.
25. **Szilard, R. (2004),** "Theories and Applications of Plate Analysis", John Wiley & Sons, USA.
26. **Thomas, w. (1990), "**Analysis of Plate on Elastic Foundations**",** A dissertation in Civil Engineering Submitted to the Graduate Faculty of Texas Tech University in Partial Fulfillment of the Requirements for The Degree of Doctor of Philosophy.
27. **Timoshenko, S.P., Woinowsky-Krieger, S. (1965), "**Theory of Plates and Shells", McGraw-Hill Company, Inc. , New York.
28. **Turhan, A. (1992),** "Consistent Vlasov Model for Analysis of Plates on Elastic Foundations Using the Finite Element Method", A dissertation in Civil Engineering Submitted to the Graduate Faculty of Texas Tech University in Partial Fulfillment of the Requirements for The Degree of Doctor of Philosophy.
29. **Vallabhan, C.V.G., and Daloglu, A.T. (1999),** "Consistent FEM-Vlasov Model for Plates on Layered Soil", Journal of Structural Engineering, Vol. 125, No. 1, ASCE.

30. **Vlasov,V.Z., and Leont'ev ,N.N., (1966),** "Beams ,plates ,and Shells on Elastic Foundations", Translated from Russian, Israel Program for Scientific Translations ,Jerusalem.

31. **Wilson, E. (2002**), "Three-Dimensional Static and Dynamic Analysis of Structures", Third Ed., Computers and Structures, Inc., USA.

32. **Worku, A. (2010),** "Part I: A Generalized Formulation of Continuum Models for Elastic Foundations", Geo Florida, ASCE.

33. **Worku, A. (2014),** "Development of a Calibrated Pasternak Foundation Model for Practical Use", International Journal of Geotechnical Engineering, W. S. Maney & Son Ltd.

34. **Worku, A. and Degu Y. (2010),** "Part II: Application of Newly Derived and Calibrated Subgrade Models in the Analysis of Beams on Elastic Foundations", ASCE, GeoFlorida.